

Archive ouverte UNIGE

https://archive-ouverte.unige.ch

Thèse 2016

Open Access

This version of the publication is provided by the author(s) and made available in accordance with the copyright holder(s).

Current fluctuations and entanglement in dynamic mesoscopic conductors

Dasenbrook, David

How to cite

DASENBROOK, David. Current fluctuations and entanglement in dynamic mesoscopic conductors. Doctoral Thesis, 2016. doi: 10.13097/archive-ouverte/unige:87601

This publication URL: https://archive-ouverte.unige.ch/unige:87601

Publication DOI: <u>10.13097/archive-ouverte/unige:87601</u>

© This document is protected by copyright. Please refer to copyright holder(s) for terms of use.

FACULTÉ DES SCIENCES Professeur E. V. Sukhorukov Professeur C. Flindt

Current Fluctuations and Entanglement in Dynamic Mesoscopic Conductors

THÈSE

présenté à la Faculté des Sciences de l'Université de Genève pour obtenir le grade de Docteur ès sciences, mention Physique

par

David Dasenbrook

né à Braunschweig (Allemagne)

Thèse No 4972

GENÈVE $\begin{array}{c} {\rm GENÈVE} \\ {\rm Atelier~de~reproduction~ReproMail} \\ 2016 \end{array}$



Doctorat ès sciences Mention physique

Thèse de Monsieur David DASENBROOK

intitulée:

"Current Fluctuations and Entanglement in Dynamic Mesoscopic Conductors"

La Faculté des sciences, sur le préavis de Monsieur E. SUKHORUKOV, professeur associé et directeur de thèse (Département de physique théorique), Monsieur C. FLINDT, professeur et codirecteur de thèse (Department of applied physics, Aalto University, Finland), Monsieur N. BRUNNER, professeur assistant (Groupe de physique appliquée), Monsieur G. BLATTER, professeur (Institut für Theoretische Physik, Eigenössische Technische Hochschule Zürich, Schweiz) et Monsieur C. GLATTLI, professeur (Service de physique de l'état condensé, Commissariat à l'énergie atomique et aux énergies alternatives Saclay, Gif-sur-Yvette, France), autorise l'impression de la présente thèse, sans exprimer d'opinion sur les propositions qui y sont énoncées.

Genève, le 2 septembre 2016

Thèse - 4972 -

Le Doyen

Abstract

In this thesis, we investigate electronic transport in mesoscopic conductors. In these systems, quantum effects play a major role and the electronic currents have to be described in a quantum mechanical setting. Of particular interest are electron quantum optics setups, a field of research which aims to take inspiration from experiments carried out with photons in quantum optics and realise them using electrons in nanoscale conductors. Edge channels in topological insulators, most notably two-dimensional electron gases in strong magnetic fields exhibiting the quantum Hall effect, can play the role of one-dimensional wave guides for electrons, and tunable constrictions, so-called quantum point contacts (QPCs), can be used as beam splitters. Finally, dynamic coherent single-electron sources have recently been realized, and new methods for the characterization of their statistical properties are required.

In the first part of this thesis, current fluctuations in periodically driven phase-coherent conductors are considered. As the electrical current is a fluctuating quantity, it is interesting to consider the distribution of charges transferred across a conductor in a certain time interval, known as full counting statistics (FCS). Alternatively, the distribution function of waiting times between two successive charge transfer events, the waiting time distribution (WTD), can be considered.

We introduce a framework to calculate electronic WTDs in periodically driven quantum systems. To this end, we make use of the non-interacting Floquet scattering formalism. A formula that relates the idle time probability (ITP) to the Floquet scattering matrix is derived. From the ITP, the WTD and other statistical quantities can be obtained by taking time derivatives. As an application, we calculate the WTD for a QPC driven by periodic Lorentzian voltage pulses. The WTD shows a clear series of peaks corresponding to the transfer of single-electron excitations across the QPC. We also modulate the transmission of the QPC in time and find signatures of the modulation in the WTD. Then, WTDs for a dynamically driven mesoscopic capacitor operated as a nonadiabatic single-electron source are calculated and compared with WTDs based on a classical model.

Next, we go one step further and calculate generalized waiting time distributions for waiting times between events in different channels and also joint WTDs for consecutive waiting times. Electron waiting times in coherent conductors are found to be correlated.

Since the measurement procedure plays a prominent role in quantum mechanics, a waiting time clock that can measure WTDs is theoretically investigated next. In an appropriate parameter regime, the WTDs without a specific reference to a detector are recovered.

To measure the extensive FCS in periodically driven conductors, a measurement pro-

cedure based on an electronic Mach-Zehnder interferometer coupled to the system of interest is proposed and its properties are analyzed.

The second part of the thesis investigates the on-demand generation and detection of entanglement in mesoscopic conductors. A periodically modulated QPC can create electronic excitations that are entangled in their electron-hole degree of freedom. To circumvent the superselection rule for particle number, a nonlocal measurement is proposed that relies on recombining the two channels that are entangled at a second QPC. An entanglement witness based on current and noise measurements is derived, and the entanglement is shown to be detectable in realistic experimental situations.

Next, the question of whether the state of a single electron split between two modes is entangled is considered. Using a simple argument, we show that the answer is yes and derive a measurement strategy to demonstrate single-electron entanglement and nonlocality in an electronic Hanbury Brown-Twiss interferometer.

This thesis advances the field of electron quantum optics, where the arrival of dynamic single-electron sources opens up new possibilities to coherently generate and manipulate few-particle states. Since these systems are periodically driven at high frequencies, characterizations of current fluctuations such as the WTD or the FCS become important. Furthermore, electronic interferometers allow for the investigation of nonclassical behaviour and entanglement.

Résumé

Dans cette thèse, nous analysons le transport électronique dans les conducteurs mésoscopiques. Dans ces systèmes, les effets quantiques jouent un rôle majeur et les courants électriques doivent être décrits par la théorie quantique. Les systèmes d'optique quantique des électrons sont particulièrement intéressants: ce domaine s'inspire des expériences faites avec des photons dans le cadre de l'optique quantique et tente de les réaliser avec des électrons dans les conducteurs à l'échelle nano.

Les canaux de bord dans les isolants topologiques, notamment des gaz d'électrons en deux dimensions démontrant l'effet quantique Hall, peuvent jouer le rôle de guide d'ondes unidimensionnel pour les électrons, et des constrictions réglables, nommés QPC (quantum point contacts), peuvent être utilisées comme diviseurs de rayons. Finalement, des sources cohérentes d'électrons uniques ont été réalisées récemment, et des nouvelles méthodes de caractérisation de leurs propriétés statistiques sont nécessaires.

La première partie de cette thèse considère les fluctuations de courant dans les conducteurs cohérents entraînés périodiquement. Comme le courant électrique est une quantité fluctuante, il est intéressant de considérer la distribution de charges transférées à travers le conducteur dans un certain intervalle temporel, ce qui est connu comme full counting statistics (FCS). Alternativement, la distribution des temps d'attente entre deux événements de transfert de charge (waiting time distribution, WTD) peut être analysée.

Nous introduisons un cadre pour calculer des WTD électroniques dans les systèmes quantiques entraînés périodiquement. A cette fin, nous faisons usage du formalisme de diffusion non-interactif de Floquet. Une formule qui relie la probabilité du temps de ralentissement (*idle time probability*, ITP) à la matrice de diffusion de Floquet est dérivée. De la ITP, la WTD et d'autres quantités statistiques peuvent être obtenues en prenant des dérivées par rapport au temps. Pour des applications, nous calculons la WTD pour un QPC entraîné par des pulses de voltage Lorentzien. La WTD montre une série de pics qui correspondent au transfert des excitations d'électrons uniques à travers le QPC. Nous modulons aussi la transmission temporale du QPC et nous trouvons des signatures de la modulation dans la WTD. Puis, les WTD d'un condensateur mésoscopique entraîné dynamiquement utilisé comme une source d'électrons uniques sont calculées et comparées avec les WTD basées sur un modèle classique.

Ensuite de quoi nous allons un peu plus loin en calculant des distributions généralisées pour des temps d'attente entre des transferts de charges dans des canaux différents, ainsi que des distributions jointes pour des temps d'attente consécutifs. Nous trouvons que les temps d'attente des électrons sont corrélés.

Comme la procédure de la mesure joue un rôle important en mécanique quantique, une horloge de temps d'attente capable de mesurer les WTD est ensuite analysée. Dans un régime approprié des paramètres, les WTD sans référence spécifique d'un détecteur sont ré-obtenues.

Pour mesurer les FCS extensifs dans les conducteurs périodiquement entraînés, une procédure de mesure basée sur un interféromètre électronique Mach-Zehnder couplé au système étudié est proposée et ses propriétés sont analysées.

La deuxième partie de cette thèse étudie la création et la détection d'intrication à la

demande dans les conducteurs mésoscopiques. Un QPC qui est modulé périodiquement peut créer des excitations électroniques qui sont intriquées par leur degré de liberté électron-trou. Pour contourner la règle de superselection pour le nombre de particules, une mesure non-locale est proposée, mesure qui repose sur la recombinaison des deux canaux intriqués par un deuxième QPC. Un témoin d'intrication basé sur la mesure du courant et du bruit électronique est dérivé. Nous montrons que l'intrication est détectable dans des situations réalistes expérimentalement.

Finalement, nous nous demandons si l'état d'un électron unique partagé entre deux canaux est intriqué. Par un argument simple, nous montrons que la réponse est oui et nous dérivons une stratégie de mesure pour montrer l'intrication et la non-localité d'un électron unique dans un interféromètre électronique Hanbury Brown-Twiss.

Cette thèse avance le domaine de l'optique quantique des électrons, où l'arrivée des source dynamiques d'électrons uniques ouvre des possibilités de créer et manipuler des états de peu d'électrons d'une façon cohérente. Comme ces systèmes sont entraînés périodiquement aux hautes fréquences, la caractérisation des fluctuations du courant comme la WTD ou le FCS gagne en importance. En outre, les interféromètres électroniques ouvrent la possibilité d'étudier les comportements non-classique ainsi que l'intrication.

List of publications

- 1. D. Dasenbrook, C. Flindt, and M. Büttiker. Floquet Theory of Electron Waiting Times in Quantum-Coherent Conductors. Phys. Rev. Lett. 112, 146801 [2014].
- 2. D. Dasenbrook, P. P. Hofer, and C. Flindt. *Electron waiting times in coherent conductors are correlated.* Phys. Rev. B 91, 195420 [2015].
- 3. P. P. Hofer, D. Dasenbrook and C. Flindt. *Electron waiting times for the mesoscopic capacitor*. Physica E 82, 3 [2015].
- 4. D. Dasenbrook and C. Flindt. Dynamical generation and detection of entanglement in neutral leviton pairs. Phys. Rev. B 92, 161412(R) [2015].
- 5. D. Dasenbrook, J. Bowles, J. Bohr Brask, P. P. Hofer, C. Flindt, and N. Brunner. Single-electron entanglement and nonlocality. New J. Phys. 18, 043036 [2016].
- 6. D. Dasenbrook and C. Flindt. Quantum theory of an electron waiting time clock. Phys. Rev. B 93, 245409 [2016].
- 7. D. Dasenbrook and C. Flindt. *Dynamical Scheme for Interferometric Measure-ments of Full Counting Statistics*. ArXiv:1605:01926 (accepted by Phys. Rev. Lett.) [2016].
- 8. P. P. Hofer, D. Dasenbrook and C. Flindt. *On-demand entanglement generation using dynamic single-electron sources*. Phys. Status Solidi Focus issue: Single-electron control in solid-state devices (in preparation) [2016].

Contents

In	trodi	uction	3
I.	Ele	ectron waiting times and counting statistics	11
1.	Floo	quet theory of electron waiting times	13
	1.1.	Introduction	13
	1.2.	Electron waiting times	13
	1.3.	Scattering theory of electron waiting times	15
		1.3.1. Stationary conductors	16
		1.3.2. Periodically driven conductors	18
	1.4.	Examples	19
		1.4.1. Levitons	19
		1.4.2. Time-varying QPC	21
		1.4.3. Mesoscopic capacitor	23
	1.5.	Conclusions	28
2.	Cor	relations between electron waiting times	31
	2.1.	Introduction	31
		2.1.1. Two-time ITP	32
		2.1.2. First passage time distribution	34
		2.1.3. Two-time WTD	35
	2.2.	Generalized idle time probability	36
		2.2.1. Multiple channels	37
		2.2.2. Multiple times	39
	2.3.	Correlated waiting times	40
		2.3.1. Single-source partitioning	40
		2.3.2. Hong-Ou-Mandel interferometry	44
	2.4.	Conclusions	46
3.	Elec	ctron waiting time clock	47
		Introduction	47
	3.2.	Time-resolved counting statistics	49
	3.3.	Waiting time distributions	51
	3.4.	Electron waiting time clock	52
	3.5.	Applications	
		3.5.1. Voltage-biased QPC	
		352 Lorentzian voltage nulses	58

Contents

	3.6. 3.7. 3.8.	3.5.3. Smooth QPC transmission	59 59 61 63
4.	Inte	rferometric measurements of full counting statistics	65
	4.1.	Introduction	65
	4.2.	Mach-Zehnder interferometer	66
		4.2.1. Basic principle	66
		4.2.2. FCS measurement	67
		Detailed analysis	68
	4.4.	Applications	72
		4.4.1. Driven quantum point contact	72
		4.4.2. Entanglement entropy	72
		Dephasing	73
	4.6.	Conclusions	74
II.	En	tanglement in mesoscopic conductors	7 5
5	Dyn	namical entanglement of neutral leviton pairs	77
υ.		Introduction	77
	5.2.		78
	5.3.	_	79
	0.0.	5.3.1. Mach-Zehnder interferometer	79
		5.3.2. Dynamical entanglement generation	80
	5.4.	·	81
	5.5.		84
		5.5.1. Realistic description	84
		5.5.2. Dephasing	86
	5.6.	Conclusions	87
6	Sing	gle-electron entanglement and nonlocality	89
υ.	6.1.	Introduction	89
	6.2.	Single-particle entanglement	89
	6.3.	Setup for the demonstration of single-electron entanglement	91
	6.4.	Floquet scattering description	94
	0.1.	6.4.1. Scattering matrix	94
		6.4.2. Zero temperature	95
		6.4.3. Finite temperature and dephasing	98
	6.5.	Single-electron entanglement at finite temperature	99
	6.6.	•	
Co	onclu	sions	105

	Contents
A. Levitons	109
B. Determinant formula for the ITP	111
C. Evaluation of the generalised ITP	115
D. Numerical evaluation of Fredholm determinants	117
E. Full scattering matrix of the electron waiting time clock	119
Acknowledgments	137

Introduction

Condensed matter physics is a vast branch of physics, comprising many distinct subfields such as the investigation of metals and insulators; exotic quantum phases such as superconductors, Bose-Einstein condensates, and other quantum liquids; semi-conductors, topological materials, and hetero-structures. Additionally, in the study of all these phenomena and materials, a wide variety of experimental and theoretical methods is used, in accordance with the large range of different physical quantities one might be interested in. Thus, all of the modern physical frameworks (quantum mechanics, electrodynamics, thermodynamics, statistical mechanics and quantum field theory) have applications in condensed matter physics [Altland and Simons, 2010]. Moreover, whenever devising new theories and viewpoints, physicists often eventually turn to condensed matter systems as a test bed for their predictions, due to the relative ease with which these systems can be investigated in modern laboratories, and also due to their potential for technological applications. For example, the AdS/CFT correspondence originally discovered in the context of string theory has provided new inputs in the study of strongly correlated systems [Cubrović et al., 2009], and the discovery of topological insulators and superconductors [Hasan and Kane, 2010] has almost revolutionised the prevalent view of thermodynamic and quantum phases and their transitions, reactivating earlier work on topological field theories and providing even new experimental possibilities for cosmology [Zurek, 1996; Rosenberg and Franz, 2010].

One way to investigate solid state materials is to apply external electric fields to them via contacts and study their response, e. g. the currents flowing through them. If quantum theory is important for the underlying physics such as typically for very low temperatures and/or small samples, this field of study is called quantum transport. The field of quantum transport has made a substantial leap forward when it became possible to fabricate nanostructures in which electrons behave phase-coherently. More precisely, in these systems, the electronic coherence length is of the same order of magnitude as the sample size. This regime is referred to as mesoscopic. Therefore, in contrast to the term "nanophysics" which explicitly refers to a length scale, mesoscopic physics is the study of the set of phenomena taking place when the wave nature of electrons becomes important, in between the microscopic and the macroscopic length scales [Datta, 1997].

Early experiments that clearly demonstrated the phase-coherence of electrons throughout the transport process were on small conducting rings pierced by a magnetic flux [Webb et al., 1985], where a periodic dependence of the conductance on the magnetic flux with period h/e was observed, h being Planck's constant and -e the electronic charge. The dependence of the conductance on the flux is due to interference of the part of the electronic wave function encircling the flux in one way with the part encircling the flux in the other way, which is known as the Aharonov-Bohm effect [Aharonov and

Bohm, 1959]. However, if the ring is larger than the electronic phase coherence length, a different periodicity is observed due to averaging effects.

In mesoscopic physics, systems of reduced dimensionality are of particular interest. If the effective degrees of freedom of the electrons are reduced, for example due to strong confinement or magnetic fields, new phenomena appear and quantum mechanics manifests itself in different ways. For example, the electronic Aharonov-Bohm rings mentioned above can in fact be described by one-dimensional models [Büttiker et al., 1984; Gefen et al., 1984]. Moreover, two-dimensional electron gases (2DEGs) can be fabricated on the surfaces of GaAs-based semiconductor heterostructures [Thornton et al., 1986]. A different way to realize two-dimensional electron gases (albeit with strikingly different properties) is to use graphene sheets [Das Sarma et al., 2011]. An advantage of the use of semiconductor hetero structures however is that it allows for electrical gating using a top layer of metal. In this way, the 2DEG can be depleted in certain regions, allowing one to engineer effective geometries in which the electrons move.

In particular, defining a small opening between two gates that otherwise completely block the transport allows for the construction of quantum point contacts (QPCs), small tunable restrictions. They provide a tunable number of one-dimensional channels for electrons to pass through. Electron motion perpendicular to the current direction through the QPC is quantised due to the confinement. Because of the variable filling of these states, one observes conductance quantisation: The conductance changes in steps if the width of the constriction is varied [van Wees et al., 1988]. It is also possible to tune the QPC such that a single channel is only partially transparent. Electrons incident on the QPC may then either be transmitted or reflected. Quantum mechanically, the situation can be described by a simple one-dimensional scattering problem. The solutions are superpositions of left- and right-moving plain waves, and due to the phase-coherent nature of the 2DEG, the transport physics of the QPC is well described by these scattering states.

Another way to provide effective one-dimensional channels for phase-coherent electron transport is to make use of the quantum Hall effect [von Klitzing et al., 1980]. If a strong magnetic field is applied perpendicular to a 2DEG, electrons in the bulk will move in cyclotron orbits, thus leading to localisation and effectively turning the bulk of the sample into an insulator. However, at the edges of the sample, electrons move in skipping orbits, being repeatedly reflected at the sample boundary [Büttiker, 1988]. This leads to the emergence of dissipationless one-dimensional edge states [Halperin, 1982]. This semiclassical picture can in fact be complemented by a full quantum-mechanical calculation of the conductance in a multi-terminal setup, and the Hall conductance can be related to a topological invariant, the Chern number [Thouless et al., 1982]. The Chern number is the number of times the phase of the quantum mechanical electronic wave function wraps around the unit circle in the complex plane as the wave number is varied across the Brillouin zone, and it turns out that it equals the number of edge states due to an intricate connection: The presence of the edge states is guaranteed by the topological properties of the bulk bands, a theme that has been recurring in the more general field of topological insulators as the bulk-boundary correspondence.

In contrast to other effectively one-dimensional electronic systems such as nanowires

or gate-defined QPCs, the electrons in quantum Hall edge states turn out to behave very robustly in response to local disorder and inelastic scattering [Laughlin, 1981]. An explanation that does not invoke phase-rigidity of the wave functions across the sample was provided by Büttiker [1988]: Carriers moving along the sample edge cannot be back scattered by a distance longer than the circumference of a cyclotron orbit, and will continue to move under the action of the confining potential.

The emergence of very clean effectively one-dimensional quantum mechanical systems such as topological edge states and quantum point contacts has made possible all kinds of novel experiments in electronic systems. Whereas the response to applied external fields was previously mostly investigated to learn more about the materials and the microscopic mechanisms governing their behaviour, the controlled injection of charge carriers into very clean two-dimensional materials and effective one-dimensional waveguides also enables the study of the physics of the charge carriers themselves, and the implementation of fundamental quantum mechanical experiments involving electrons in the same way photons have traditionally been used in quantum optics. Consequently, this particular field of study was termed electron quantum optics [Bocquillon et al., 2012, 2014].

High-mobility two-dimensional electron gases in strong magnetic fields made it possible to experimentally implement electron interferometers in which fermionic anti-bunching [Henny et al., 1999; Bocquillon et al., 2013a] and interference effects due to the quantum mechanical wave nature of electrons [Ji et al., 2003; Roulleau et al., 2007] could be observed. A missing ingredient from the quantum optical toolbox was provided with the advent of dynamic on-demand single-electron emitters [Fève et al., 2007; Dubois et al., 2013b]. Before this, electron sources were implemented as statically biased contacts attached to the sample. In contrast to stationary bosonic particle sources (such as lasers), the fact that electrons are fermions and therefore anti-bunch already provides a fundamental source of regularity to such a static electron stream, which in fact can be modelled as a periodic succession of wave packets spaced by time intervals h/eV, where V is the applied voltage [Martin and Landauer, 1992].

A single-electron source based on a dynamically driven mesoscopic capacitor [Büttiker et al., 1993] instead injects electrons at well-defined instants in time and allows one to tune the overlap of successive wave packets [Fève et al., 2007]. Combining two such sources also permits tuning their relative time delay, making possible Hong-Ou-Mandel-like electron collision experiments [Bocquillon et al., 2013a]. A different way to inject single-electron wave packets on-demand was proposed by Levitov et al. [1996]: Applying Lorentzian-shaped voltage pulses to a contact injects exactly n charges on top of the otherwise undisturbed Fermi sea without any accompanying electron-hole pairs if the time integral of the voltage V(t) is ne, e being the elementary charge. This technique was experimentally implemented almost twenty years later by Dubois et al. [2013b] and subsequently used to perform tomography of the reduced single-electron density matrix [Jullien et al., 2014]. The particular single-electron excitation created in this way was named leviton.

To characterise these systems, suitable observables have to be chosen. In electronic quantum transport, mostly electric currents in response to applied fields are studied and

measured. The electric current is however a fluctuating quantity (there are thermal as well as quantum fluctuations), and therefore it is meaningful to study also correlation functions of currents [Blanter and Büttiker, 2000], also known as the noise spectrum. As the current operator is time-dependent, in principle a second order current correlator depends on two-time arguments. However, for a system that is invariant under time translations, the noise will only depend on the difference of the two times. Most often, the Fourier transform of such a stationary correlation function is considered. This is called the noise spectral density. Experimentally, it is usually measured in a small frequency range close to zero, and a lot of information about the charge transport can be inferred from zero-frequency noise. For periodically driven systems, the current correlator depends on two times separately and its Fourier transform can be investigated as a function of two frequencies [Moskalets and Büttiker, 2007].

For a phase-coherent mesoscopic conductor, the scattering theory of quantum transport can be used to calculate current and noise spectra [Büttiker, 1990b; Lesovik and Sadovskyy, 2011]. In this approach, which is valid as long as electron interactions can be neglected, the contacts are assumed to be sources of thermally distributed fermions and their creation and annihilation operators are related to those of the electrons that have traversed the sample by means of a scattering matrix. In this way, the non-equilibrium distribution functions of the outgoing electrons can be found and in principle all current correlation functions can be calculated at arbitrary temperatures. This approach also works for periodically driven systems where electrons can change their energy by scattering. In this case, the approach is called Floquet scattering theory.

The advent of single-electron sources made it necessary to devise new observables that characterise transport processes and that are sensitive to the particular properties of the sources, such as the shapes of the wave packets they emit and the accuracy of the emission timing. Fermionic anti-bunching provides a natural regularisation also to a continuous stream of electrons, and in fact the difference between a statically biased contact and a dynamic single-electron source is not visible from a measurement of the current or a zero-frequency current correlation function: For these observables, an average over many emissions of electrons is implicitly performed. Instead, one particular intuitive way of characterising the accuracy and properties of single-electron emitters is provided by the waiting time distribution (WTD), which is one of the two major topics of this thesis. The electron waiting time is defined as the time that passes between two successive emissions (or detections) of electrons. For an ideal periodic single-particle emitter, it is just given by the period of the driving, which is a constant. If there are cycle-missing events where an electron fails to be emitted due to e. g. some back-scattering mechanism or if the precise emission time fluctuates, the electron waiting time is a random quantity, and the WTD is the corresponding probability distribution function.

The WTD contains more information about the transport process than just the average current, which is (for obvious reasons) equal to the inverse mean waiting time, $\langle \tau \rangle = e/I$. There are other quantities which describe fluctuations of the current around its mean and often give complementary information. For example, moments and cumulants of the current distribution are often studied. In the zero-frequency limit, they are encoded in the full counting statistics (FCS) P(n) [Levitov et al., 1996], defined as the probability

to observe n charge transfer events across a conductor in a long measurement time. Full counting statistics has generated an enormous amount of research activity mainly on the theoretical side. It has been evaluated for, among many other examples, voltage pulses in mesoscopic conductors [Ivanov et al., 1997; Vanević et al., 2007], quantum pumps [Makhlin and Mirlin, 2001; Muzykantskii and Adamov, 2003], charge transfer between superconductors [Belzig and Nazarov, 2001], persistent currents [Komnik and Langhanke, 2014], Luttinger liquids [Gutman et al., 2010] and quantum impurity models [Komnik and Saleur, 2006].

While it is possible to study also the time-dependent FCS P(n,t), i. e. the probability distribution to observe n charge transfers in a finite measurement time t [Hassler et al., 2008; Schönhammer, 2007], in many cases the WTD can provide a more intuitive view-point. Finite-time FCS can sometimes be related to finite-frequency current cumulants, which are measurable in modern experiments and have been used among others to characterise the accuracy of single-electron emitters [Mahé et al., 2010; Parmentier et al., 2012]. The WTD on the other hand provides a clear series of peaks when evaluated for single-electron sources based on levitons [Dasenbrook et al., 2014] or the mesoscopic capacitor [Hofer et al., 2015] that simply correspond to the possible delay times between charge emissions, and features such as regularity or sharpness of the peaks can be related to physical interpretations in a straightforward way.

The first part of this thesis is dedicated to waiting time distributions and counting statistics for periodically driven quantum systems, especially focusing on single-electron sources. In addition to presenting the Floquet scattering formalism for WTDs and results for levitons and the mesoscopic capacitor (chapter 1), in chapter 2 we investigate WTDs depending on multiple times and also generalisations to many channels. The WTDs considered here are distributions of waiting times between electrons above the Fermi level. To leave out the Fermi sea from the analysis is convenient since the interest is in the additional electrons above the Fermi level produced by the sources, but it raises fundamental questions about the measurability of such distributions, since in real systems the Fermi sea is always present and it is not straightforward to separate it from the electrons above it. This is especially true in the case of time-dependent measurements [Gavish et al., 2001]. For this reason, in chapter 3 we present the theory of an electron waiting time clock that is capable of measuring electron waiting times above the Fermi sea and that reproduces the results of the calculations simply disregarding the Fermi sea in an appropriate parameter regime.

While the FCS has been studied quite intensely on the theory side, experimental measurements for phase-coherent mesoscopic conductors are still lacking. A detector that can measure the FCS was proposed by Levitov et al. [1996]. It consists of a quantum two-level system that is coupled to the magnetic field generated by the current in the conductor. Experimentally, the coupling of a qubit to a quantum conductor in a controlled and tunable way is challenging. In chapter 4, we propose a measurement scheme for the FCS in mesoscopic conductors using an electronic Mach-Zehnder interferometer coupled to the nearby conductor. To access the full probability distribution, the coupling between the system and the detector must be tunable. In our proposal, the tunability is achieved by varying the time-delay between electrons periodically injected into the

interferometer and the system to be measured. Hence, the proposal explicitly relies on the availability of coherent on-demand single-electron sources.

An important further step in the investigation of electron quantum optical systems is the controlled generation and characterisation of entangled few-particle states, in analogy to what is routinely achieved in quantum optics. Entanglement is perhaps one of the most puzzling features of quantum mechanics and had been identified as one of its defining concepts early on [Schrödinger, 1935]. Later, Bell famously showed that entanglement can lead to peculiar statistical correlations between spatially separated subsystems that cannot be explained by any locally realistic (or "hidden-variables") model [Bell, 1964]. This was later termed "Bell nonlocality" and opened up a whole new field of ongoing research [Brunner et al., 2014].

In the context of condensed matter physics, the concept of Bell nonlocality is less interesting in itself due to the small size of the systems considered. However, Bell tests are widely used to certify the presence of entanglement between spatially separate parts of the system, which is a highly sought-after resource for many reasons [Bennett and DiVincenzo, 2000]. For example, it is expected that quantum effects can provide exponential speedups for classically intractable calculations, and schemes for fundamentally unbreakable information encryption have been proposed. Apart from that, entanglement plays a major role in concepts such as dense coding (the transmission of more than one bit of classical information using a quantum bit) or teleportation (the transfer of a quantum state onto a distant particle using entanglement and classical communication).

In electron quantum optics, the challenge is to find strategies to generate and detect entanglement between electrons or electronic modes, preferably in a controlled way. Ondemand single-electron sources might play an important role in this endeavour. However, it is equally important to find ways to encode quantum information in electronic degrees of freedom and to devise and implement observables that can read out this information and ideally distinguish between entangled and separable states. One way to create entangled electron pairs is to use the spin degree of freedom, as the electron spin is an ideal two-level system and therefore provides a realisation of a quantum bit (qubit). A spin-entangled electron pair may be considered a direct analogue of a polarisation-entangled photon pair in quantum optics.

An s-wave superconductor provides a natural source of spin-singlets in the form of Cooper pairs, and as proposed by Recher et al. [2001] and Lesovik et al. [2001], they can in principle be split using a double quantum-dot setup connected to leads. Many Cooper-pair splitting devices have since been realised in semiconductors [Hofstetter et al., 2009], carbon nanotubes [Herrmann et al., 2010; Schindele et al., 2012] and graphene [Tan et al., 2015], some approaching very high efficiencies such as those required for Bell tests [Kawabata, 2001; Samuelsson et al., 2003] or entanglement witnesses [Burkard et al., 2006].

Apart from Cooper-pair splitting, Beenakker et al. [2003] noted that spin-entanglement also naturally occurs when an electron tunnels through a barrier, leaving behind a hole which is entangled with the electron through its spin. A teleportation effect results from the same physical mechanism [Beenakker and Kindermann, 2004]. On the other hand, in quantum Hall systems, electrons can be in different channels or modes, which

can also be used to encode quantum information even using spin-less electrons. If two electrons are entangled in their channel quantum number, they are said to be orbitally entangled. A setup in which orbital entanglement can be created and detected has been theoretically proposed by Samuelsson et al. [2004]. It consists of an electronic analogue of the Hanbury-Brown Twiss interferometer, and a Bell inequality for the orbital entanglement can be formulated in terms of experimentally measurable zero-frequency current-current correlators. The proposal was subsequently realised experimentally by Neder et al. [2007c], but the observed visibility in the noise oscillations was too low to unambiguously demonstrate the presence of entanglement [Samuelsson et al., 2009b].

A conceptually different type of entanglement is entanglement using the fermionic occupation number of modes. In this case, one cannot strictly speak about entanglement between two particles or excitations, since the information about the presence or absence of a particle is directly used to encode the quantum information needed for an entangled quantum state. Indeed, this case is called entanglement between modes, since now the spatially separated modes (e. g. quantum Hall edge channels) are entangled. However, it can be challenging to formulate Bell inequalities or derive entanglement witnesses based on experimentally measurable quantities. The reason is that for a certification of entanglement, it is necessary to perform measurements along two vectors in the state space which are not orthogonal [Horodecki et al., 2009]. In principle, to certify entanglement using the occupation number, one must therefore locally prepare superpositions of states with different particle numbers, which is forbidden by charge and parity superselection rules [Bartlett et al., 2007]. In quantum optics, these issues are by now well-understood and occupation-number entangled states are routinely generated and detected by providing a shared phase reference to bypass the superselection rules. For fermions however, these procedures cannot be straightforwardly applied. Yet, there are different ways to circumvent the superselection rules and certify the presence of mode-entanglement.

This is the topic of the second part of this thesis. In chapter 5, we investigate a scheme to create and detect entangled leviton pairs using the electron-hole degree of freedom. In this case, the quantum information is encoded in the charge of the electronic excitation, namely whether the excitation is electron-like or hole-like. Since the many-body state of an electron-like leviton differs from a hole-like leviton by two particles, the entanglement uses the fermionic occupation number and the difficulties described above appear. However, the entanglement can be detected using a nonlocal measurement scheme. We derive an entanglement witness for the electron-hole entanglement. The combined setup with the generation and detection of electron-hole entanglement then looks like the electronic Mach-Zehnder interferometer.

In chapter 6, we go one step further and ask the question of whether the state of a single-electronic excitation above the Fermi sea in a superposition between two spatial modes is entangled. For photons, it is by now well-established that the answer is yes [van Enk, 2005], but for electrons, the situation is more subtle. However, we rigorously demonstrate that the answer is positive also in this case, and that the entanglement can be revealed using two independently generated copies of the single-electron state. We furthermore

¹This is of course also true in the case of spin- or orbital entanglement.

Introduction

show that the demonstration of single-electron entanglement and nonlocality is possible in an electronic Hanbury-Brown Twiss interferometer with two single-electron sources using only zero-frequency current and noise measurements, also at finite temperatures.

The material presented in this thesis is compiled from a number of papers that the author published during his PhD work. Large parts of the main text are taken verbatim from these papers. The relevant references are [Dasenbrook et al., 2014; Hofer et al., 2015] (chapter 1), [Dasenbrook et al., 2015] (chapter 2), [Dasenbrook and Flindt, 2016b] (chapter 3), [Dasenbrook and Flindt, 2016a] (chapter 4), [Dasenbrook and Flindt, 2015] (chapter 5) and [Dasenbrook et al., 2016] (chapter 6).

Part I.

Electron waiting times and counting statistics

1. Floquet theory of electron waiting times

1.1. Introduction

In this chapter, we will introduce the concept of the waiting time distribution (WTD) in electronic transport. It is defined as the distribution of times τ that pass between successive electron detection events. We will review its definition and formulation for a phase-coherent electronic conductor connected to two single-channel leads. In this case, neglecting interactions between electrons, the scattering theory of electronic transport provides a convenient framework and the WTD can be related to the scattering matrix of the conductor. We then generalise the formalism to systems that are periodically time-dependent. Examples of such systems are quantum pumps, single-electron sources and periodically operated quantum switches. In this case, electrons can exchange energy with the system during the scattering process. The appropriate generalisation of the scattering matrix is then the Floquet scattering matrix, and again the WTD can be calculated based on its knowledge. As applications for this formalism, we consider the emission of single-charged voltage-pulses (levitons) onto a quantum point contact (QPC), a statically-biased QPC with a time-dependent transmission, and a single-electron source based on the mesoscopic capacitor.

The generalisations to multi-channel conductors and joint distributions of several waiting times will be the subject of chapter 2. In chapter 3, we will present the theory of a mesoscopic single-electron detector capable of measuring electron waiting time distributions.

1.2. Electron waiting times

Traditionally, the study of charge transport in mesoscopic conductors has focused on finding the average current $\langle I \rangle$ through the sample and its fluctuations, i. e. the noise $\propto \langle I^2 \rangle$ and higher-order cumulants. The latter are encoded in the full counting statistics (FCS) $P(n,\tau)$, the probability for n charges to be transferred through the conductor in a (typically long) measurement time τ .

An alternative characterisation on short-time scales is provided by the second-order coherence $g^{(2)}(t, t + \tau)$. It is defined as the joint probability of detecting an electron at time t and one at a later time $t + \tau$. Initially, it was proposed in quantum optics to characterise anti-bunching of photons emitted by a coherently driven two-level system [Carmichael and Walls, 1976; Kimble and Mandel, 1976].

Subsequently, as a more intuitive characterisation of the photo detection statistics, the waiting time distribution (WTD) $W(\tau)$ was proposed in this context by Cohen-Tannoudji

1. Floquet theory of electron waiting times

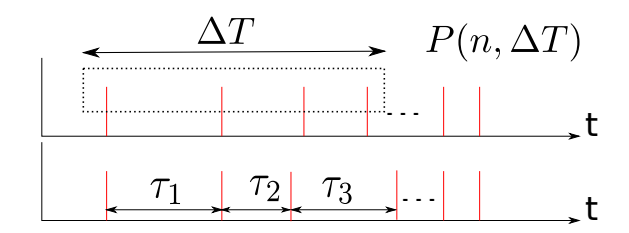


Figure 1.1.: Difference between FCS and WTD. Given a time series of detection events (red vertical lines), the problem of obtaining the FCS involves specifying a large measurement interval of length ΔT and finding the probability that n events are within this interval. In contrast, the WTD is the statistical distribution of the waiting times τ_i between two successive events. The WTD is therefore better suited to investigating short-time physics.

and Dalibard [1986] and developed further by Zoller et al. [1987]; Carmichael et al. [1989]. In contrast to the second-order coherence, the WTD is defined as the probability distribution for the time τ that passes between two subsequent photo detection events. It is therefore a conditional probability distribution. One of its appeals in quantum optics is that anti-bunching can be conveniently detected as the WTD is then suppressed at $\tau = 0$ and typically peaked around the mean waiting time. In contrast, for coherent light, the WTD is just exponentially decaying.

In electronic quantum conductors, the particles participating in transport are electrons and they therefore naturally anti-bunch due to their fermionic nature. Thus, it seems natural to also define the WTD for electronic transport and use it to investigate these issues. However, mostly due to the difficulties associated with measuring time-resolved quantities, proposals to consider the WTD also for electronic systems are fairly recent [Brandes, 2008]. Before that, usually the full counting statistics (FCS) was investigated instead [Levitov et al., 1996], the distribution function for the number of charges that pass through the conductor in a certain time interval. This approach usually does not capture effects on short time-scales. The difference between the FCS and the WTD is summarized in Fig. 1.1.

For systems weakly coupled to leads or in the limit of a high voltage bias, transport can often be described by a generalised master equation (GME). In this case, the question of what exactly constitutes a "detection event" in the definition of the WTD is straightforward since the process can be unravelled into a stochastic time-series series of quantum jumps, which are essentially classical. The formalism to extract the WTD from the GME was first given by Brandes [2008] and later generalised to non-markovian GMEs by Thomas and Flindt [2013]. Furthermore, the waiting time distribution for a dynamic single-electron emitter described by a classical stochastic model was obtained by Albert et al. [2011].

In the phase-coherent transport regime where the Landauer-Büttiker scattering formalism applies, the situation is a priori less clear. In this case, electrons are described by scattering states which are completely delocalised across the sample. Thus, the mathematical description provides no indication of when an electron is detected. To remedy this, either a quantum-mechanical model of a measurement device has to be included in the description, or the WTD has to be related to other, more directly accessible quantities. Both possibilities will be subjects of this thesis. In the following, we will introduce the concept of the idle time probability ITP, the probability that no electrons are detected in a time-interval of length τ . If this quantity originates from a stochastic time series of detection events, it has a simple relation to the WTD between these events. Furthermore, in scattering theory, it can be evaluated by a suitable function of the single electron density operator. The question of when this procedure is valid for a realistic electronic conductor and what kind of detector is implicitly assumed will be treated in chapter 3.

1.3. Scattering theory of electron waiting times

We consider a central scatterer connected to electronic leads. We are interested in the distribution $W(\tau)$ of waiting times τ between electrons scattered from the left to the right lead, passing a particular point x_0 in the right lead. A fundamental building block of our theory is the idle time probability (ITP) $\Pi(\tau, t_0)$: The ITP is the probability that no charges are observed at x_0 in the time interval $[t_0, t_0 + \tau]$. For stationary systems, the ITP is independent of t_0 such that $\Pi(\tau, t_0) = \Pi(\tau)$. The WTD can then be expressed as

$$W(\tau) = \langle \tau \rangle \partial_{\tau}^{2} \Pi(\tau), \tag{1.1}$$

where $\langle \tau \rangle$ is the mean waiting time [Vyas and Singh, 1988; Albert et al., 2012]. In contrast, for the periodically driven systems of interest here, the ITP is a two-time quantity depending on both t_0 and τ . In that case, the WTD can be evaluated by averaging the ITP over a period of the driving \mathcal{T} , using

$$\Pi(\tau) = \int_0^{\mathcal{T}} dt_0 \Pi(\tau, t_0) / \mathcal{T}$$
(1.2)

in Eq. (1.1).

We will now proceed to demonstrate both Eqs. (1.1) and (1.2). $\Pi(\tau,t_0)$, denotes the probability that there is no detection in the time interval $[t_0,t_0+\tau]$. At the time t_0 , there might or might not be a detection of an electron. We denote the last detection time of an electron prior to t_0 by t_e . Under the assumption of a detection at t_e , we define the temporal probability density of a subsequent detection to be the two-time waiting time distribution (WTD) $\widetilde{W}(t_e,\tau)$. Therefore, the probability for no detection in the interval $[t_e,t_0+\tau]$ is given by $1-\int_0^{t_0+\tau-t_e} \widetilde{W}(t_e,t) dt$. Since we do not know when the last detection of an electron prior to t_0 was, we integrate over all possible times to arrive at the two-time ITP. This integration is done with a weighting function I(t) denoting the temporal distribution of detection events:

$$\Pi(\tau, t_0) = \int_{-\infty}^{t_0} I(t_e) \left(1 - \int_0^{t_0 + \tau - t_e} \widetilde{\mathcal{W}}(t_e, t) dt \right) dt_e.$$

$$(1.3)$$

1. Floquet theory of electron waiting times

I(t) is the average current at time t.

If we differentiate Eq. (1.3) twice with respect to τ , we arrive at

$$\frac{\partial^2 \Pi}{\partial \tau^2}(\tau, t_0) = -\int_{-\infty}^{t_0} I(t_e) \frac{\partial \widetilde{\mathcal{W}}}{\partial \tau}(t_e, t_0 + \tau - t_e) dt_e. \tag{1.4}$$

Similarly, taking a mixed derivative, we get

$$\frac{\partial^{2}\Pi}{\partial t_{0}\partial \tau}(\tau, t_{0}) = -I(t_{0})\widetilde{W}(t_{0}, \tau) - \int_{-\infty}^{t_{0}} I(t_{e}) \frac{T}{\langle \tau \rangle} \frac{\partial \widetilde{W}}{\partial t_{0}}(t_{e}, t_{0} + \tau - t_{e}) dt_{e}$$

$$= -I(t_{0}) \frac{\langle \tau \rangle}{\mathcal{T}} \frac{\mathcal{T}}{\langle \tau \rangle} \widetilde{W}(t_{0}, \tau) + \frac{\partial^{2}\Pi}{\partial \tau^{2}}(\tau, t_{0}). \tag{1.5}$$

In the second line, we have inserted a factor of unity. $\mathcal{T}/\langle \tau \rangle$ is the average current integrated over one period, so that $I(t_0)\langle \tau \rangle/\mathcal{T}$ becomes a dimensionless probability distribution that integrates to one. We now recognise $I(t_0)\langle \tau \rangle \widetilde{\mathcal{W}}(t_0,\tau)/\mathcal{T}$ as the joint probability of a detection at t_0 and the next detection at $t_0 + \tau$. The waiting time distribution is now defined as the probability for the next detection at $t_0 + \tau$ regardless of the time t_0 . We therefore only have to integrate this quantity over all possible times, arriving at the relation

$$W(\tau) = \frac{\langle \tau \rangle}{\mathcal{T}} \int_0^{\mathcal{T}} \left(\frac{\partial^2 \Pi}{\partial \tau^2} (\tau, t_0) - \frac{\partial^2 \Pi}{\partial t_0 \partial \tau} (\tau, t_0) \right) dt_0, \tag{1.6}$$

which is automatically normalised such that $\int_0^\infty W(\tau) d\tau = 1$. For a periodically driven system, the ITP must itself be periodic in its second argument t_0 , so in this case the second term in Eq. (1.6) drops out. Thus, Eq. (1.1) with $\Pi(\tau)$ defined as in Eq. (1.2) follows.

1.3.1. Stationary conductors

Next, we evaluate the ITP for the outgoing many-body state of the scattering problem. Since all relevant energies are close to the Fermi energy, we can linearise the dispersion relation around the Fermi level, $E_k = \hbar v_F k$, such that all electrons scattered into the right lead propagate with the Fermi velocity v_F towards x_0 . The probability of finding no charges at x_0 in the temporal interval $[t_0, t_0 + \tau]$ is then equal to the probability of finding no charges in the spatial interval $[x_0, x_0 + v_F \tau]$ at time $t_0 + \tau$. We thus define the single-particle projection operator

$$\widehat{Q}_{\tau} = \int_{x_0}^{x_0 + v_F \tau} \mathrm{d}x \, |x\rangle \langle x| \tag{1.7}$$

which measures the probability of finding a given particle in the spatial interval $[x_0, x_0 + v_F \tau]$ [Hassler et al., 2008; Albert et al., 2012]. The complementary projector $1 - \hat{Q}_{\tau}$ similarly measures the probability of *not* finding the particle. To evaluate the ITP for the outgoing many-body state we proceed with a general second-quantized formulation

by introducing the operators $\hat{b}_{\alpha}^{(\dagger)}(E)$ which annihilate (create) electrons in an outgoing state of lead $\alpha = L, R$ at energy E. We may then write

$$\widehat{Q}_{\tau} = \sum_{E,E'} \int_{x_0}^{x_0 + v_F \tau} dx \varphi_{R,E'}^*(x) \varphi_{R,E}(x) \widehat{b}_R^{\dagger}(E) \widehat{b}_R(E'), \tag{1.8}$$

where $\varphi_{R,E}(x) = \langle x | \hat{b}_R^{\dagger}(E) | 0 \rangle$ and $| 0 \rangle$ is the vacuum.

The corresponding many-body operator that measures the probability of not finding any particles in the spatial interval is the normal-ordered exponential of $-\hat{Q}_{\tau}$, see e. g. the presentations by Vyas and Singh [1988]; Levitov et al. [1996]; Saito et al. [1992]. The ITP is then

$$\Pi(\tau) = \left\langle : e^{-\widehat{Q}_{\tau}} : \right\rangle_{\tau},\tag{1.9}$$

with :...: denoting normal-ordering of operators and the expectation value is taken with respect to the outgoing many-body state evaluated at the time $t_0 + \tau$. Equation (1.9) is a powerful formal result. It is also of practical use as it can be applied in a wide range of problems. Below, we consider non-interacting electrons, but Eq. (1.9) may equally well form the basis of a theory of WTDs in interacting systems. For stationary scattering problems, Eq. (1.9) reduces to the first-quantized result

$$\Pi(\tau) = \left\langle \bigotimes_{i=1}^{N} [1 - \widehat{Q}_{\tau}] \right\rangle_{t_0 + \tau} \tag{1.10}$$

by Albert et al. [2012] with the expectation value taken with respect to a time-evolved Slater determinant describing N particles.

In Eq. (1.8), the creation and annihilation operators for the electrons in the outgoing states appear. Using the scattering matrix approach [Blanter and Büttiker, 2000; Lesovik and Sadovskyy, 2011], we can map these operators onto linear combinations of operators of incoming electrons. These are assumed to be in thermal equilibrium, allowing us to evaluate averages as in Eq. (1.9). The operators of the outgoing states are expressed in terms of the operators of the incoming states as

$$\hat{b}_{\alpha}(E) = \sum_{\beta} S_{\alpha\beta} \hat{a}_{\beta}(E) \tag{1.11}$$

Inserting this relation into Eq. (1.9), the ITP can be written in terms of the operators $\hat{a}_{\beta}(E)$ for the incoming states. The evaluation of the ITP then amounts to calculating equilibrium averages of linear combinations of operators for the incoming states $\hat{a}_{\beta}(E)$.

We consider applying a constant voltage eV to the left lead, while the right lead remains grounded. For now, we are only interested in the waiting times between particles above the Fermi level and explicitly consider only the contribution of the states in the voltage window $[E_F, E_F + eV]$. (A discussion of the question if this corresponds to any physical measurement is the subject of chapter 3.)

1. Floquet theory of electron waiting times

Evaluating Eq. (1.9) with Eq. (1.11) and restricting to particles scattered from above the Fermi level of the left reservoir to the right one, we arrive at (see Appendix B)

$$\Pi(\tau) = \det(1 - \mathbf{Q}_{\tau}) \tag{1.12}$$

where the single-particle matrix elements of \mathbf{Q}_{τ,t_0} are

$$\mathbf{Q}_{\tau,t_0}(E, E') = \mathcal{S}_{RL}^*(E)\mathcal{S}_{RL}(E')K_{\tau}(E_m, E_n')\Theta(-E)\Theta(-E')$$
(1.13)

having introduced the kernel

$$K_{\tau}(E, E') = 2e^{-iqv_F\tau/2}\sin(qv_F\tau/2)/q$$
 (1.14)

with $q = (E - E')/\hbar v_F$ [Hassler et al., 2008; Albert et al., 2012].

1.3.2. Periodically driven conductors

Single-particle emitters such as mesoscopic capacitors or the QPC in the recent experiment by Dubois et al. [2013b] demonstrating clean electron excitations by applying voltage pulses can be described as mesoscopic scatterers driven with frequency $\Omega = 2\pi/\mathcal{T}$. Our next goal is to evaluate the ITP for these systems using Eq. (1.9).

To this end, Floquet scattering theory provides us with a convenient framework [Moskalets and Büttiker, 2002; Moskalets, 2011]. The scatterer is described by the Floquet scattering matrix S whose matrix elements $S_{\alpha\beta}(E_n, E)$ with $E_n = E + n\hbar\Omega$ are the amplitudes for an in-coming electron in lead β with energy E to scatter into lead α having absorbed (n > 0) or emitted (n < 0) |n| energy quanta of size $\hbar\Omega$. The generalisation of the formalism presented in the previous subsection for the case of static conductors to periodically time-dependent systems is now straightforward. The operators for the outgoing states are now related to the incoming operators via the Floquet scattering matrix [Moskalets and Büttiker, 2002; Moskalets, 2011],

$$\hat{b}_{\alpha}(E) = \sum_{\beta} \sum_{E_n} \mathcal{S}_{\alpha\beta}(E, E_n) \hat{a}_{\beta}(E_n). \tag{1.15}$$

A constant or time-dependent voltage bias between leads can always be gauged away at the expense of a time-dependent scattering phase, thus allowing us to treat the plethora of different devices on the same footing.

Eq.
$$(1.12)$$
 now becomes

$$\Pi(\tau, t_0) = \det(1 - \mathbf{Q}_{\tau, t_0}) \tag{1.16}$$

with

$$\mathbf{Q}_{\tau,t_0}(E,E') = \sum_{\substack{m=-\lfloor E/\hbar\Omega \rfloor\\n=-\lfloor E'/\hbar\Omega \rfloor}}^{\infty} \mathcal{S}_{RL}^*(E_m,E) \mathcal{S}_{RL}(E'_n,E') \times K_{\tau,t_0}(E_m,E'_n) \Theta(-E) \Theta(-E')$$
(1.17)

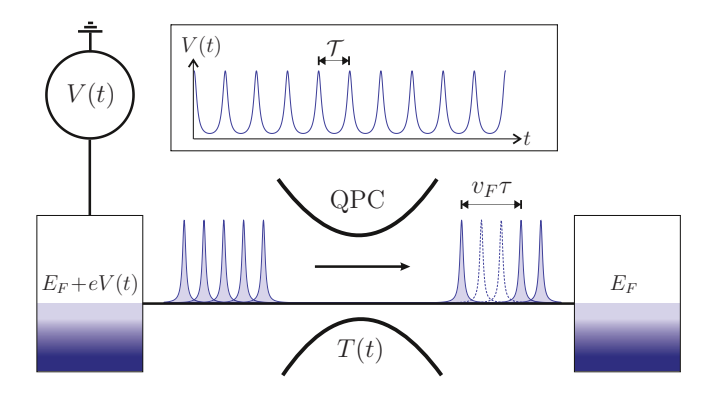


Figure 1.2.: Driven quantum point contact. Lorentzian-shaped voltage pulses V(t) with period \mathcal{T} generate a train of clean single-electron excitations (levitons) above the Fermi level E_F . The levitons propagate with the Fermi velocity v_F towards a quantum point contact (QPC) whose transmission T(t) can be controlled. We are interested in the distribution of waiting times τ between transmitted electrons. Reflected (missing) levitons are indicated by dashed lines. ([Dasenbrook et al., 2014], (C) 2014 American Physical Society.)

and the kernel $K_{\tau,t_0}(E,E') = 2e^{iqv_F(t_0-\tau/2)}\sin(qv_F\tau/2)/q$ with $q = (E-E')/\hbar v_F$. In deriving Eq. (1.17), we concentrated again on situations where all particles scattered into the right lead originate from the left lead (see also Appendix C). The Heaviside- Θ -functions are inserted into the equations by hand for now in order to filter out the Fermi sea. In contrast to the determinant in Eq. (1.12), the determinant is now taken over energies in the range $[0, E_F]$ and any voltage can be included as a time-dependent scattering phase in the Floquet S-matrix.

1.4. Examples

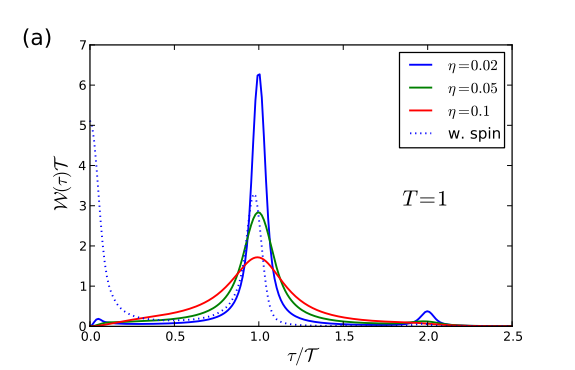
We now turn to the setup depicted in Fig. 1.2, consisting of a QPC connected to source (left) and drain (right) electrodes. We first apply a periodic voltage V(t) to the left electrode and later discuss a time-dependent transmission T(t).

1.4.1. Levitons

We consider the periodic application of Lorentzian voltage pulses of unit charge to the contact. The derivation of the Floquet scattering matrix for this situation is briefly reviewed in Appendix A. With the Floquet scattering matrix at hand we proceed by calculating the matrix \mathbf{Q}_{τ,t_0} in Eq. (1.17) and the determinant in Eq. (1.16) to find the WTD.

Figure 1.3a shows WTDs for different pulse widths with the QPC fully open. The WTDs are all suppressed to zero at $\tau = 0$, independently of the pulse width. This is due to the fermionic statistics which prevents two electrons from being detected at the same

1. Floquet theory of electron waiting times



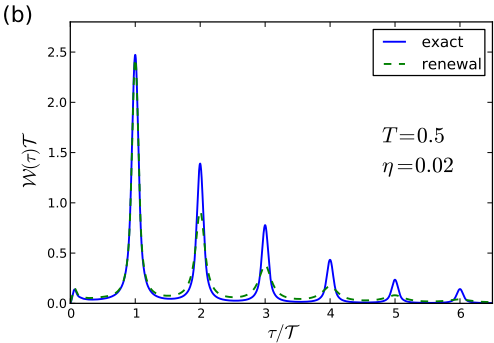


Figure 1.3.: Waiting times between levitons. (a) WTDs for levitons with different relative widths η and the QPC fully open (T=1). For small widths, a clear peak in the WTD is observed at the period of the voltage pulses, $\tau = \mathcal{T}$, together with small side peaks. As the pulses start to overlap, the peaks are smeared out. (b) WTD for levitons with the QPC tuned to half transmission (T=0.5). Cycle missing events may now occur as levitons reflect back on the QPC, giving rise to clear peaks at multiples of the period. We compare exact results to the approximation in Eq. (1.21) based on a renewal assumption. ([Dasenbrook et al., 2014], (C) 2014 American Physical Society.)

time [Albert et al., 2012]. With sharp pulses, most levitons are separated by one period of the driving as reflected by the large peak at $\tau = \mathcal{T}$. However, although one excitation is created in each period, the detection of an electron may happen in the (long) tails of the leviton, such that a period is skipped. This gives rise to the small but visible side-peaks at multiples of the period as well as the small peak just after $\tau = 0$ and shows that even a perfect single-electron source will suffer from cycle-missing events. In a quantum circuit, this information is important to synchronise the arrival of single electrons. As the pulse width is increased, the peak in the WTD broadens as the waiting time becomes less regular. Finally, for strongly overlapping pulses, the voltage is essentially constant and we recover the results for a dc-biased QPC (not shown) [Albert et al., 2012].

We now turn to the experimental situation realized by Dubois et al. [2013b], where the electronic spin is important. For two independent electronic spin channels, the idle time probability factorizes as $\Pi(\tau) = \Pi_1(\tau)^2$, where $\Pi_1(\tau)$ is the ITP for a single electronic channel. (For the case of correlated channels, see chapter 2.) In this case, the WTD (dotted line) develops a large peak around $\tau = 0$ corresponding to one electron in each spin channel being emitted nearly simultaneously. A second peak appears for waiting times slightly shorter than the period \mathcal{T} . This peak corresponds to the waiting time between the pairs of electrons that are emitted almost periodically with period \mathcal{T} .

Figure 1.3b shows the WTD with the QPC tuned to half transmission. Levitons may now reflect back on the QPC, and cycle-missing events, in which no levitons reach the right electrode within several periods, are very likely. The cycle-missing events give rise to clear peaks at multiples of the period.

Renewal theory

The effect of the QPC can be understood in a simple picture by resolving the WTD with respect to the number of reflections that have occurred as

$$\mathcal{W}(\tau) = T\mathcal{W}_1^{\text{in}}(\tau) + TR\mathcal{W}_2^{\text{in}}(\tau) + TR^2\mathcal{W}_3^{\text{in}}(\tau) + \dots$$
(1.18)

The reflection probability is R = 1 - T and the $W_n^{\text{in}}(\tau)$'s are the distributions of waiting times between n+1 incoming levitons. These are related to the joint probability distributions $W_n^{\text{in}}(\tau_1, \ldots, \tau_n)$ for n successive waiting times between incoming levitons, for example

$$W_2^{\text{in}}(\tau) = \int_0^{\tau} dt_1 W_2^{\text{in}}(t_1, \tau - t_1). \tag{1.19}$$

Introducing the Laplace transform $\widetilde{\mathcal{W}}(z) = \int_0^\infty d\tau \mathcal{W}(\tau) e^{-z\tau}$, we have

$$\widetilde{\mathcal{W}}_{n}^{\text{in}}(z) = \widetilde{\mathcal{W}}_{n}^{\text{in}}(z, \dots, z).$$
 (1.20)

We now make the renewal assumption that successive waiting times are uncorrelated [Cox, 1962] such that the joint WTDs factorise as $\widetilde{\mathcal{W}}_n^{\mathrm{in}}(z,\ldots,z)\simeq [\widetilde{\mathcal{W}}_1^{\mathrm{in}}(z)]^n$. We can then re-sum the geometric series $\widetilde{\mathcal{W}}(z)\simeq T\widetilde{\mathcal{W}}_1^{\mathrm{in}}(z)\sum_{n=0}^\infty [R\widetilde{\mathcal{W}}_1^{\mathrm{in}}(z)]^n$ as

$$\widetilde{\mathcal{W}}(z) \simeq \frac{T\widetilde{\mathcal{W}}_{1}^{\text{in}}(z)}{1 - R\widetilde{\mathcal{W}}_{1}^{\text{in}}(z)}.$$
 (1.21)

The WTD of the incoming levitons, $\widetilde{W}_1^{\text{in}}(z)$, is the WTD at full transmission (T=1) shown in Fig. 1.3a.

Equation (1.21) provides us with a direct test of the renewal assumption of uncorrelated waiting times. Reverting it to the time domain, we can compare Eq. (1.21) with the exact results in Fig. 1.3b. The first peak around $\tau = \mathcal{T}$ is governed by the term $TW_1^{\text{in}}(\tau)$, which does not depend on the renewal assumption, and good agreement is found. In contrast, the following peaks are increasingly smeared out under the renewal assumption. This demonstrates that successive waiting times are correlated: The external driving produces a quasi-periodic train of incoming levitons. Thus, a waiting time that is shorter (longer) than the period \mathcal{T} will likely be followed by a waiting time that is longer (shorter) than the period. These correlations, which are responsible for the sharp peaks in Fig. 1.3b, are omitted under the renewal assumption. We note that the full counting statistics for this problem is always binomial with success probability T and therefore does not distinguish between a static voltage and a series of Lorentzian pulses [Ivanov et al., 1997]. In contrast, the WTD fully captures the influence of the width of the pulses and of correlations between single-electron emissions, which is crucial information for the synchronised operation of a quantum device.

1.4.2. Time-varying QPC

We now fix the voltage V(t) = V and instead modulate the transmission probability periodically in time as $T(t) = T_0[1 - \epsilon \sin(\Omega t)]^2$ [Klich and Levitov, 2009; Zhang et al.,

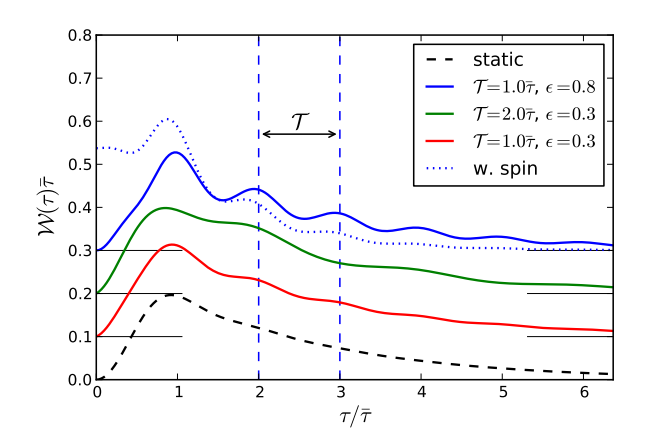


Figure 1.4.: Periodically modulated QPC transmission. The WTDs are shifted vertically for clarity. Oscillations with a period \mathcal{T} are superimposed on the WTD for a static QPC with $T_{\rm av}=0.4$ (black dashed lines). The dotted lines show the WTDs for spin-1/2 particles, which show a lifting of the suppression at $\tau=0$ as well as a damping of the oscillations compared to the spin-less case (dashed lines). ([Dasenbrook et al., 2014], (C) 2014 American Physical Society.)

2009]. The average transmission probability is $T_{\rm av}=T_0(1+\epsilon^2/2)$ and the maximal transmission $T_{\rm max}=T_0(1+\epsilon)^2$ must be smaller than unity. The frozen transmission amplitude from the left to the right lead reads $\mathcal{S}^f_{RL}(E,t)=\sqrt{T(t)}e^{-ieVt/\hbar}$. For the Floquet scattering matrix we find in the adiabatic limit

$$S_{RL}(E_n, E) = \sqrt{T_0} \left[\delta_{n,p} + i\epsilon \left(\delta_{n,p-1} - \delta_{n,p+1} \right) / 2 \right], \tag{1.22}$$

assuming for the sake of simplicity that the applied voltage is a multiple of the modulation quantum, $eV = p\hbar\Omega$, where p is an integer, so that the problem is \mathcal{T} -periodic. (The case $qeV = p\hbar\Omega$ with p and q being integers can easily be treated, although the problem becomes $q\mathcal{T}$ -periodic). Apart from the central energy band (the Kronecker delta $\delta_{n,p}$) due to the voltage bias, there are two side bands corresponding to electrons emitting $(\delta_{n,p-1})$ or absorbing $(\delta_{n,p+1})$ a modulation quantum.

Figure 1.4 shows the WTD for different modulation frequencies. As we treat the experimentally most relevant case of two independent spin channels, the WTDs do not vanish for $\tau=0$, contrary to what happens for spin-less electrons. Compared to the static case, the external driving introduces new oscillations in the WTD. They are most dominant for a large oscillation amplitude (blue curve) and show that the modulation regulates the stream of incoming electrons: Since transmission at the peak of the modulation is more likely, electrons are most likely spaced by multiples of the period. For small oscillations however, the presence of the second spin-channel renders these oscillations almost invisible, since the WTD is now dominated by electrons that are transmitted close after each other, within the same period of the oscillation.

For weak modulations ($\epsilon \ll 1$) and low transmissions ($T_0 < 1$), the determinant in Eq. (1.16) can be expanded to lowest order in ϵ and T_0 . A detailed calculation then yields

$$\mathcal{W}(\tau) \simeq T_0 \left(\frac{g_{\bar{\tau}}^{(2)}(\tau)}{\bar{\tau}} + \epsilon^2 \left[\frac{g_{\bar{\tau}_{\Omega}}^{(2)}(\tau)}{\bar{\tau}_{\Omega}} + \frac{g_{\bar{\tau}_{-\Omega}}^{(2)}(\tau)}{\bar{\tau}_{-\Omega}} \right] \right), \tag{1.23}$$

where $g_x^{(2)}(\tau) = 1 - \sin^2(\pi \tau/x)/(\pi \tau/x)^2$ is the two-point correlation function for a static voltage-biased conductor. The expansion is expected to be valid at short times [Albert et al., 2012]. In Eq. (1.23), time-scales related to the driving $\bar{\tau}_{\pm\Omega} = h/(eV \pm \hbar\Omega)$ appear in addition to the time-scale associated with the static voltage, $\bar{\tau} = h/eV$. Equation (1.23) is simply a superposition of correlation functions for a static voltage-biased QPCs with voltages eV and $eV \pm \hbar\Omega$, respectively, reflecting the three energy bands in Eq. (1.22). Interferences between the bands show up at longer waiting times, leading to the oscillations with period \mathcal{T} in Fig. 1.4.

1.4.3. Mesoscopic capacitor

A different approach to create on-demand single-electron excitations above the Fermi level is provided by the mesoscopic capacitor. It consists of a small electronic cavity in the quantum Hall regime with quantized energy levels tunnel-coupled to an edge state. By varying a top gate potential periodically in time, the energy levels in the dot can be moved above and below the Fermi level in the edge state. The mesoscopic capacitor then periodically emits electrons and holes into the nearby channel. This has been experimentally realized by Fève et al. [2007]; Bocquillon et al. [2013a]. In this section, we will consider the WTD of a mesoscopic capacitor operated using a non-adiabtic driving protocol.

Scattering matrix

We now describe the mesoscopic capacitor using non-interacting scattering theory [Moskalets, 2011]. This approach can account for many experimental observations.

The capacitor is shown schematically in Fig. 1.5. Electrons propagate along chiral edge states that form when a two-dimensional electron gas is subject to a strong magnetic field. A small loop is tunnel coupled to an edge state via a QPC. The loop constitutes one plate of the capacitor. The other plate is a top-gate with potential V(t). An electron travelling along the edge state can either be reflected on the capacitor and continue its motion along the edge, or it can be transmitted into the capacitor and make several turns inside the loop before eventually escaping. Since there is only a single incoming and outgoing channel, the scattering matrix of the capacitor is just a complex number of unit length which can be obtained by summing up the quantum mechanical amplitudes for all possible scattering paths.

We first consider the capacitor with a constant top-gate potential $V(t) = V_0$. The

1. Floquet theory of electron waiting times

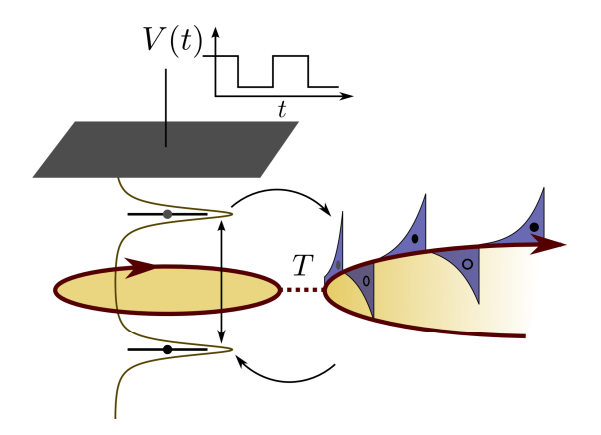


Figure 1.5.: The driven mesoscopic capacitor. A small cavity is tunnel coupled to an edge state (in red) via a quantum point contact with transmission probability T. By applying a time-dependent voltage V(t) to the top gate of the capacitor (in grey) the levels of the capacitor are shifted up and down. If a filled level is moved above the Fermi energy of the external reservoir, the capacitor can emit an electron into the edge state. The empty level is then refilled by an electron as the level is moved below the Fermi energy. This leads to exponential current pulses (in blue) with alternating signs in the outgoing edge state. ([Hofer et al., 2015], (C) 2015 Elsevier.)

reflection amplitude is then

$$S(\epsilon) = r - T \sum_{n=1}^{\infty} r^{n-1} e^{in(\epsilon - eV_0)\tau_0/\hbar}$$

$$= \frac{r - e^{i(\epsilon - eV_0)\tau_0/\hbar}}{1 - re^{i(\epsilon - eV_0)\tau_0/\hbar}},$$
(1.24)

where r is the reflection amplitude of the QPC (here chosen to be real), $T = 1 - r^2$, and $\tau_0 = \ell/v_F$ is the time it takes an electron with Fermi velocity v_F to complete one turn in the loop of circumference ℓ . In this case, no (additional) current is generated in the outgoing edge state.

To generate an AC current, the top-gate potential must be time-dependent. To see this, it is instructive to consider the density of states of the capacitor without driving

$$\rho(\epsilon) = \frac{1}{2\pi i} \mathcal{S}^*(\epsilon) \frac{d\mathcal{S}(\epsilon)}{d\epsilon}$$

$$= \frac{1}{\pi} \sum_{j=-\infty}^{\infty} \frac{\frac{1}{2}\gamma}{(\epsilon - eV_0 - j\Delta)^2 + (\frac{1}{2}\gamma)^2}.$$
(1.25)

The density of states consists of a series of Lorentzian peaks with spacing $\Delta = h/\tau_0$ and widths

$$\gamma = -\frac{\Delta}{\pi} \ln \left(\sqrt{1 - T} \right) \simeq \frac{\Delta T}{2\pi}, \quad T \ll 1.$$
 (1.26)

A time-dependent potential V(t) will shift the positions of the levels. If a filled level is moved above the Fermi energy, an electron can escape the capacitor and when an empty level is moved below the Fermi energy, an electron can be absorbed, or equivalently, a hole be emitted from the capacitor. Moving an energy level periodically above and below the Fermi energy will thus result in the periodic emission of a single electron followed by a single hole. If this is done adiabatically, the Lorentzian width of the level determines the wave-function of the emitted particles and the current consists of a series of Lorentzian pulses with alternating signs [Keeling et al., 2008]. Experimentally, a square-shaped potential has been applied to a capacitor with period $\mathcal T$ and peak-to-peak amplitude equal to the level spacing Δ [Fève et al., 2007]. Within one period, the potential has the form

$$eV(t) = \begin{cases} \Delta/2 & 0 < t \le \mathcal{T}/2 \\ -\Delta/2 & \mathcal{T}/2 < t \le \mathcal{T} \end{cases}$$
 (1.27)

The current pulses then have the shape of decaying exponentials with alternating signs. We focus throughout this work on this square-shaped potential.

To describe a periodic potential we use Floquet scattering theory [Moskalets, 2011]. We start by noting that an electron that completes n turns in the capacitor picks up the phase [Parmentier et al., 2012]

$$\phi_n(t) = \frac{e}{\hbar} \int_{t-n\tau_0}^t V(\tau) d\tau, \qquad (1.28)$$

upon leaving the capacitor at time t. By substituting this expression for the static phase $(e/\hbar)V_0n\tau_0$ in the first line of Eq. (1.24), we obtain the mixed energy-time representation of the scattering amplitude $\mathcal{S}(t,\epsilon)$ for electrons that enter the capacitor with energy ϵ to leave it at time t. Since the potential is periodic, $V(t) = V(t + \mathcal{T})$, we can expand the scattering phase in a Fourier series as

$$e^{-i\frac{e}{\hbar}\int_0^t V(\tau)d\tau} = \sum_{m=-\infty}^{\infty} c_m e^{-im\Omega t},$$
(1.29)

where $\Omega = 2\pi/\mathcal{T}$ is the frequency of the driving. In addition, by Fourier transforming $\mathcal{S}(t,\epsilon)$ as

$$S_F(\epsilon_n, \epsilon) = \frac{1}{\mathcal{T}} \int_0^{\mathcal{T}} e^{in\Omega t} S(t, \epsilon) dt, \qquad (1.30)$$

we obtain the Floquet scattering matrix

$$S_F(\epsilon_n, \epsilon) = \sum_{m = -\infty}^{\infty} c_{m+n} c_m^* S(\epsilon_{-m}), \qquad (1.31)$$

where we have defined the energies

$$\epsilon_n = \epsilon + n\hbar\Omega. \tag{1.32}$$

1. Floquet theory of electron waiting times

Equation (1.31) is valid for an arbitrary periodic top-gate potential V(t) expressed in terms of its Fourier components c_m . With this expression one may calculate the time-dependent current or the finite-frequency noise of the capacitor [Moskalets, 2011], or the ITP using Eq. (1.16).

The mesoscopic capacitor works best as a single-electron source if the density of states is symmetric around the Fermi energy. In this case, an analytic expression for the Floquet scattering matrix has been derived by Moskalets et al. [2013]. In addition, the charge relaxation resistance

$$R_q = \frac{h}{e^2} \left(\frac{1}{T} - \frac{1}{2} \right) \simeq \frac{h}{e^2 T}, \quad T \ll 1$$
 (1.33)

equals the resistance of the QPC for small transmissions [Parmentier et al., 2012]. By contrast, the capacitance becomes independent of the transmission

$$C_q = \frac{e^2}{\Lambda}. (1.34)$$

The dwell (or relaxation) time of the capacitor reads

$$\tau_D = R_q C_q \simeq \frac{h}{T\Lambda} = \frac{\tau_0}{T}.$$
 (1.35)

The capacitor is expected to operate as a nearly perfect single-electron emitter if the dwell time is (much) shorter than the period, $\tau_D \ll \mathcal{T}$. In this case, a single electron and a single hole should be emitted in almost every cycle. However, even under these optimal conditions, there can be noise at finite frequencies associated with the uncertainty of the emission time within a period and the shape of the wave packets. This type of noise has been investigated theoretically and experimentally by Mahé et al. [2010]; Albert et al. [2010]; Parmentier et al. [2012].

If the QPC transmission is too low, the dwell time can become comparable to the period. In this case, cycle-missing events may occur, where the capacitor fails to emit an electron within a period or an empty level is not refilled. An electron and a hole will then be missing from the otherwise periodic stream of particles. Several methods have been employed to assess the accuracy of the mesoscopic capacitor as a single-electron source. These include analysing the finite-frequency noise [Moskalets et al., 2008; Parmentier et al., 2012; Moskalets, 2013] or the full counting statistics of emitted charge [Albert et al., 2010]. Instead, we here analyse the WTD.

Results

The numerical calculations are demanding. We discretize the kernel in the energy windows $[-n\hbar\Omega, -(n+1)\hbar\Omega]$ with $n \in \mathbb{N}$ using a five-point Gauss-Legendre quadrature rule following a recently developed method by Bornemann [2010] (see Appendix D) to evaluate Fredholm determinants. To calculate the matrix Q_{t^s,t^e} , we have to sum over all Floquet scattering amplitudes. We find that we can cut off the summation with about $n_{\text{max}} \approx 2\Delta/(\hbar\Omega)$ amplitudes. This is the maximum number of energy quanta that a scattered particle can absorb or emit. The determinant is then taken over all the energies

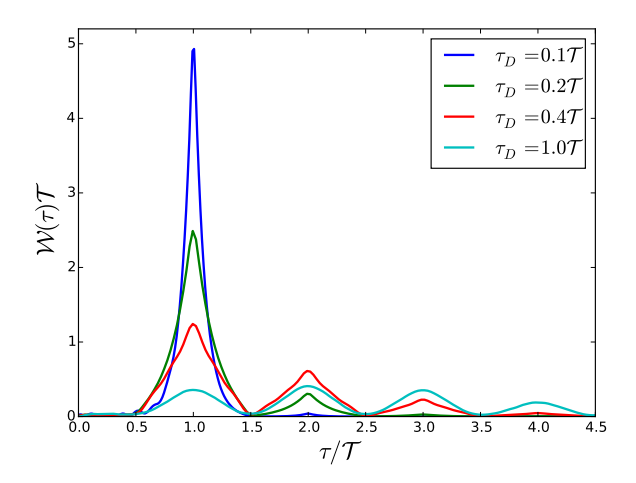


Figure 1.6.: Floquet calculations of the WTD. Results are shown for different values of the dwell time τ_D . The QPC transmission is T=0.2. The results agree very well with those obtained from a wave packet approach. ([Hofer et al., 2015], (C) 2015 Elsevier.)

in the n_{max} compartments. Finally, we integrate numerically the ITP over one period of the driving and evaluate the WTD according to Eq. (1.1).

Figure 1.6 shows WTDs for the mesoscopic capacitor obtained using Floquet scattering theory. For $\tau_D \ll \mathcal{T}$, the central peak at the period of the driving is clearly reproduced with small but visible satellite peaks at multiples of the period. As the dwell time is increased by lowering the level spacing Δ , the peaks become smoother and less sharp compared to the wave packet approach. This happens as the broadened energy levels start to overlap.

The results can be compared to those based on a wave packet approach [Hofer et al., 2015; Albert et al., 2011], where the WTD depends only on the ratio of the dwell time over the period. The dwell time is given by the product of the level spacing and the QPC transmission according to Eq. (1.35). By contrast, in the full scattering problem the level spacing and the transmission are independent parameters which thus provide an additional time scale in the problem. Indeed, a calculation of the finite-frequency noise of the driven capacitor Parmentier et al. [2012] has shown that the noise vanishes at measurement frequencies that are higher than the level spacing, unlike what is found based on the rate equation description.

With this in mind, we show in Fig. 1.7 distributions of waiting times for a fixed dwell time, but with different transmissions of the QPC. As the transmission is increased, the energy levels of the capacitor are broadened and the peaks in the WTD get smeared out. In addition, the peaks at multiples of the period are reduced, as it is increasingly likely that the capacitor will emit an electron in each period. Even with a large transmission, the mesoscopic capacitor seems to function well as a single-electron emitter. In the

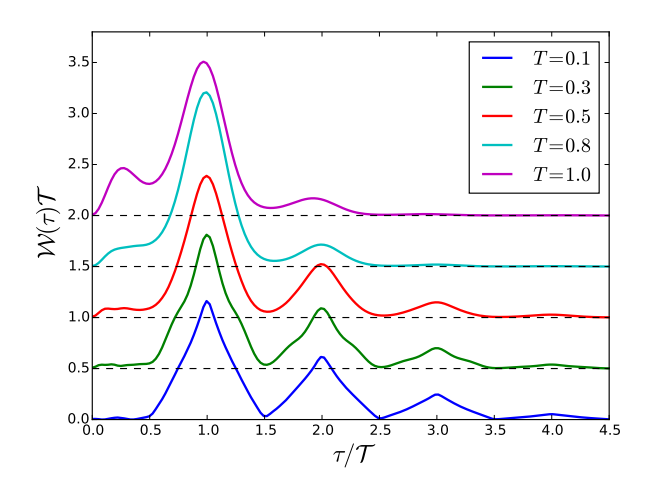


Figure 1.7.: Floquet calculations of the WTD for different QPC transmission. The dwell time is $\tau_D = 0.4\mathcal{T}$. The different curves have been shifted vertically for the sake of better visibility. ([Hofer et al., 2015], (C) 2015 Elsevier.)

extreme case of full transmission, the capacitor consists merely of an elongation of the edge state and the level quantization is completely lost. It may then happen that more than one electron is lifted above the Fermi level within one period, giving rise to the satellite peak at $\tau \approx \mathcal{T}/4$, similarly to what has been found for Lorentzian-shaped voltage pulses (Fig. 1.3a) [Dasenbrook et al., 2014; Albert and Devillard, 2014].

1.5. Conclusions

In this chapter, we have presented a Floquet scattering formalism to calculate waiting time distributions (WTDs) for mesoscopic conductors with an external periodic time-dependence. The WTD is related to the idle time probability, the probability for no charge transfers in a certain time interval τ . The idle time probability for electrons above the Fermi level can be expressed as a compact determinant formula involving the Floquet scattering matrix of the system. We have applied our formalism to a quantum point contact driven by Lorentzian voltage pulses, a statically biased quantum point contact whose transmission is periodically modulated in time, and a driven mesoscopic capacitor acting as a single-electron source. In all cases, the external driving period provides a new time scale that appears in the WTDs.

The shape of the WTDs provides information about the shape of the electron wave packets and the properties of the scatterer. If we neglect correlations between subsequent waiting times, the effect of a finite transmission of the QPC can be understood by resolving the WTD with respect to the number of reflections that have occurred, and the WTD at finite transmission can be obtained by a Laplace transform technique from the WTD at unit transmission. In the following section, we will further investigate correlations

between electron waiting times.

2. Correlations between electron waiting times

2.1. Introduction

So far, we have focused on the distribution of individual electron waiting times. Such distributions, however, do not address the question of correlations between subsequent waiting times. One may ask if the observation of one waiting time will affect the following waiting time. Some results have already indicated that subsequent electron waiting times indeed are correlated, see e. g. the discussion of renewal theory in Sec. 1.4.1. However, to fully answer this question, a theory of joint WTDs is needed. Such a theory is provided in this chapter.

Figure 2.1 shows an example of a joint WTD. Using a method that we develop in this chapter, we have calculated the joint distribution of waiting times $W(\tau_1, \tau_2)$ between electrons transmitted through a fully open conduction channel. Albert et al. [2012]; Haack et al. [2014] showed that the distribution of individual electron waiting times in this case is well-approximated by the Wigner-Dyson distribution

$$W_{WD}(\tau) = \frac{32\tau^2}{\pi^2 \bar{\tau}^3} e^{-4\tau^2/\pi \bar{\tau}^2},$$
 (2.1)

with the mean waiting time

$$\bar{\tau} = \frac{h}{eV},\tag{2.2}$$

determined by the applied voltage V. If subsequent waiting times are uncorrelated, the joint WTD in Fig. 2.1 should factorise as $W(\tau_1, \tau_2) = W_{\rm WD}(\tau_1)W_{\rm WD}(\tau_2)$. Such a factorisation is referred to as a renewal property [Cox, 1962]. However, as we find, the joint WTD in Fig. 2.1 cannot be written in this simple form. This demonstrates that subsequent electron waiting times are correlated. In fact, based on the analogy between WTDs and level spacing statistics exploited by Albert et al. [2012]; Haack et al. [2014], the joint WTD is expected to take the form [Herman et al., 2007]

$$W_{WD}(\tau_1, \tau_2) = \frac{4b^4}{\pi\sqrt{3}\bar{\tau}^6} \tau_1^2 \tau_2^2 (\tau_1 + \tau_2)^2 e^{-\frac{2b}{3\bar{\tau}^2} (\tau_1^2 + \tau_2^2 + \tau_1 \tau_2)}, \tag{2.3}$$

with $b = 729/(128\pi)$. Figure 2.1 shows that our results are well-approximated by this generalised Wigner-Dyson distribution, which cannot be factorised into products of the WTD in Eq. (2.1).

Our method for calculating joint WTDs further exploits the relation between WTDs and the idle time probability (ITP) [Albert et al., 2012; Thomas and Flindt, 2013; Dasenbrook et al., 2014]. We saw that for stationary processes, the WTD can be expressed as

2. Correlations between electron waiting times

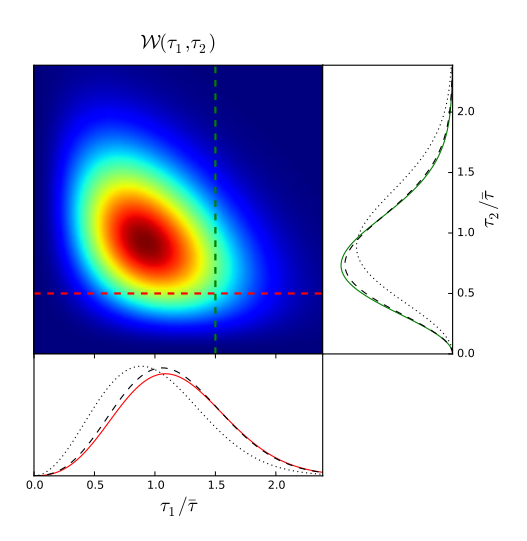


Figure 2.1.: Joint WTD for a fully open conduction channel. The two side panels show the joint WTD along the cuts indicated with coloured dashed lines in the main panel. The joint WTD is well-captured by the generalised Wigner-Dyson distribution (dashed lines) in Eq. (2.3). The dotted lines in the side panels show the waiting time distributions if there were no correlations between subsequent waiting times. Exact results have been obtained using Eq. (2.29). ([Dasenbrook et al., 2015], (C) 2015 American Physical Society.)

the second derivative of the ITP with respect to τ . Each derivative corresponds to the detection of an electron. Building on this principle, we obtain WTDs for detections in different channels and joint distributions of successive electron waiting times.

To illustrate our formalism, we consider a chiral setup where two incoming conduction channels are partitioned on a quantum point contact (QPC), Fig. 2.2. One or both inputs may be voltage biased, either by a static voltage or with a series of Lorentzian-shaped voltage pulses [Levitov et al., 1996; Ivanov et al., 1997; Keeling et al., 2006] as recently realised experimentally [Dubois et al., 2013b; Jullien et al., 2014]. We calculate the joint WTD and discuss correlations between electron waiting times together with WTDs for detections in different channels. Our findings generalise the results presented in chapter 1 and provide insights into the correlations between subsequent electron waiting times in phase-coherent conductors.

2.1.1. Two-time ITP

For the purpose of this chapter, it is useful to adopt a slightly different notion of the idle time probability, in that it depends on the starting and ending time of the measurement interval (instead of the starting time and the duration as in chapter 1). Thus, $\Pi(t^s, t^e)$ is the probability of observing no transmitted electrons in the time interval $[t^s, t^e]$ at a point x_0 after the scatterer. The operator that counts the number of particles, Eq. (B.13), now

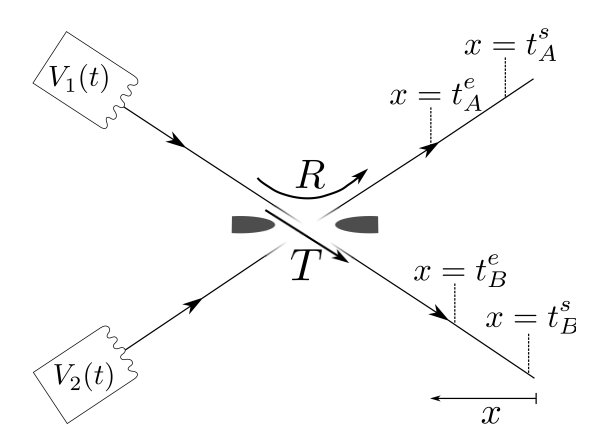


Figure 2.2.: Chiral setup with electrons in two incoming channels being partitioned on a QPC. A (time-dependent) voltage can be applied to the contacts of the incoming channels. The QPC has transmission T and reflection R. The transmitted and reflected electrons are detected in the outgoing channels at different positions $x = t_{A/B}^{s/e}$ with $v_F = 1$. ([Dasenbrook et al., 2015], (C) 2015 American Physical Society.)

becomes

$$\widehat{Q} = \int_{v_F t^s}^{v_F t^e} \widehat{b}^{\dagger}(x)\widehat{b}(x)dx, \tag{2.4}$$

where $\hat{b}^{\dagger}(x)$ and $\hat{b}(x)$ are the creation and annihilation operators of electrons at position x. To keep the notation simple, we have omitted the explicit time arguments of \hat{Q} . We will later on make use of the relations

$$\partial_{t^s} \widehat{Q} = -\hat{b}^{\dagger}(t^s) \hat{b}(t^s),
\partial_{t^e} \widehat{Q} = \hat{b}^{\dagger}(t^e) \hat{b}(t^e),$$
(2.5)

setting $v_F = 1$ throughout the rest of this chapter.

As before, the ITP can be expressed as the expectation value of the normal-ordered exponential of $-\hat{Q}$,

$$\Pi(t^s, t^e) = \left\langle : e^{-\widehat{Q}} : \right\rangle, \tag{2.6}$$

where the expectation value is taken with respect to the many-body state at t=0. To obtain a unidirectional process, we once again limit our analysis to particles in the transport window above the Fermi energy. We note that any time evolution of the many-body state from t=0 to $t=t^o$ can be absorbed into a shift of the spatial interval $(v_F=1)$ from $[t^s,t^e]$ to $[t^s+t^o,t^e+t^o]$. With this in mind, we always evaluate the expectation value at t=0 and treat time-dependent systems by shifting the integration interval in the definition of \hat{Q} in Eq. (2.4).

In general, the ITP is a two-time quantity depending both on t^s and t^e . However, for

2. Correlations between electron waiting times

stationary processes it depends only on the time difference $\tau = t^e - t^s$ such that

$$\Pi(t^s, t^e) = \Pi(t^e - t^s) = \Pi(\tau),$$
(2.7)

just as for the WTD.

2.1.2. First passage time distribution

To illustrate the correspondence between derivatives of the ITP and detection events, we first show how one can obtain the first passage time distribution $\mathcal{F}(t^s, t^e)$ from the ITP. The first passage time distribution is the probability density for the first detection of a particle to occur at the time t^e , given that observations were started at the earlier time t^s . Such a distribution has recently been evaluated for electron transport through a quantum dot, with t^s being the time at which the external electronic reservoirs are connected to the quantum dot [Tang et al., 2014]. To obtain the first passage time distribution from the ITP, we notice that the ITP may be expressed as

$$\Pi(t^s, t^e) = 1 - \int_{t^s}^{t^e} \mathcal{F}(t^s, t) dt.$$
 (2.8)

Here, the integral equals the probability that at least one electron is observed in the interval $[t^s, t^e]$. Now, by differentiating the ITP with respect to t^e , we obtain

$$\mathcal{F}(t^s, t^e) = -\partial_{t^e} \Pi(t^s, t^e). \tag{2.9}$$

Furthermore, using Eqs. (2.5) and (2.6) we find

$$\mathcal{F}(t^s, t^e) = \left\langle \hat{b}^{\dagger}(t^e) : e^{-\widehat{Q}} : \hat{b}(t^e) \right\rangle. \tag{2.10}$$

Equation (2.10) is very similar to Eq. (2.6), however, the expectation value of the normal-ordered exponential is taken with respect to the many-body state with a particle removed at time t^e . This removal constitutes the detection event in the definition of the first passage time distribution.

A related quantity is the probability density $\overline{\mathcal{F}}(t^s, t^e)$ for detecting a particle at t^s with no subsequent detections until the time t^e . Following the line of arguments above, we readily find

$$\overline{\mathcal{F}}(t^s, t^e) = \partial_{t^s} \Pi(t^s, t^e) \tag{2.11}$$

and

$$\overline{\mathcal{F}}(t^s, t^e) = \left\langle \hat{b}^{\dagger}(t^s) : e^{-\widehat{Q}} : \hat{b}(t^s) \right\rangle. \tag{2.12}$$

We see that the expectation value of the normal-ordered exponential is now taken with respect to the many-body state with a particle removed at the initial time t^s . For stationary problems, the first passage time only depends on the time difference $\tau \equiv t^e - t^s$ and we have

$$\mathcal{F}(\tau) = \overline{\mathcal{F}}(\tau) = -\partial_{\tau}\Pi(\tau),$$
 (2.13)

as a direct consequence of Eq. (2.7).

The derivations of Eqs. (2.9,2.10,2.11,2.12) illustrate an important principle that we will use in the following: By differentiating the ITP with respect to its time arguments, pairs of operators are pulled down from the exponential function corresponding to detection events at the beginning or at the end of the interval $[t^s, t^e]$.

2.1.3. Two-time WTD

We next apply our redefinition of the two-time ITP to the WTD. We define the WTD to be the conditional probability density of detecting a particle at a time t^e given that the last detection occurred at the earlier time t^s . The joint probability density of detecting a particle both at t^s and t^e with no detection events in between is equal to the WTD multiplied by the probability density of a detection at t^s . The joint probability density can be obtained by differentiating the ITP with respect to both the initial time t^s and the final time t^s . Moreover, for uni-directional charge transport, the probability density of a detection at t^s is simply the average particle current $I(t^s)$ at time t^s . We then find

$$I(t^s)\mathcal{W}(t^s, t^e) = -\partial_{t^e}\partial_{t^s}\Pi(t^s, t^e), \tag{2.14}$$

where the minus sign comes together with the partial derivative with respect to t^e , c.f. Eq. (2.9). Using Eq. (2.6) we now arrive at the second quantized expression

$$I(t^s)\mathcal{W}(t^s, t^e) = \left\langle \hat{b}^{\dagger}(t^e)\hat{b}^{\dagger}(t^s) : e^{-\hat{Q}} : \hat{b}(t^s)\hat{b}(t^e) \right\rangle. \tag{2.15}$$

For stationary processes, the average particle current equals the inverse mean waiting time, $I(t^s) = 1/\langle \tau \rangle$. Combining Eqs. (2.7) and (2.14), we then arrive at Eq. (1.1). For conductors driven with period \mathcal{T} , we define a one-time ITP by averaging over all possible starting times t^s , keeping the interval $\tau \equiv t^e - t^s$ fixed, as in Eq. (1.2). This yields the relevant ITP if the observation starts at a random time. Employing Eqs. (2.13), (1.1), we obtain one-time distributions which are independent of the detection time of the first electron. For the first passage time distribution, we find

$$\mathcal{F}(\tau) = \frac{1}{\mathcal{T}} \int_0^{\mathcal{T}} \mathcal{F}(t^s, t^s + \tau) dt^s$$

$$= \frac{1}{\mathcal{T}} \int_0^{\mathcal{T}} \overline{\mathcal{F}}(t^s, t^s + \tau) dt^s,$$
(2.16)

and for the WTD

$$W(\tau) = \frac{\langle \tau \rangle}{\mathcal{T}} \int_0^{\mathcal{T}} I(t^s) W(t^s, t^s + \tau) dt^s.$$
 (2.17)

Figure 2.3 shows the ITP, the first passage time distribution, and the WTD for a static voltage as well as for a train of voltage pulses. Interestingly, the two ITPs are nearly indistinguishable despite the very different voltages applied to contact 1. In both cases, the ITP decays monotonously with time from $\Pi(0) = 1$ at $\tau = 0$. Turning next to the first passage time distribution, some structure starts to be visible and the two

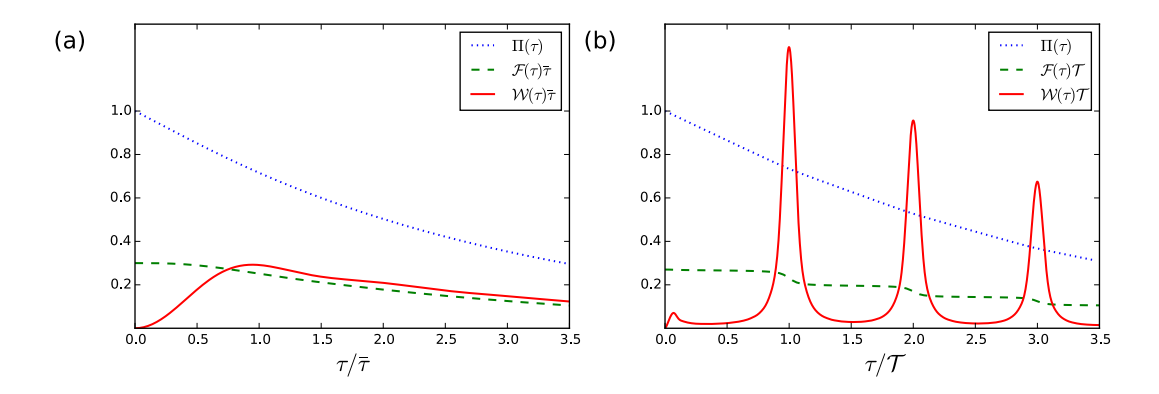


Figure 2.3.: Idle time probability (ITP), first passage time distribution, and waiting time distribution (WTD). (a) Results for a static voltage applied to contact 1, $V_1(t) = V$, and no voltage applied to contact 2, $V_2(t) = 0$. The QPC is tuned to T = 0.3. We consider the electrons that are transmitted into outgoing channel B. The time is given in units of $\bar{\tau} = h/(eV)$. (b) Results for a series of Lorentzian-shaped voltage pulses of unit charge applied to contact 1, see Eq. (A.1). The width of the pulses is $\Gamma = 0.02\mathcal{T}$. The time is given in units of the period of the pulses \mathcal{T} . ([Dasenbrook et al., 2015], (C) 2015 American Physical Society.)

voltage cases can now be distinguished. Finally, considering the WTDs, we see how they clearly differentiate between the two voltages. For the static voltage, the electronic wave packets are strongly overlapping and the WTD is rather structureless. By contrast, the application of Lorentzian-shaped voltage pulses leads to the emission of well-localised electron wave packets with a small overlap, giving raise to clear peaks at multiples of the period of the driving \mathcal{T} . For a fully transmitting QPC (T=1), the WTD essentially consists of a single peak around $\tau \simeq \mathcal{T}$ (see the results of chapter 1). For a QPC with a finite transmission, as in Fig. 2.3, levitons may reflect back on the QPC, giving rise to the series of peaks in the WTD. We note that the period and the width of the Lorentzian-shaped pulses, which determine the overall structure of the WTD, are easily tunable in an experiment.

2.2. Generalized idle time probability

We now generalise the concepts from the last section to an arbitrary number of channels and to an arbitrary number of successive waiting times. To this end, we introduce a generalised ITP from which we obtain the joint WTDs as well as other distributions. In the following section we illustrate our formalism with specific examples.

We consider a scatterer which is connected to N_i incoming and N_o outgoing channels. The generalised ITP is the probability that no particles are detected in any of the outgoing channels during the channel-dependent time-intervals $[t_{\alpha}^s, t_{\alpha}^e]$ (Fig. 2.2). The generalised ITP reads

$$\Pi(t_1^s, t_1^e; \dots; t_{N_o}^s, t_{N_o}^e) = \left\langle : e^{-\sum_{\alpha=1}^{N_o} \widehat{Q}_{\alpha}} : \right\rangle, \tag{2.18}$$

having defined projectors for each channel

$$\widehat{Q}_{\alpha} = \int_{t_{\alpha}^{e}}^{t_{\alpha}^{e}} \widehat{b}_{\alpha}^{\dagger}(x)\widehat{b}_{\alpha}(x)dx. \tag{2.19}$$

The evaluation of the generalised ITP is analogous to the evaluation of the single-channel ITP, and discussed in Appendix C. The introduction of individual starting and ending times for each channel allows us to compute a variety of WTDs. In each channel, the idle time interval $[t_{\alpha}^s, t_{\alpha}^e]$ can be modified and detection events can be inserted by differentiation with respect to the time arguments. The single-channel ITP can always be recovered by letting the length of the intervals in all other channels go to zero

$$\Pi(t_{\alpha}^{s}, t_{\alpha}^{e}) = \Pi(t_{\alpha}^{s}, t_{\alpha}^{e}; \{t_{i \neq \alpha}^{s} = t_{i \neq \alpha}^{e}\}), \tag{2.20}$$

where the curly brackets imply $\forall i$. The operators \widehat{Q}_{α} in Eq. (2.19) count the number of particles in the spatial intervals $[t^s_{\alpha}, t^e_{\alpha}]$. For this reason, the generalised ITP is closely related to the joint particle number statistics in spatial sub-regions [Shelankov and Rammer, 2003; Rammer and Shelankov, 2012].

2.2.1. Multiple channels

For the sake of simplicity, we consider only two outgoing channels labelled as A and B. The generalisation to more channels is straightforward. With two outgoing channels, the ITP has four time arguments $\Pi(t_A^s, t_A^e; t_B^s, t_B^e)$. We consider two different types of WTDs: The two-channel WTD is the distribution of waiting times between detections in either of the two channels. The cross-channel WTD is the distribution of waiting times between a detection in one channel and the next detection in the other channel. These WTDs generally have two time arguments but become one-time quantities for driven systems by averaging over a period following Eq. (2.17).

We first discuss the two-channel WTD. This is the conditional probability density of detecting an electron at time t^e in either channel, given that the last prior detection happened at the earlier time t^s in any of the two channels. This WTD follows from the generalised ITP by differentiation with respect to the time arguments

$$I(t^s)\mathcal{W}_{AB}(t^s, t^e) = -\partial_{t^s}\partial_{t^e}\Pi(t^s, t^e; t^s, t^e), \tag{2.21}$$

where we have set $t^s = t_A^s = t_B^s$ and $t^e = t_A^e = t_B^e$, since we do not differentiate between the two channels, and $I = I_A + I_B$ is the sum of the particle currents in each channel. If the two channels are uncorrelated, the ITP factorises as [Haack et al., 2014]

$$\Pi^{uc}(t_A^s, t_A^e; t_B^s, t_B^e) = \Pi_A(t_A^s, t_A^e) \Pi_B(t_B^s, t_B^e), \tag{2.22}$$

2. Correlations between electron waiting times

where Π_{α} is the ITP in channel α and the superscript uc stands for uncorrelated. In this case, the two-channel WTD takes on a particularly illuminating form

$$I(t^{s})\mathcal{W}_{AB}^{uc}(t^{s}, t^{e}) = I_{A}(t^{s})\mathcal{W}_{A}(t^{s}, t^{e})\Pi_{B}(t^{s}, t^{e}) + \mathcal{F}_{B}(t^{s}, t^{e})\bar{\mathcal{F}}_{A}(t^{s}, t^{e}) + A \leftrightarrow B.$$
(2.23)

The first term represents contributions where both detections happen in channel A, while no detections occur in channel B. The second term corresponds to contributions where the first detection happens in channel A at time t^s and the next detection occurs in channel B at time t^e . Finally, the term $A \leftrightarrow B$ indicates that the roles of the two channels can be interchanged.

In contrast to the single-channel WTD, the Pauli principle does not force the twochannel WTD to vanish at short times (detections in the two channels can occur simultaneously). Evaluating Eq. (2.21) at $t^s = t^e$, we find

$$\mathcal{W}_{AB}(t^s, t^s) = 2 \frac{\langle \hat{I}_A(t^s) \hat{I}_B(t^s) \rangle}{I(t^s)}, \tag{2.24}$$

showing that the two-channel WTD at $t^s = t^e$ is (twice) the coincidence rate in the two channels divided by the total particle current at t^s . The factor of two accounts for the fact that either of the two detections can be interpreted as being the first one. For two uncorrelated channels, the expectation value factorises and we find

$$W_{AB}^{uc}(t^s, t^s) = 2\frac{I_A(t^s)I_B(t^s)}{I(t^s)},$$
(2.25)

where I_{α} is the average particle current in channel α .

Next we discuss the cross-channel WTD. This is the conditional probability density of waiting until t^e for the first detection in channel B to happen after a detection has occurred in channel A at the earlier time t^s . We note that additional detections may occur in channel A after the time t^s . The cross-channel WTD follows from the ITP as

$$I_A(t^s)\mathcal{W}_{A\to B}(t^s, t^e) = -\left.\partial_{t_A^s}\partial_{t^e}\Pi(t_A^s, t^s; t^s, t^e)\right|_{t_A^s = t^s}$$

$$= \left\langle \hat{b}_A^{\dagger}(t^s)\hat{b}_B^{\dagger}(t^e) : e^{-\hat{Q}_B} : \hat{b}_B(t^e)\hat{b}_A(t^s) \right\rangle.$$
(2.26)

We set $t_A^s = t_A^e = t^s$ after taking the derivatives since additional detections in channel A may occur following the first detection. For two uncorrelated channels, we recover the first passage time distribution in channel B since the detection in channel A only defines t^s without influencing channel B

$$\mathcal{W}_{A\to B}^{uc}(t^s, t^e) = \mathcal{F}_B(t^s, t^e). \tag{2.27}$$

For $t^s = t^e$, we again obtain the coincidence rate in the two channels. However, this time without the factor of two since the event in channel A by definition is the first one

$$\mathcal{W}_{A\to B}(t^s, t^s) = \frac{\langle \hat{I}_A(t^s)\hat{I}_B(t^s)\rangle}{I_A(t^s)}.$$
 (2.28)

For uncorrelated channels this expression reduces to $I_B(t^s)$ in accordance with Eq. (2.27). In the following section, we evaluate the two WTDs and show how waiting times may be correlated.

2.2.2. Multiple times

We are now in position to formulate our theory of joint WTDs. The joint distribution of n waiting times is the conditional probability to find a given sequence of n waiting times. As we will see, the joint WTD can be obtained from the multi-channel ITP defined in Eq. (2.18) by introducing auxiliary channels. For the sake of brevity, we consider the case of just two successive waiting times in a single channel. The extension to several channels or waiting times is straightforward.

To find the joint WTD, we consider the two-channel ITP $\Pi(t_{\alpha}^s, t_{\alpha}^e; t_{\beta}^s, t_{\beta}^e)$, where β denotes an auxiliary channel. Eventually, we set $t_{\beta}^s = t_{\beta}^e = t^m$ and $\alpha = \beta$ and skip the channel index. Specifically, we express the joint WTD as

$$I(t^{s})\mathcal{W}(t^{s}, t^{m}, t^{e}) = \partial_{t_{\alpha}^{s}} \partial_{t_{\alpha}^{e}} \partial_{t_{\beta}^{e}} \Pi(t_{\alpha}^{s}, t_{\alpha}^{e}; t_{\beta}^{s}, t_{\beta}^{e}) \Big|_{t_{\beta}^{s} = t_{\beta}^{e} = t^{m}}$$

$$= \left\langle \hat{b}^{\dagger}(t^{s})\hat{b}^{\dagger}(t^{m})\hat{b}^{\dagger}(t^{e}) : e^{-\hat{Q}} : \hat{b}(t^{e})\hat{b}(t^{m})\hat{b}(t^{s}) \right\rangle,$$

$$(2.29)$$

where the operator \widehat{Q} is given in Eq. (2.4). Using the auxiliary channel a detection event is inserted at time t^m between the starting t^s and the end time t^e of the interval $[t^s, t^e]$. In a similar way, additional detection events within the interval can be introduced. Equation (2.29) is a central result for the joint distribution of two successive electron waiting times in a single conduction channel. Based on this expression we calculated the joint WTD in Fig. 2.1 and we will make further use of it in the following section, where we illustrate our method with specific examples.

For a driven conductor, a two-time WTD is obtained by integrating over the period \mathcal{T} , cf. Eq. (2.17),

$$\mathcal{W}(au_1, au_2) = rac{\langle au
angle}{\mathcal{T}} \int_0^{\mathcal{T}} I(t^s) \mathcal{W}(t^s,t^s+ au_1,t^s+ au_1+ au_2) dt^s.$$

In addition, we recover the standard WTD by integrating over the time at which the last detection event occurred

$$\mathcal{W}(t^s, t^m) = \int_{t^m}^{\infty} dt^e \mathcal{W}(t^s, t^m, t^e). \tag{2.30}$$

As discussed in Sec. 1.4.1, the joint WTD appears in the expansion of the WTD for a QPC. Returning to the results in Fig. 2.1, the ITP reads

$$\Pi(t^s, t^e) = \left\langle : e^{-T\widehat{Q}_1} : \right\rangle = \left\langle : e^{(R-1)\widehat{Q}_1} : \right\rangle, \tag{2.31}$$

where \widehat{Q}_1 acts on the incoming channel 1. We can formally expand this expression in either T or R [Albert et al., 2012; Dasenbrook et al., 2014]. To zeroth order in T, the ITP is unity as no electrons are transmitted through the QPC. The n'th order term in the expansion yields the reduction of the ITP due to the probability that n particles were transmitted through the QPC. To zeroth order in R, the ITP equals the ITP for a fully

transmitting QPC. The n'th order term in the expansion in R equals the increase in the ITP due to the probability that n particles were reflected.

Here we perform an expansion in R, and by differentiating the ITP with respect to t^s and t^e we obtain

$$W(t^{s}, t^{e}) = T \sum_{n=0}^{\infty} R^{n} W^{(n)}(t^{s}, t^{e})$$
(2.32)

where

$$W^{(n)}(t^s, t^e) = \frac{1}{n!} \int_{t^s}^{t^e} dt^1 \cdots dt^n W_{\text{in}}(t^s, t^1, \cdots, t^n, t^e)$$
 (2.33)

is the WTD given than n reflections on the QPC have occurred and $W_{\rm in}(t^s,t^1,\cdots,t^n,t^e)$ is the joint WTD for n+2 detection events in the incoming channel 1. Each term in the expansion is the probability density for n particles to be reflected (corresponding to the prefactor R^n) followed by a transmission (corresponding to the prefactor T). We integrate over all possible times that the reflections can occur and the factor 1/n! corrects for multiple counting of reflections. We see that joint WTDs occur already in the expansion of the WTD for a QPC. By averaging over t^s and making a renewal assumption, we can recover the results from Sec. 1.4.1.

We now illustrate our formalism for joint WTDs using the setup in Fig. 2.2. First we consider the partitioning of electrons emitted from one source. In the second example we discuss an electronic analogue of the Hong-Ou-Mandel interferometer, where electrons from different input channels interfere on the QPC [Burkard et al., 2000; Ol'khovskaya et al., 2008; Giovannetti et al., 2006; Jonckheere et al., 2012; Bocquillon et al., 2013a].

2.3. Correlated waiting times

2.3.1. Single-source partitioning

We consider the setup in Fig. 2.2 with contact 2 grounded and contact 1 biased with a constant voltage or a train of Lorentzian-shaped voltage pulses. Figures 2.3 and 1.3 show single-channel WTDs for this setup. We now go on to calculate two-channel and joint WTDs.

The two-channel WTD is the distribution of waiting times between successive electrons irrespective of the channel in which they are detected. As the QPC merely distributes the incoming electrons into the two outgoing channels, we expect simply to recover the WTD of the incoming electrons from channel 1. Indeed, using our formalism we find from Eq. (2.21) that

$$I(t^{s})\mathcal{W}_{AB}(t^{s}, t^{e}) = -\partial_{t^{s}}\partial_{t^{e}} \left\langle : e^{-\widehat{Q}_{A} - \widehat{Q}_{B}} : \right\rangle$$
$$= -\partial_{t^{s}}\partial_{t^{e}} \left\langle : e^{-\widehat{Q}_{1}} : \right\rangle,$$
(2.34)

where the integrations in the \widehat{Q} operators run from t^s to t^e and $I(t^s)$ is the average current in channel 1. In addition, we have used the scattering matrix to relate \widehat{Q}_{α} to

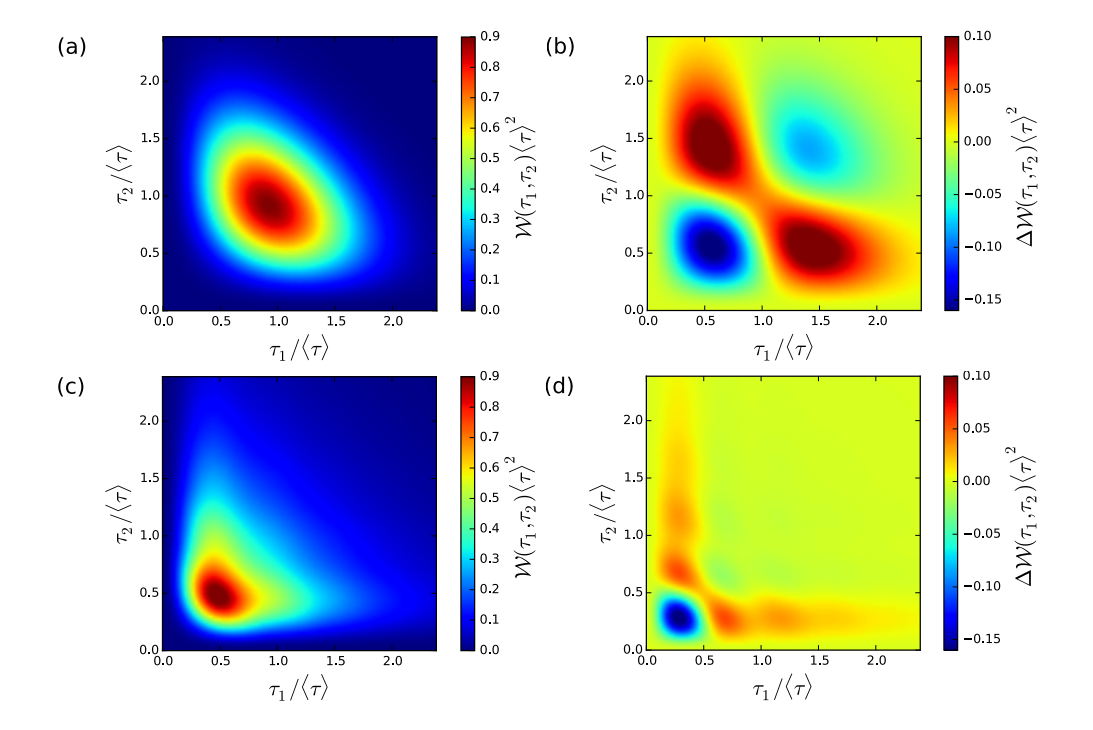


Figure 2.4.: Joint waiting time distributions for a static voltage. (a) Results for the voltage $V_1(t) = V$ applied to contact 1 and no voltage applied to contact 2, $V_2(t) = 0$. The QPC is fully transmitting T = 1 and we consider the electrons that are transmitted into outgoing channel B. The time is given in units of $\langle \tau \rangle = h/(TeV)$. (b) Difference $\Delta W(\tau_1, \tau_2) = W(\tau_1, \tau_2) - W(\tau_1)W(\tau_2)$ between exact results and results for uncorrelated waiting times. Positive correlations are indicated with red, while areas of negative correlations are blue. (c,d) Similar results for a half-transmitting QPC, T = 1/2. ([Dasenbrook et al., 2015], (C) 2015 American Physical Society.)

2. Correlations between electron waiting times

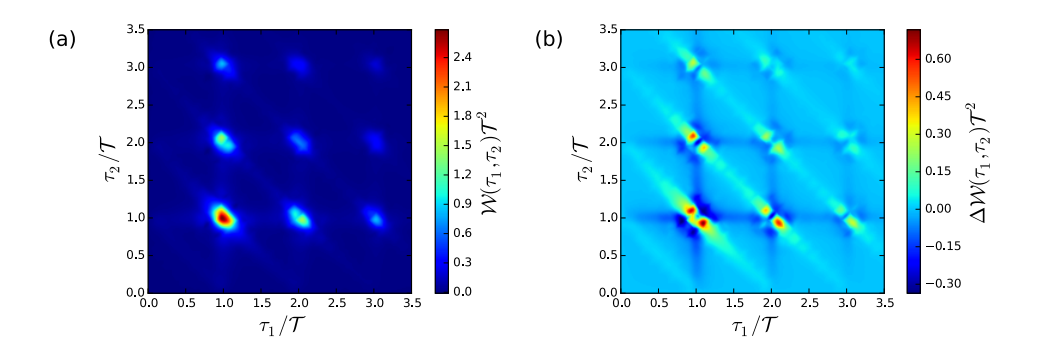


Figure 2.5.: Joint waiting time distribution for levitons. (a) Results for a series of Lorentzian-shaped voltage pulses of unit charge applied to contact 1. The width of the pulses is $\Gamma = 0.05\mathcal{T}$ and the QPC is tuned to T = 1/2. The time is given in units of the period of the pulses \mathcal{T} . (b) Difference $\Delta \mathcal{W}(\tau_1, \tau_2) = \mathcal{W}(\tau_1, \tau_2) - \mathcal{W}(\tau_1)\mathcal{W}(\tau_2)$ between exact results and results for uncorrelated waiting times. Positive correlations are indicated with red, while areas of negative correlations are blue. ([Dasenbrook et al., 2015], (C) 2015 American Physical Society.)

 \widehat{Q}_1 combined with the probability conservation condition T+R=1. For a constant voltage, the WTD was found to be well-approximated by a Wigner-Dyson distribution reflecting Fermi correlations between the incoming electrons. For a train of Lorentzian-shaped voltage pulses, the WTD was found to be peaked around the period of the driving with small satellite peaks due to the finite overlap of the voltage pulses. As we see here, the QPC has no effect on the WTD if we consider detections irrespective of the channel where they happen. This argument only applies if the QPC partitions electrons emitted by a single source. In that case, detections in the outgoing channels are not statistically independent, and the suppression of the WTD at $\tau=0$ remains.

Next, we consider the cross-channel WTD. This is the distribution of waiting times between a detection in one outgoing channel and the next detection in the other channel. Since the QPC just randomly partitions the incoming electrons into the outgoing channels, we expect the cross-channel WTD to equal the single-channel WTD. The cross-channel WTD is conditioned on the first detection happening in channel A, whereas the single-channel WTD is conditioned on the first detection happening in channel B. In either case, the reflection or transmission of the first particle does not influence the particles that traverse the QPC at a later time. Indeed, within our formalism we readily find, cf. Eq. (2.26),

$$\mathcal{W}_{A\to B}(t^s, t^e) = \mathcal{W}_B(t^s, t^e)
= \frac{RT}{I_A(t^s)} \left\langle \hat{a}_1^{\dagger}(t^s) \hat{a}_1^{\dagger}(t^e) : e^{-T\hat{Q}_1} : \hat{a}_1(t^e) \hat{a}_1(t^s) \right\rangle,$$
(2.35)

having used $I_A(t^s)/R = I_B(t^s)/T = I(t^s)$.

For the partitioning of electrons emitted from a single source, we see that the twochannel WTD and the cross-channel WTD do not provide additional information compared with the WTD itself. This is a direct consequence of the operator proportionality $\hat{Q}_A \propto \hat{Q}_B$ and it does not hold when both contacts emit electrons above the Fermi sea as we will see in the following example.

We now consider just one of the outgoing channels and calculate the joint probability distribution of finding two successive waiting times τ_1 and τ_2 using Eq. (2.29). For a constant voltage V, the joint WTD at full transmission is shown in Fig. 2.1. As mentioned in the introduction, the joint WTD is well-approximated by the generalised Wigner-Dyson distribution in Eq. (2.3). We find that the joint WTD is symmetric with respect to an exchange of the waiting times, $\tau_1 \leftrightarrow \tau_2$. This symmetry implies that the WTD does not change if we invert the spatial arguments of all the \hat{b} operators in Eq. (2.29). The symmetry in the WTD is thus a consequence of the spatial inversion symmetry of the many-body wave function.

In Fig. 2.4, we show joint WTDs both for full transmission and at half transmission. To highlight possible correlations, we also show the difference

$$\Delta \mathcal{W}(\tau_1, \tau_2) = \mathcal{W}(\tau_1, \tau_2) - \mathcal{W}(\tau_1) \mathcal{W}(\tau_2), \tag{2.36}$$

between the joint WTD and a factorised WTD corresponding to uncorrelated waiting times [Cox, 1962]. The figure clearly demonstrates that electron waiting times are correlated. The probability to observe a waiting time which is shorter (longer) than the mean waiting time $\langle \tau \rangle$ is reduced if the previous waiting time was already shorter (longer) than the mean waiting time. On the other hand, a short waiting time will likely be followed by a long waiting time and vice versa. This conclusion holds for both values of the transmission.

A similar analysis can be carried out for levitons emitted by a train of Lorentzianshaped voltage pulses. In Fig. 2.5 we show $W(\tau_1, \tau_2)$ and $\Delta W(\tau_1, \tau_2)$ for levitons incident on a QPC tuned to half transmission. Again, we observe a symmetry under the interchange of waiting times due to the spatial inversion symmetry of the fermionic manybody state. The joint WTD displays a lattice-like structure in contrast to the results for the dc-biased source in Fig. 2.4. This reflects the regular on-demand nature of the leviton source. Also here, the probability to observe two short or two long waiting times after each other is suppressed, while a short (long) waiting time is likely followed by a long (short) waiting time.

Due to the external driving, the sum of two subsequent waiting times is likely to equal a multiple of the period. If a particular waiting time is shorter than the average waiting time, this will not affect the absolute emission time of the next electron. Consequently, the next waiting time will most likely be longer. Thus, a strong regularity in the absolute electron emission times leads to strong dependencies of the waiting times on each other. For the case that the voltage pulses overlap more and more until the limit of a constant voltage is reached, the regularity in the emission times is provided by the Pauli principle. Moreover, this effect is independent of the QPC transmission. In the low transmission regime however (not shown), electron emission becomes increasingly rare and transport

resembles a Poisson process [Albert et al., 2012]. Correlations between waiting times will then eventually be negligible.

2.3.2. Hong-Ou-Mandel interferometry

As a second application, we consider the electronic analogue of the Hong-Ou-Mandel experiment developed in quantum optics [Burkard et al., 2000; Ol'khovskaya et al., 2008; Giovannetti et al., 2006; Jonckheere et al., 2012; Bocquillon et al., 2013a]. In this case, a driven on-demand source in each incoming channel emits single electrons onto the QPC in Fig. 2.2 with a possible time delay $\Delta \tau$ between the emissions from the two sources. Such experiments have recently been realised with two mesoscopic capacitors [Bocquillon et al., 2013a] and two leviton sources [Dubois et al., 2013a]. Here we treat the periodic emission of levitons onto the QPC.

Figure 2.6a shows the distribution of waiting times between detection events in either of the two outgoing channels. With zero time delay, incoming levitons anti-bunch on the QPC and there is a large probability of detecting the two outgoing levitons nearly simultaneously. The peak in the WTD around the period \mathcal{T} corresponds to the waiting time between the last leviton in one cycle and the first one in the next cycle. Since the probability of measuring the waiting time between two levitons within one cycle is equal to the probability of measuring the waiting time between levitons in different cycles, the areas underneath the two peaks are the same.

In general, for a given time delay $\Delta \tau$, we find peaks in the WTD at $\Delta \tau$ and at $\mathcal{T} - \Delta \tau$, corresponding to the waiting times between levitons within the same cycle and the waiting between levitons in different cycles. In the special case $\Delta \tau = \mathcal{T}/2$, the two peaks merge into one, except for a small remaining feature at $\tau = \mathcal{T}$. This feature is related to the satellite peak seen in the WTD for levitons in a single channel with perfect transmission. The WTD decays strongly for waiting times beyond the period, since all levitons will be detected independently of the QPC. This reflects the high reliability of the leviton sources which emit exactly one electron per cycle. This example demonstrates how the two-channel WTD provides information about the synchronisation of the two sources. Importantly, this detailed characterisation does not depend on the transmission of the QPC.

In Fig. 2.6b we turn to the distribution of waiting times between detections in different channels. This distribution is rather similar to the WTD for a single channel, shown in the left inset for comparison. Unlike the single-channel WTD, the cross-channel WTD is not suppressed to zero at $\tau = 0$, since detections can occur simultaneously in the two channels. For finite delay times between the two sources, the particles can go into the same outgoing channel, and both WTDs show a peaked structure even for waiting times larger than the period.

Due to the Pauli principle, two levitons arriving simultaneously at the QPC will go into different outgoing channels with unit probability, independently of the transmission. Thus, for zero time delay all results are independent of the QPC transmission T and reduce to the results for full transmission. As the time delay between the two sources is increased, the overlap between levitons arriving at the QPC decreases, and simultaneous

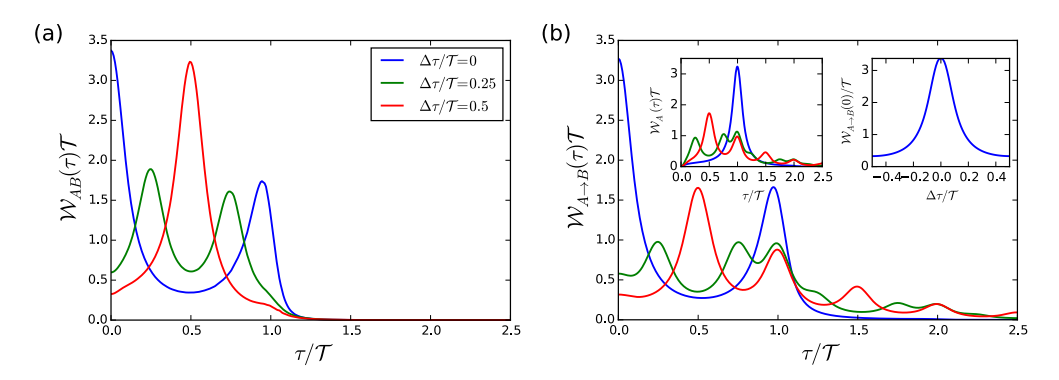


Figure 2.6.: Distributions of waiting times for a Hong-Ou-Mandel experiment with levitons. Two sources emit levitons of pulse width $\Gamma=0.05\mathcal{T}$ toward a QPC with transmission T=1/2. The tunable time delay between the sources is denoted as $\Delta\tau$. (a) WTD for waiting times between events occurring in either of the two outgoing channels for different values of the time delay. (b) WTD for waiting times between detection events in different channels. The left inset shows the WTD for just a single channel. The right inset shows the WTD at $\tau=0$ as a function of the time delay $\Delta\tau$ between the sources. ([Dasenbrook et al., 2015], (C) 2015 American Physical Society.)

detections in the outgoing channels become increasingly rare. For $\Delta \tau = \mathcal{T}/4$, the cross-channel WTD essentially shows four peaks within the first period. The peak at $\tau = 0$ is a relic of the fermionic anti-bunching due to the finite overlap of the pulses. The peaks at $\Delta \tau$ and at $\mathcal{T} - \Delta \tau$ are caused by two successive particles entering opposite arms of the interferometer, while the peak at \mathcal{T} corresponds to two successive particles entering the same arm and the next particle entering the opposite arm. For the maximal detuning $\Delta \tau = \mathcal{T}/2$, the WTD resembles that of just a single channel.

Due to the Pauli principle the cross-channel WTD of a single source is suppressed for zero waiting times. By contrast, with two sources we observe a local maximum due to the anti-bunching of electrons that arrive simultaneously at the QPC. The right inset of Fig. 2.6b shows the cross-channel WTD at $\tau=0$ as a function of the time delay, with a maximum for zero time delay in analogy with the Hong-Ou-Mandel peak found in the zero-frequency current cross-correlations [Jonckheere et al., 2012; Bocquillon et al., 2013a].

We see that the two-channel and cross-channel WTDs contain different information about the emission processes. The two-channel WTD mostly contains information about the sources alone, in particular their synchronisation. The cross-channel WTD contains additional information about the QPC and shows more prominent signatures of fermionic anti-bunching.

2.4. Conclusions

In this chapter, we have developed a general framework for calculating joint WTDs in electronic multi-channel conductors. The central building block of our formalism is the generalised idle time probability, i. e. the joint probability for no detections to occur in the outgoing channels. By calculating the joint WTD for a single conduction channel, we have explicitly demonstrated that the electron waiting times in coherent conductors are correlated due to the fermionic statistics encoded in the many-body state.

Drawing on the analogy between random matrices and free fermions, we have shown that the joint WTD for a fully transmitting conduction channel is well-approximated by a generalised Wigner-Dyson distribution. In contrast to a renewal process with uncorrelated waiting times, we find that the probability of observing a long (short) waiting time following a short (long) waiting time is increased, while finding two long or two short waiting times in succession is less likely. This holds both for electrons coming from a dc-biased contact and for levitons emitted on top of the Fermi sea by applying Lorentzian-shaped voltage pulses to the contact.

Correlations between electrons in different outgoing channels also show up in the distributions of waiting times between detections in different channels. We have defined multi-channel and cross-channel WTDs and illustrated these concepts for a QPC in a chiral setup where electrons are injected in either one or both incoming channels. In a fermionic Hong-Ou-Mandel experiment, where electrons interfere on the QPC, the two-channel WTD provides information about the synchronisation of the sources, while the cross-channel WTD shows signatures of the scatterer and the fermionic anti-bunching.

Our formalism as well as the results presented in chapter 1 rely on the ability to detect single electrons above the Fermi level. In the next chapter, we develop a quantum theory of a detector capable of measuring the idle time probability.

3. Electron waiting time clock

3.1. Introduction

In the preceding chapters of this thesis, we have seen how the distribution of electron waiting times can be a powerful tool to analyse short-time characteristics of quantum transport processes. Especially for dynamically driven single-electron emitters, the WTD turns out to be useful to characterise the uncertainty in the emission time and cyclemissing events. We have also presented a useful framework to calculate WTDs in noninteracting systems using the scattering approach to quantum transport.

While certainly useful, one might have doubts about some aspects of the formalism presented so far. The relation between the WTD and the ITP given in Eq. (1.1) assumes that the underlying statistical process can be described as a time series of discrete events. This assumption might not be justified in a mesoscopic conductor. Furthermore, the Fermi sea electrons should play a profound role in contributing to short-time and finite-frequency observables, and the WTD would certainly necessitate measurements on short time scales. The Fermi sea has so far simply been disregarded, and the focus was on a theory for an empty band consisting of just a beam of electrons without an underlying Fermi sea. It is interesting to investigate whether the theory is still applicable in the case of a "normal" conductor where a Fermi sea is present.

In some Coulomb-blockade structures, the tunneling of individual electrons can be monitored in real-time [Fujisawa et al., 2006; Gustavsson et al., 2006, 2009; Flindt et al., 2009; Ubbelohde et al., 2012; Maisi et al., 2014], and the electron waiting time is clearly defined as the time that passes between two subsequent detections of a tunneling event. By contrast, in mesoscopic conductors, where the electronic transport is phase-coherent, the concept of electron waiting times is more subtle. In particular, it is not immediately obvious what physical process constitutes a detection event. As such, a proper definition of the electron waiting time relies on a careful description of a specific detector. In the context of full counting statistics, a quantum theory of a detector was developed by Levitov et al. [1996].

The theory of electron waiting times in mesoscopic conductors presented above considers the electrons above the Fermi sea. For typical voltages in the micro-volt regime, the mean waiting time is on the order of nano-seconds. This is a feasible time-scale from an experimental point of view. By contrast, if electrons in the Fermi sea are included, the mean waiting time would be given by the inverse Fermi energy, implying that a measurement of the electron waiting time essentially would be out of reach. Moreover, for dynamic single-electron sources, one is interested in the waiting time between the emission of electrons above the Fermi surface rather than in the intrinsic fluctuations in the Fermi sea. For these reasons, theories of waiting times between electrons above the

3. Electron waiting time clock

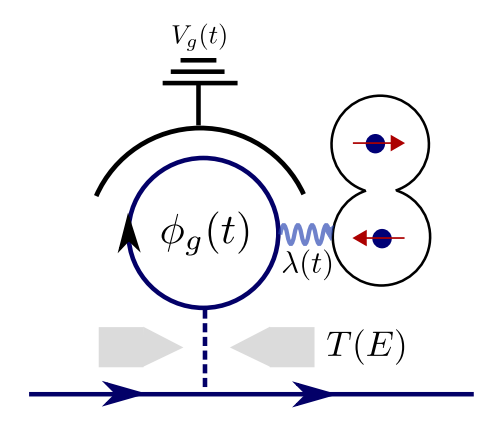


Figure 3.1.: Electron waiting time clock. The clock consists of a mesoscopic capacitor coupled via a quantum point contact to a chiral edge state. Due to the energy-dependent transmission T(E), only electrons above the Fermi level of the external reservoir can enter and leave the capacitor. Electrons inside the capacitor interact with a two-level system via the controllable coupling $\lambda(t)$. The top-gate potential $V_g(t)$ is used to empty the capacitor and leads to the time-dependent scattering phase $\phi_g(t)$. By monitoring the two-level system, the distribution of electron waiting times can be measured. This detector can be placed after the scatterer whose WTD is to be measured. ([Dasenbrook and Flindt, 2016b], (C) 2016 American Physical Society.)

Fermi sea are attractive.

It is well-known that measurements of zero-frequency quantities like the average current and the shot noise only concern the electrons above the Fermi level [Büttiker, 1990c; Blanter and Büttiker, 2000]. On the other hand, measurements of the finite-frequency noise (and other short-time measurements) with standard current detectors are generally also sensitive to the underlying Fermi sea [Gavish et al., 2001]. Bearing this in mind, it is clear that a theory of electron waiting times in mesoscopic conductors should include a description of a detector. This is the central goal of this chapter. Specifically, we devise a quantum theory of a waiting time clock that is capable of measuring the distribution of waiting times between electrons above the Fermi sea in a mesoscopic conductor. When operated under ideal conditions, our waiting time clock recovers the results of earlier theories without a detector. Within our theoretical description, we can also investigate possible deviations due to imperfect operating conditions.

The rest of this chapter is organized as follows. In Sec. 3.2 we discuss the scattering theory of full counting statistics (FCS) in mesoscopic conductors with a specific emphasis on the detector. In Sec. 3.3 we relate the idle time probability to the finite time FCS. In Sec. 3.4 we describe our electron waiting time clock and its building blocks as indicated in Fig. 3.1. In Sec. 3.5 we illustrate the use of the waiting time clock with two specific applications. A possible implementation of the measurement scheme is described in Sec. 3.6. Finally, in Sec. 3.8, we present our conclusions and give an outlook on future work.

3.2. Time-resolved counting statistics

We start by recapitulating the scattering theory of time-dependent FCS with a special emphasis on the detector. An absorptive electron detector has been investigated theoretically by Saito et al. [1992]. As an alternative, Levitov et al. [1996] later on considered a detector which conserves the number of electrons. In this approach, the detector consists of a quantum two-level system, such as a spin-1/2 particle, which rotates coherently in the magnetic field induced by the electrical current in the conductor. The moment generating function of the FCS can then be measured directly as a function of the coupling strength between the spin and the conductor.

To see this, we consider the combined system, including the detector, described by the Hamiltonian

$$\hat{H}(t) = \hat{H}_{el}(t) + \hat{H}_{int}(t) = \hat{H}_{el}(t) - \lambda(t) \frac{\hbar}{2e} \hat{\sigma}_z \hat{I}.$$
 (3.1)

The Hamiltonian of the conductor is denoted as $\hat{H}_{\rm el}(t)$, $\hat{\sigma}_z$ is the Pauli matrix for the z-component of the spin, and \hat{I} is the operator for the electrical current through a given cross-section of the conductor. The particular form of the coupling between the spin and the conductor makes the spin rotate in the x-y plane of the Bloch sphere due to the magnetic field induced by the electrical current. The coupling strength $\lambda(t)$ is assumed to be controllable and generally time-dependent. We evolve the combined system from $t=-\infty$ to $t=\infty$ and describe the finite duration of a measurement by having a coupling which is only non-zero during the measurement. (In a different approach [Muzykantskii and Adamov, 2003; Schönhammer, 2007], one detects the total charge in one of the leads at the beginning and at the end of the measurement and then defines the number of transferred charges as the difference between the two measurement outcomes.) After the complete time evolution, the electronic conductor is integrated out and the density matrix of the spin is obtained.

By evaluating the off-diagonal element of this reduced density matrix, one arrives at the function [Belzig and Nazarov, 2001; Nazarov and Kindermann, 2003; Beaud et al., 2013]

$$\chi(\lambda) = \left\langle T \left\{ e^{i \int_{-\infty}^{\infty} dt \hat{H}_{-\lambda}(t)/\hbar} \right\} \widetilde{T} \left\{ e^{-i \int_{-\infty}^{\infty} dt \hat{H}_{\lambda}(t)/\hbar} \right\} \right\rangle, \tag{3.2}$$

where T and \tilde{T} denote time and anti-time ordering, respectively. The Hamiltonian $\hat{H}_{\lambda}(t)$ is obtained from Eq. (3.1) by replacing $\hat{\sigma}_z$ by unity so that it only acts on the electronic degrees of freedom. The electronic conductor consists of a central scatterer connected to electronic leads and is described by $\hat{H}_{\rm el}(t)$. The electrons are non-interacting so that a scattering problem can be formulated in terms of a scattering matrix that we denote by \mathcal{S} . To include the coupling to the spin, we solve the scattering problem of the electrons interacting with the spin via the time-dependent coupling $\lambda(t)$ and denote the resulting scattering matrix by U_{λ} . Since both $\lambda(t)$ and $\hat{H}_{\rm el}(t)$ can be time-dependent, neither U_{λ} nor \mathcal{S} are necessarily diagonal in the energy representation. The combined scattering matrix is denoted as \mathcal{S}_{λ} and will be specified in more detail in the following sections.

Eq. (3.2) can be evaluated by means of the Keldysh technique [Kamenev, 2011]. Specif-

3. Electron waiting time clock

ically, it can be written as

$$\chi(\lambda) = \det\left(1 - n_F \left[1 - \mathcal{S}_{-\lambda}^{\dagger} \mathcal{S}_{\lambda}\right]\right), \tag{3.3}$$

which is known as the Levitov-Lesovik determinant formula. Here, n_F is the occupation matrix of the leads and the involved matrices have indices both in the channel and energy spaces.

For the special case of a single-channel chiral system, e. g. a quantum Hall edge state, there is no channel index. However, due to the general time-dependence of the problem, S_{λ} is not diagonal in the energy representation. At zero temperature, n_F is just a projector onto the filled states in the lead from which electrons enter the conductor. We can then write Eq. (3.3) as

$$\chi(\lambda) = \det\left(\mathcal{S}_{-\lambda}^{\dagger} \mathcal{S}_{\lambda}\right),\tag{3.4}$$

where the matrix elements of $\mathcal{S}_{-\lambda}^{\dagger}\mathcal{S}_{\lambda}$ have been restricted to the initially filled states.

We now specify the interaction between the electrons and the spin. Due to the spin, electrons pick up the additional scattering phase $\exp(i\lambda(t)/2)$. The scattering matrix U_{λ} therefore has the matrix elements

$$[U_{\lambda}]_{t,t'} = e^{i\lambda(t)/2}\delta(t-t') \tag{3.5}$$

in the time representation. We take an abrupt switching,

$$\lambda(t) = \lambda \Theta(t - t_0)\Theta(\tau - t + t_0), \tag{3.6}$$

where $\Theta(t)$ is the Heaviside step function, t_0 is the starting point of the measurement, τ is the duration, and λ is the coupling strength. In the energy representation, the matrix elements of U_{λ} then become

$$[U_{\lambda}]_{E,E'} = \delta(E - E') + K_{\tau}^{\lambda}(E - E'),$$
 (3.7)

having defined

$$K_{\tau}^{\lambda}(E) = \left(e^{i\lambda/2} - 1\right) K_{\tau}(E) \tag{3.8}$$

in terms of the sine kernel given in Eq. (1.14).

If the reservoirs at $t = t_0$ are not in a superposition of different number eigenstates, Eq. (3.3) can be interpreted as the moment generating function of the FCS [Shelankov and Rammer, 2003]. Specifically, from the inverse Fourier transformation

$$P(n) = \frac{1}{2\pi} \int_0^{2\pi} \chi(\lambda) e^{in\lambda} d\lambda, \qquad (3.9)$$

we obtain the probability P(n) that n charges have passed through the conductor while the detector was on. We note that backaction effects due to the measurement device are fully included in this formalism.

It is instructive to consider the limit of long measurement times. In this case, we can take $\lambda(t) \equiv \lambda$ to be constant in Eq. (3.6), such that U_{λ} becomes diagonal in the energy representation. If, furthermore, the Hamiltonian $\hat{H}_{el}(t) = \hat{H}_{el}$ is not time-dependent, the determinant over energies in Eq. (3.3) reduces to a product,

$$\chi(\lambda) = \prod_{E>0} \det \left(1 - [n_F]_{E,E} \left\{ 1 - [S_{-\lambda}^{\dagger} S_{\lambda}]_{E,E} \right\} \right), \tag{3.10}$$

where the determinant is now taken only over the channel indices of the matrices. For a single-channel two-terminal conductor with the energy-dependent transmission probability T(E), contributions from left and right moving electrons below the Fermi level cancel each other at zero temperature and only electrons above the Fermi level need to be included,

$$\chi(\lambda) = \prod_{E_F < E < E_F + eV} \left[(e^{i\lambda} - 1)T(E) + 1 \right]. \tag{3.11}$$

This type of FCS is known as generalized binomial statistics [Hassler et al., 2008; Abanov and Ivanov, 2008, 2009]. The result shows us that observables measured over a long time, for instance the mean current or any zero-frequency current correlator, are only affected by the electrons in the voltage window $[E_F, E_F + eV]$ above the Fermi level. In the following we will see that finite-time measurements are more involved as they may also be influenced by electrons below the Fermi level.

3.3. Waiting time distributions

Building on the previous section, we are now ready to develop a quantum theory of an electron waiting time clock. We begin by establishing the general relationship of WTDs to short time electron counting statistics, before moving on to a detailed description of our detector

Given a series of detection events, the waiting time is the time that elapses between two successive detections. The distribution of waiting times is denoted as $W(\tau)$. For a stationary process, it can be related to the idle time probability $\Pi(\tau)$ as in Eq. (1.1). By contrast, for periodically driven systems, the idle time probability is a two-time quantity $\Pi(t_0,\tau)$ which explicitly depends on t_0 . The idle time probability entering Eq. (1.1) is then obtained as an average over the period of the driving \mathcal{T} as in Eq. (1.2).

The idle time probability can be expressed in terms of the time-dependent FCS as

$$\Pi(\tau) = P(n=0,\tau) \tag{3.12}$$

which is the n=0 component of the probability $P(n,\tau)$ to observe n detections during a time interval of length τ . Alternatively, the idle time probability can be expressed in terms of the moment generating function of the FCS

$$\chi(\lambda, \tau) = \sum_{n=0}^{\infty} P(n, \tau) e^{in\lambda}.$$
 (3.13)

Specifically, we get $P(n=0,\tau)$ by an inverse Fourier transformation as

$$P(n=0,\tau) = \frac{1}{2\pi} \int_0^{2\pi} \chi(\lambda,\tau) d\lambda, \tag{3.14}$$

or, since the number of detector clicks is non-negative, by formally taking the limit $\lambda \to i\infty$,

$$P(n=0,\tau) = \chi(\lambda \to i\infty, \tau). \tag{3.15}$$

Experimentally, one may measure the moment generating function $\chi(\lambda, \tau)$ for different values of the coupling strength λ and from those measurements evaluate the idle time probability using the Fourier transformation in Eq. (3.14). On the theory side, it will be useful rather to take the limit $\lambda \to i\infty$ according to Eq. (3.15). This also holds at finite temperatures, if the detector can only produce a non-negative number of clicks.

The considerations above rely on a detector that produces a series of clicks. Since single-electron detection remains challenging in mesoscopic conductors, we proceed here along a different route and instead develop a detector than can measure the idle time probability of electrons above the Fermi sea in a mesoscopic conductor. As we will see, this leads to a well-defined distribution of waiting times between subsequent electron transfers.

3.4. Electron waiting time clock

The electron waiting time clock is depicted in Fig. 3.1. It consists of a mesoscopic capacitor [Büttiker et al., 1993; Prêtre et al., 1996] coupled to a two-level quantum system, such as a spin-1/2 particle, in a similar spirit to the proposal to measure FCS by Levitov et al. [1996]. The coupling $\lambda(t)$ between the spin and the capacitor is controllable and time-dependent. We assume that the capacitor is initially depleted of electrons. As we will see, this setup makes it possible to measure the idle time probability and thus the WTD of electrons above the Fermi level in the incoming channel.

We start by constructing the scattering matrix of the electron waiting time clock. The capacitor is implemented with chiral edge states in the quantum Hall regime [Fève et al., 2007]. Incoming electrons in the edge state on the left may be transmitted into the capacitor via a QPC and make one or several round trips inside the capacitor before leaving via the outgoing edge state to the right. While being inside the capacitor, the electrons interact with the spin that we monitor. Importantly, as we discuss below, we use a QPC with a cut-off in the transmission close the the Fermi level.

The scattering matrix of the waiting time clock is obtained by summing up the amplitudes of all possible scattering processes. Formally, we can express it as

$$S_{\lambda} = \mathcal{P}_{R} - \mathcal{P}_{T} \left[S_{\lambda}^{(l)} \sum_{n=0}^{\infty} \left(\mathcal{P}_{R} S_{\lambda}^{(l)} \right)^{n} \right] \mathcal{P}_{T}, \tag{3.16}$$

where the first term describes processes where electrons are reflected on the QPC and never enter the capacitor. The second term describes processes where electrons enter the capacitor and complete n + 1 round trips (or loops) inside the capacitor before leaving via the outgoing edge state. We now specify each matrix in this expression.

We consider a QPC with an energy-dependent transmission T(E). In a strong magnetic field, the transmission takes the form [Büttiker, 1990a]

$$T(E) = \frac{1}{e^{\mathcal{B}(E_F - E)} + 1},\tag{3.17}$$

where the parameter \mathcal{B} can be controlled by the magnetic field. The QPC is tuned such that the transmission is cut off at the Fermi energy E_F . For a sharp cuf-off, only electrons above the Fermi level are allowed to enter and leave the capacitor. For a smooth cut-off, the measurement may be affected by electrons in the Fermi sea as we discuss in Sec. 3.5.3. The corresponding transmission and reflection matrices in Eq. (3.16) read

$$[\mathcal{P}_T]_{E,E'} = \sqrt{T(E)}\delta(E - E'),$$

$$[\mathcal{P}_R]_{E,E'} = \sqrt{1 - T(E)}\delta(E - E').$$
(3.18)

Next, we define the scattering matrix $\mathcal{S}_{\lambda}^{(l)}$ describing one round trip inside the capacitor. An electron inside the capacitor can make one or several round trips. For each completed loop, it picks up the scattering phase

$$[S_{\lambda}^{(l)}]_{t,t'} = e^{i(\phi_g(t) + \lambda(t)/2)} \delta(t - t' - \tau_0), \tag{3.19}$$

where $\tau_0 = \ell/v_F$ is the time it takes to complete one loop with ℓ being the circumference of the capacitor and v_F the Fermi velocity. The specific times when the electron enters and leaves the capacitor are denoted as t' and t, respectively. The phase $\phi_g(t)$ picked up during one loop due to the time-dependent gate-voltage $V_g(t)$ reads

$$\phi_g(t) = \frac{e}{\hbar} \int_{t-\tau_0}^t V_g(t') dt'. \tag{3.20}$$

As we will see below, it is convenient to apply a linearly rising gate voltage of the form

$$V_a(t) = \delta V_a(t/\tau_0 + 1/2),$$
 (3.21)

where δV_g is the increase of the voltage during one loop. In this case, the phase takes the simple form

$$\phi_g(t) = \frac{e\delta V_g}{\hbar}t. \tag{3.22}$$

Finally, the coupling to the spin $\lambda(t)$ is given by Eq. (3.6).

In the energy representation, the scattering matrix is non-diagonal with matrix elements reading

$$[S_{\lambda}^{(l)}]_{E,E'} = \left[\delta(E' - E' - e\delta V_g) + K_{\tau}^{\lambda}(E - E' - e\delta V_g)\right] \times e^{i(E' + e\delta V_g)\tau_0/\hbar}.$$
(3.23)

3. Electron waiting time clock

This is the probability amplitude for a particle with incoming energy E' to change its energy to E due to the interaction with the spin and the time-dependent voltage.

Having specified the various scattering matrices, we can construct the scattering matrix of the electron waiting time clock according to Eq. (3.16). Moreover, if an additional scatterer (whose WTD we wish to measure) with scattering matrix S_{sys} is placed before the waiting time clock, the full scattering matrix becomes

$$S_{\lambda}^{(\text{tot})} = S_{\lambda} S_{\text{sys}}. \tag{3.24}$$

In the following section, where we apply our method, we specify S_{sys} for two particular scatterers.

We start by considering the limit of a sharp cut-off in Eq. (3.17), where $\mathcal{B} \gg 1/E$ for all relevant energies. In this case, only electrons above the Fermi level are allowed to enter and leave the capacitor. Mathematically, the transmission and reflection matrices in Eq. (3.18) become projectors onto energies above and below the Fermi level which we denote as P_T and P_R , respectively. We can then evaluate the geometric series in Eq. (3.16) and write the scattering matrix as

$$S_{\lambda} = P_R - P_T S_{\lambda}^{(l)} P_T$$

$$- P_T S_{\lambda}^{(l)} P_R (1 - P_R S_{\lambda}^{(l)} P_R)^{-1} P_R S_{\lambda}^{(l)} P_T,$$
(3.25)

having used properties of the projectors. This expression has a clear physical interpretation as we now discuss.

The first term corresponds to electrons below the Fermi level which are reflected on the QPC and never enter the capacitor. The second term describes electrons above the Fermi level that enter the capacitor, interact with the spin and the time-dependent voltage, but stay above the Fermi level, so that they leave the capacitor after having completed just one loop. The third term describes electrons that complete more than one loop. Read from right to left, this term corresponds to processes, where an electron above the Fermi level enters the capacitor and is scattered below the Fermi level during the first loop as described by the matrix product $P_R S_{\lambda}^{(l)} P_T$. The electron then completes a number of loops (possibly none) below the Fermi level. This is described by the matrix inversion $(1 - P_R S_{\lambda}^{(l)} P_R)^{-1}$, which can be re-expanded as a geometric series. Finally, in one last loop, the electron is scattered back above the Fermi level and leaves the capacitor as described by the matrix product $P_T S_{\lambda}^{(l)} P_R$.

Ideally, the electron waiting time clock would be described by only the two first terms of the scattering matrix in Eq. (3.25). Electrons above the Fermi level then interact only once with the spin, while electrons below the Fermi level are filtered out. However, due to the time-dependence of the measurement procedure, the third term is generally present. To suppress processes where electrons complete several loops and interact with the spin more than once, we apply the top-gate voltage. With a sufficiently large voltage increase, we can ensure that essentially all electrons end up with an energy above the Fermi level after having completed the first loop, even if they may have lost energy by interacting with the spin. They will then leave the capacitor via the QPC after having interacted with the spin only once.

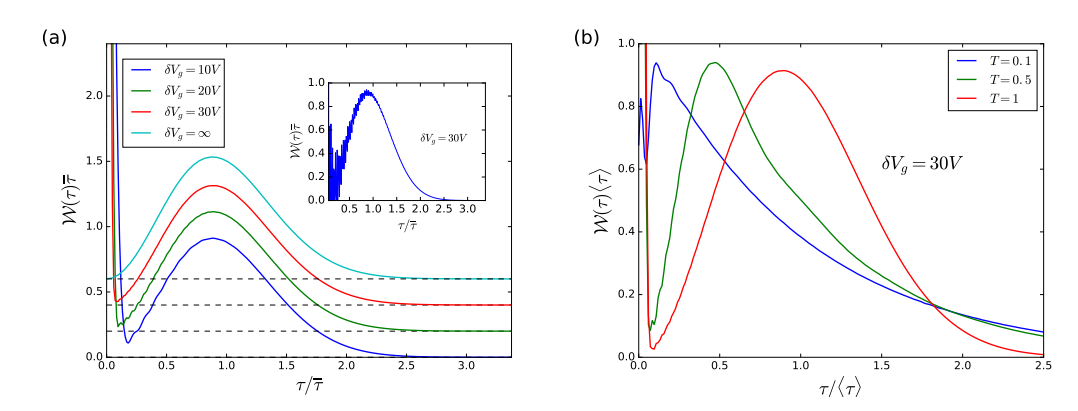


Figure 3.2.: WTDs for a voltage-biased QPC. (a) Distribution of waiting times for a fully transmitting QPC (T=1) with an applied voltage V. The mean waiting time is $\bar{\tau} = h/(eV)$. We show results for different values of the gate voltage increase δV_g . With $\delta V_g = 30V$, we essentially recover the prediction $(\delta V_g = \infty)$ of earlier theories without a detector [Albert et al., 2012; Haack et al., 2014]. The curves have been shifted vertically by multiples of 0.2 and we have applied a low pass filter to remove high-frequency oscillations. The inset shows the WTD for $\delta V_g = 30V$ without the low pass filter. (b) Distribution of waiting times for different values of the QPC transmission T. ([Dasenbrook and Flindt, 2016b], (C) 2016 American Physical Society.)

In this case, we can write the scattering matrix as

$$S_{\lambda} = P_R - P_T S_{\lambda}^{(l)} P_T, \tag{3.26}$$

without processes involving several loops. In the following section, we discuss the values of δV_g in Eq. (3.21) needed for this to be a good approximation. To evaluate the determinant formula in Eq. (3.3), we first note that

$$(\mathcal{S}_{-\lambda}^{(\text{tot})})^{\dagger} \mathcal{S}_{\lambda}^{(\text{tot})} = \mathcal{S}_{\text{sys}}^{\dagger} \left(P_R + P_T (\mathcal{S}_{-\lambda}^{(l)})^{\dagger} \mathcal{S}_{\lambda}^{(l)} P_T \right) \mathcal{S}_{\text{sys}}, \tag{3.27}$$

having used $[P_T, \mathcal{S}_{\lambda}^{(l)}] = 0$, since electrons that enter the capacitor remain above the Fermi level. This holds for large values of δV_g . A simple calculation now shows that

$$(\mathcal{S}_{-\lambda}^{(l)})^{\dagger} \mathcal{S}_{\lambda}^{(l)} = 1 + (e^{i\lambda} - 1)\mathcal{K}_{\tau}, \tag{3.28}$$

with the matrix elements

$$[\mathcal{K}_{\tau}]_{E,E'} = K_{\tau}(E - E')$$
 (3.29)

given by the sine kernel in Eq. (1.14). Inserting these expressions into Eq. (3.4) we find at zero temperature

$$\chi(\lambda) = \det\left(1 + \left(e^{i\lambda} - 1\right) \mathcal{S}_{\text{sys}}^{\dagger} P_T \mathcal{K}_{\tau} P_T \mathcal{S}_{\text{sys}}\right), \tag{3.30}$$

3. Electron waiting time clock

having used that the scattering matrix S_{sys} is unitary and $P_T + P_R = 1$. In this expression, the increase of the gate voltage δV_q has dropped out. Moreover, by introducing the matrix

$$Q_{\tau} = S_{\text{sys}}^{\dagger} P_T \mathcal{K}_{\tau} P_T S_{\text{sys}}, \tag{3.31}$$

we may express the moment generating function as

$$\chi(\lambda) = \det\left(1 + \left(e^{i\lambda} - 1\right)Q_{\tau}\right). \tag{3.32}$$

Finally, by taking the limit $\lambda \to i\infty$, we recover the determinant formula for the idle time probability above the Fermi level

$$\Pi(\tau) = \det\left(1 - \mathcal{Q}_{\tau}\right) \tag{3.33}$$

previously derived by Albert et al. [2012] without specifying a detector. For a static scatterer with an applied voltage V, the matrix Q_{τ} only has non-zero elements in the transport window $[E_F, E_F + eV]$.

Next, we consider the non-ideal situation where electrons may complete several loops inside the capacitor and interact with the spin more than once. This is described by the scattering matrix in Eq. (3.25). We then evaluate the idle time probability by inserting this scattering matrix into Eq. (3.4). In contrast to Eq. (3.30), the function $\chi(\lambda)$ now contains terms that are proportional to $\exp(i\lambda/2)$ as shown in Appendix E. Consequently, the function is not 2π -periodic in λ as required for a moment generating function according to Eq. (3.13), and the transport process cannot be described by a time series of discrete detection events. This is not a consequence of measurement back action in particular, but may possibly be related to the occurrence of negative probabilities in FCS due to interference effects [Hofer and Clerk, 2016]. Still, we can take the limit $\lambda \to i\infty$ and calculate the resulting WTD using Eq. (1.1). However, as we will see, the WTD may then become negative for certain waiting times. This is due to processes where an electron interacts more than once with the spin and thereby tampers with the measurement of the idle time probability.

3.5. Applications

We are now ready to illustrate the electron waiting time clock with two specific applications: A voltage-biased QPC and lorentzian voltage pulses. We also investigate the influence of a smooth transmission profile. In Sec. 3.7 we consider a smooth coupling to the spin instead of the abrupt switching given by Eq. (3.6). Technically, it is worth mentioning that the Fredholm determinants that appear for example in Eq. (3.4) can be evaluated efficiently using the algorithm described in Appendix D [Bornemann, 2010].

3.5.1. Voltage-biased QPC

We start by considering a QPC with transmission probability T and applied voltage V. In this case, we have $S_{\text{svs}} = \sqrt{T}$. Earlier works [Albert et al., 2012; Haack et al., 2014]

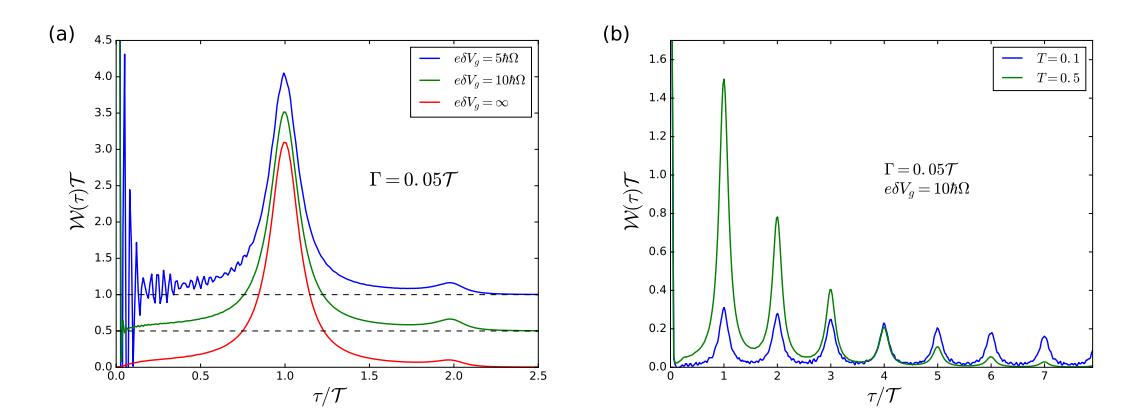


Figure 3.3.: WTDs for levitons transmitted through a QPC. (a) Results for full transmission (T=1) with different values of the gate voltage increase δV_g . Already with $e\delta V_g=10\hbar\Omega$, the waiting time clock reproduces results $(\delta V_g=\infty)$ of earlier theories without a detector [Dasenbrook et al., 2014; Albert and Devillard, 2014]. The curves have been shifted vertically for the sake of a better visibility. (b) Results for a QPC with a finite transmission T. In this case, levitons may reflect back on the QPC, and the WTD has peaks at multiplies of the period. ([Dasenbrook and Flindt, 2016b], (C) 2016 American Physical Society.)

without a detector have shown that the WTD should display a cross-over from Wigner-Dyson statistics at full transmission (T=1) to a Poisson distribution close to pinch-off $(T \simeq 0)$ with the mean waiting time given as

$$\langle \tau \rangle = \frac{\bar{\tau}}{T},\tag{3.34}$$

where

$$\bar{\tau} = \frac{h}{eV},\tag{3.35}$$

is the meaning waiting time at full transmission.

Figure 3.2 shows WTDs obtained with the waiting time clock. We calculate the idle probability using Eqs. (3.4, 3.25), see also App. E, and differentiate it twice with respect to τ according to Eq. (1.1). In panel (a) we show the WTD for a fully open QPC with different increments of the gate voltage δV_g . To measure the WTD, the coupling to the spin is only non-zero during a period of time on the order of $\bar{\tau}$. Such short detector pulses can change the energy of an electron by an amount on the order of $h/\bar{\tau}=eV$. Thus, to ensure that no electrons are scattered below the Fermi level during the measurement, the increase of the gate voltage must be much larger than this energy scale, i. e. $\delta V_g \gg V$. This physical picture is confirmed by panel (a). As we increase δV_g , we approach the results of an ideal clock obtained from Eq. (3.33).

The time resolution of the waiting time clock depends on δV_g . A finite value of δV_g introduces fluctuations in the WTD on the time scale $h/(e\delta V_g)$. The fluctuations es-

3. Electron waiting time clock

sentially disappear for waiting times that are longer than the mean waiting time, where the measurement-induced disturbances are almost negligible. By contrast, for very short waiting times, the WTD may become negative as seen in the inset. To remove any spurious fluctuations, we apply a low pass filter that suppresses frequencies on the order of $e\delta V_q/h$. The inset of panel (a) shows the WTD without the low pass filter.

In panel (b) we consider the WTD for different values of the QPC transmission T. The figure illustrates how our electron waiting time clock allows a observation of the cross-over from Wigner-Dyson distribution at full transmission to Poisson statistics close to pinch-off as previously predicted by theories without a detector.

3.5.2. Lorentzian voltage pulses

Next, we consider lorentzian voltage pulses applied to the input lead [Dubois et al., 2013a; Jullien et al., 2014; Levitov et al., 1996; Keeling et al., 2006; Ivanov et al., 1997; Lebedev et al., 2005]. The applied voltage has the form

$$V(t) = \sum_{j=-\infty}^{\infty} \frac{2\hbar\Gamma}{(t-j\mathcal{T})^2 + \Gamma^2},$$
(3.36)

where Γ denotes the pulse width and \mathcal{T} is the period. The voltage can be encoded in a time-dependent scattering phase picked up by electrons as they leave the lead,

$$e^{i\phi(t)} = e^{-i\frac{e}{\hbar} \int_{-\infty}^{t} V(t') dt'}$$
(3.37)

By Fourier transforming this scattering phase, we obtain a Floquet scattering matrix with elements given by Eq. (A.5). Each pulse excites just a single electron-hole pair out of the Fermi sea without creating any additional disturbances, known as levitons. The corresponding scattering matrix reads [Moskalets, 2011]

$$[S_{\text{sys}}]_{E,E'} = \sqrt{T} \sum_{n} \delta(E' - E_n) S_F(E, E'), \qquad (3.38)$$

having included a QPC that reflects a fraction R = 1 - T of the levitons before they reach the waiting time clock.

Figure 3.3 shows the distribution of waiting times between levitons measured with the waiting time clock. For a fully transmitting QPC, the WTD is peaked around the period of the driving \mathcal{T} , panel (a). Unlike the results for the voltage-biased QPC, there is no need to apply a low pass filter. We still observe small oscillations with a period of $h/e\delta V_g$, but they essentially disappear already for $\delta V_g = 10\hbar\Omega/e$. Physically, the levitons are well-localized in time and space, and one would expect that they are easier to distinguish from the underlying Fermi sea than electrons emitted from a constant voltage source. This is indeed confirmed by our results.

In panel (b) we consider the WTD of levitons transmitted through a partially reflecting QPC. In this case, levitons may reflect back on the QPC. As a consequence, the WTD develops peaks at multiples of the period, with each peak corresponding to the number of subsequent reflections that have occurred. Again, we find good agreement with earlier theories without a detector [Dasenbrook et al., 2014; Albert and Devillard, 2014].

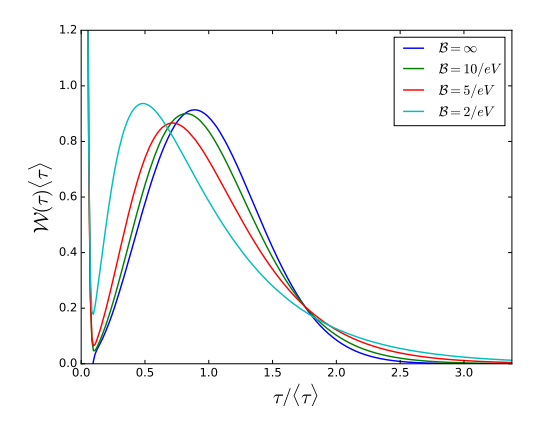


Figure 3.4.: WTDs obtained with a smooth transmission profile. The sharpness of the transmission in Eq. (3.17) is determined by the parameter \mathcal{B} . We consider here the WTD for a single edge channel with an applied voltage V and have used $\delta V_g = 30V$. ([Dasenbrook and Flindt, 2016b], (C) 2016 American Physical Society.)

3.5.3. Smooth QPC transmission

So far, we have considered a waiting time clock with a sharp cut-off in the transmission. In reality, however, the cut-off might be smooth, corresponding to having a finite value of \mathcal{B} in Eq. (3.17). In this case, electrons below the Fermi level can enter and leave the capacitor, and electrons above the Fermi level may reflect back on the QPC and never enter the capacitor. Figure 3.4 shows the WTD for a constant voltage V with different values of the cut-off parameter \mathcal{B} . For values of \mathcal{B} that are much larger than the inverse voltage, the influence on the WTD is small compared to the ideal case with a sharp cut-off. For smaller values of \mathcal{B} , the shape of the distribution gets somewhat distorted. Still, a measurement of the WTD is clearly possible with a smooth QPC transmission.

3.6. Measurement scheme

The electron waiting time clock relies on measuring the moment generating function $\chi(\lambda,\tau)$ for different values of the counting field λ to obtain the idle time probability via the Fourier transformation in Eq. (3.14). To this end, it should be possible not only to turn the coupling on and off, but also to accurately change the strength of the coupling as well as measure the off-diagonal element of the spin density matrix. In principle, this is possible. However, as we will show now, a better strategy might be to couple several spins to the mesoscopic capacitor.

We start by considering just a single spin coupled to the capacitor during the time τ . The coupling strength is denoted as λ_1 . The spin is initialized in the pure state

$$|\Psi\rangle = \frac{1}{\sqrt{2}}(|\uparrow\rangle + |\downarrow\rangle) \tag{3.39}$$

3. Electron waiting time clock

with the corresponding density matrix

$$\hat{\rho}_0^{(1)} = |\Psi\rangle\langle\Psi| = \frac{1}{2} \begin{pmatrix} 1 & 1\\ 1 & 1 \end{pmatrix}. \tag{3.40}$$

After the coupling is turned off, the density matrix reads

$$\hat{\rho}^{(1)} = \frac{1}{2} \begin{pmatrix} 1 & \chi^*(\lambda_1, \tau) \\ \chi(\lambda_1, \tau) & 1 \end{pmatrix}. \tag{3.41}$$

Since the coupling is fixed we cannot extract the moment generating function. However, we can calculate the probabilities of the individual precession angles of the spin. In particular, the probability that the spin is in its initial state after the coupling has been switched off reads

$$\Pi^{(1)}(\tau) = \operatorname{tr}[\hat{\rho}_0^{(1)}\hat{\rho}^{(1)}] = \frac{1}{2} \left[1 + \operatorname{Re}\chi(\lambda_1, \tau) \right]. \tag{3.42}$$

For $\lambda_1 = \pi$, this is a crude approximation of the integral in Eq. (3.14). To improve the approximation, we couple a second spin to the capacitor. The coupling strength of this spin is denoted as λ_2 . Both spins are initially in the state given by Eq. (3.39). If the couplings have been switched on during a time interval of length τ , the elements of the density matrix of the spins become

$$[\hat{\rho}^{(2)}]_{ij,kl} = \frac{1}{4} \chi^{(2)} \left((i-j)\lambda_1, (k-l)\lambda_2, \tau \right). \tag{3.43}$$

Here, the indices i, j = 0, 1 (k, l) refer to the first (second) spin and $\chi^{(2)}(\lambda_1, \lambda_2, \tau)$ is a joint moment generating function obtained from Eq. (3.3) by including the additional scattering phases due to the second spin. If the two spins are directly attached to the capacitor one after another, we find that the joint moment generating function can be expressed as

$$\chi^{(2)}(\lambda_1, \lambda_2, \tau) = \chi(\lambda_1 + \lambda_2, \tau) \tag{3.44}$$

in terms of the moment generating function $\chi(\lambda, \tau)$ corresponding to a single spin. Calculating the probability that the spins are in their initial states after the couplings have been switched off, we find

$$\Pi^{(2)}(\tau) = \frac{1}{4} \left[1 + \text{Re} \left\{ \chi(\pi/2, \tau) + \chi(\pi, \tau) + \chi(3\pi/2, \tau) \right\} \right], \tag{3.45}$$

taking $\lambda_1 = \pi/2$ and $\lambda_2 = \pi$. This is now a four-point approximation of the integral in Eq. (3.14). Following this line of thoughts, one can extend the idea to three or more spins, and thereby further improve the approximation of the idle time probability. For example with 3 spins with couplings $\lambda_1 = \pi/3$, $\lambda_2 = 2\pi/3$, and $\lambda_1 = \pi$, one obtains a six-point approximation of the integral.

In Fig. 3.5 we show WTDs based on idle time probabilities $\Pi^{(n)}(\tau)$ measured with n (= 1, 2, 3) spins. With just one spin, the WTD is only qualitatively correct for very short waiting times compared with the mean waiting time. At longer times, the WTD

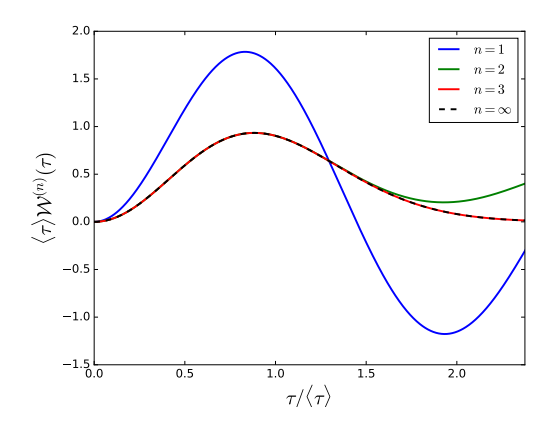


Figure 3.5.: WTDs obtained with n spins coupled to the capacitor. We consider here the WTD for a single edge channel with an applied voltage V and have used $\delta V_g \gg V$. The WTD obtained with a perfect detector is shown with a dashed line. ([Dasenbrook and Flindt, 2016b], (C) 2016 American Physical Society.)

turns negative which is clearly not correct. However, already with two spins coupled to the capacitor, the results are much closer to the WTD obtained with a perfect detector. Only for long waiting times, deviations become visible. With three spins coupled to the capacitor, we find essentially perfect agreement with the expected WTD for the range of waiting times shown in Fig. 3.5.

3.7. Lorentzian switching

As an interesting aside, we consider a smooth coupling to the spin. Specifically, we take $\lambda(t)$ to be the integral of a lorentzian,

$$\lambda(t) = \int_{-\infty}^{t} \frac{-2\tau}{t'^2 + \tau^2/4} dt' = -2\pi - 4 \arctan(2t/\tau), \tag{3.46}$$

such that

$$[U_{\tau}^{\text{lor}}]_{t,t'} = e^{i\lambda(t)/2}\delta(t-t') = \frac{t+i\tau/2}{t-i\tau/2}\delta(t-t'). \tag{3.47}$$

It should be noted that $\lambda(t) \simeq 0$ for $t < -\tau/2$ and $\lambda(t) \simeq -4\pi$ for $t > \tau/2$. However, due to the 4π -periodicity in Eq. (3.47), the value $\lambda = -4\pi$ is equivalent to $\lambda = 0$. Thus, one may think of the coupling in Eq. (3.46) as being non-zero only during the time interval $[-\tau/2, \tau/2]$.

In the energy representation, the elements of U_{τ}^{lor} are

$$[U_{\tau}^{\text{lor}}]_{E,E'} = \delta(E - E') - K_{\tau}^{\text{lor}}(E - E'), \tag{3.48}$$

where we have defined the exponential kernel

$$K_{\tau}^{\text{lor}}(E) = \tau e^{-\tau E/2} \Theta(E). \tag{3.49}$$

3. Electron waiting time clock

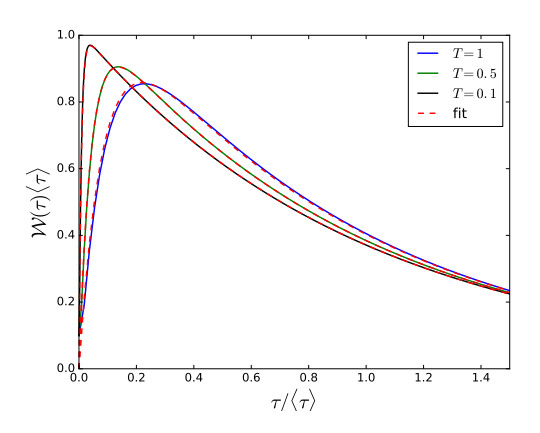


Figure 3.6.: WTDs with a lorentzian switching of the coupling. We show results for a QPC with different transmission probabilities T. The dashed curves are based on Eqs. (3.53, 3.54). ([Dasenbrook and Flindt, 2016b], (C) 2016 American Physical Society.)

Unlike the sine kernel in Eq. (1.14), this kernel is only non-zero for positive energies. Thus, electrons can only absorb energy by interacting with the spin and are thus not scattered into the Fermi sea.

Next, we evaluate Eq. (3.4) and find

$$\chi(\lambda) = \det\left(1 - Q_{\tau}^{\text{lor}}\right) \tag{3.50}$$

with

$$Q_{\tau}^{\text{lor}} = \mathcal{S}_{\text{sys}}^{\dagger} P_T \mathcal{K}_{\tau}^{\text{lor}} P_T \mathcal{S}_{\text{sys}}$$
 (3.51)

and

$$[\mathcal{K}_{\tau}^{\text{lor}}]_{E,E'} = \tau e^{-|E-E'|\tau/2}.$$
 (3.52)

Surprisingly, by comparing these expressions with Eqs. (3.31,3.33), we see that Eq. (3.50) takes the form of an idle time probability, however, with the kernel given by Eq. (3.52). Thus, without further justification, we consider in the following $\chi(\lambda)$ as the idle time probability and evaluate the corresponding WTD by differentiating it twice with respect to τ .

In Fig. 3.6 we show WTDs for a QPC with transmission T obtained in this way. The mean waiting time is still given by Eq. (3.34), however, the WTDs are different from those in Fig. 3.2b. The WTD appears to depend linearly on τ at short times and eventually decays exponentially at long times. This resembles the WTD for a resonant level in the high-bias limit [Brandes, 2008]

$$W(\tau) = \frac{\Gamma_L \Gamma_R}{\Gamma_R - \Gamma_L} (e^{-\Gamma_L \tau} - e^{-\Gamma_R \tau}), \tag{3.53}$$

where Γ_L and Γ_R are the rates at which electrons enter and leave the level. The mean waiting time reads

 $\langle \tau \rangle = \frac{\Gamma_L + \Gamma_R}{\Gamma_L \Gamma_R}.$ (3.54)

Based on the similarity, we surmise that Eq. (3.53) also describes the WTDs in Fig. 3.6. The rate Γ_R can be determined from the mean waiting time. We then use Γ_L to fit our results for full transmission and find excellent agreement. For the results with finite transmission, we keep Γ_L fixed and extract Γ_R from the mean waiting time which depends on the transmission. With this approach, we can fully account for all results in Fig. 3.6.

It would be interesting to investigate these findings further. For example, the reason for the correspondence between the WTD obtained by a Lorentzian switching protocol and the resonant tunneling WTD Eq. (3.53) is currently not known.

3.8. Conclusions

We have presented a quantum theory of a waiting time clock which can measure the distribution of waiting times between electrons above the Fermi sea in a mesoscopic conductor. This is an important element which so far has been missing in theories of electron waiting times. Our waiting time clock consists of a mesoscopic capacitor coupled to a quantum two-level system whose coherent precession is measured. We have demonstrated explicitly that the waiting time clock under ideal operating conditions recovers the predictions of earlier theories without a detector. We have also investigated the influence of imperfect operating conditions with two specific applications. With these advances, theories of electron waiting times can now be discussed based on a specific detector.

Our work leaves a number of questions for future investigations. The waiting time clock presented here may not be the only one that can measure the distribution of waiting times between electrons above the Fermi sea. It would be interesting to devise alternative implementations of such waiting time clocks. It might also be interesting to investigate waiting time clocks that are sensitive to correlations between waiting times, or to the electrons below the Fermi level. The distribution of electron waiting times between electrons in the Fermi sea constitutes a line of research which has not yet been addressed. Finally, the ideas presented here may form the basis for future investigations of the influence of interactions on the distribution of electron waiting times.

4. Interferometric measurements of full counting statistics

4.1. Introduction

Full counting statistics (FCS) is a central concept in mesoscopic physics [Levitov et al., 1996; Blanter and Büttiker, 2000; Nazarov and Kindermann, 2003]. The distribution of charge transfers contains information about the elementary conduction processes [Vanević et al., 2007, 2008; Hassler et al., 2008; Abanov and Ivanov, 2008, 2009]. Full counting statistics has found widespread use in theories of quantum electronic circuits, for instance in proposals for detecting entanglement [Beenakker and Kindermann, 2004; Di Lorenzo and Nazarov, 2005], revealing interactions [Kambly et al., 2011; Stegmann et al., 2015], understanding quasi-probabilities [Belzig and Nazarov, 2001; Bednorz and Belzig, 2010; Clerk, 2011; Hofer and Clerk, 2016], or observing Majorana modes [Soller and Komnik, 2014; Li et al., 2015; Gnezdilov et al., 2015; Liu et al., 2015; Strübi et al., 2015]. Intimate connections to fluctuation relations at the nano-scale [Tobiska and Nazarov, 2005; Förster and Büttiker, 2008; Esposito et al., 2009; Utsumi and Saito, 2009; Nagaev et al., 2010; Utsumi et al., 2010; Küng et al., 2012; Saira et al., 2012] and to entanglement entropy in fermionic many-body systems [Klich and Levitov, 2009; Song et al., 2011, 2012; Petrescu et al., 2014; Thomas and Flindt, 2015] have also been discovered.

Despite these promising applications, experiments remain scarce. Measurements of FCS are demanding as they require accurate detection of rare events in the tails of the distributions. For quantum-dot systems, progress has been made using real-time charge detectors [Fujisawa et al., 2006; Gustavsson et al., 2006; Flindt et al., 2009; Gustavsson et al., 2009; Ubbelohde et al., 2012; Maisi et al., 2014]. By contrast, for phase-coherent transport in mesoscopic conductors, only the first few cumulants of the current have been measured [Reulet et al., 2003; Bomze et al., 2005; Timofeev et al., 2007; Gershon et al., 2008; Gabelli and Reulet, 2009]. To measure the FCS, it has been suggested to use a spin to sense the magnetic field generated by the electrical current in a mesoscopic conductor [Levitov et al., 1996; Lesovik et al., 2006; Lebedev et al., 2016]. However, being experimentally challenging, this proposal has not yet come to fruition.

Now, progress in giga-hertz quantum electronics is changing these perspectives [Bocquillon et al., 2014]. Coherent electrons can be emitted on demand from quantum capacitors [Gabelli et al., 2006; Fève et al., 2007] and clean single-particle excitations can be generated using Lorentzian voltage pulses [Dubois et al., 2013a; Jullien et al., 2014]. In parallel with these developments, electronic interferometers have emerged as powerful detectors of weak signals [Henny et al., 1999; Oliver et al., 1999]. Mach-Zehnder interferometers can be realized using quantum Hall edge states with quantum point contacts

4. Interferometric measurements of full counting statistics

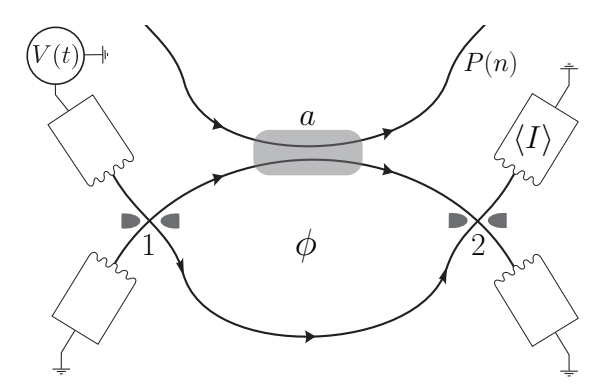


Figure 4.1.: Interferometric measurements of FCS. Single electrons are injected into a Mach-Zehnder interferometer enclosing the reduced magnetic flux ϕ . The average current measured at the outputs is sensitive to a phase shift caused by the capacitive coupling to a nearby conductor. The length of the interaction region is denoted as a. The phase shift is proportional to the number of transferred electrons in the conductor. By varying the magnetic flux and the time delay between two separate voltage signals applied to the conductor and the interferometer, the FCS of the conductor can be obtained from average current measurements only. [Dasenbrook and Flindt, 2016a].

(QPCs) acting as electronic beam splitters [Ji et al., 2003; Neder et al., 2007c,b,a; Roulleau et al., 2008; Litvin et al., 2010; Helzel et al., 2015]. When combined, these building blocks may form the basis for the next generation of quantum electronic circuits, including future measurements of FCS.

Motivated by these experimental advances we develop in this chapter a dynamical scheme for measuring the FCS in mesoscopic conductors. The detector consists of an electronic Mach-Zehnder interferometer driven by periodic voltage pulses [Hofer and Flindt, 2014; Gaury and Waintal, 2014]. One arm of the interferometer is capacitively coupled to a nearby conductor that causes a phase shift which is proportional to the number of transferred charges, Fig. 4.1. As we will see, the FCS of the conductor can be inferred from current measurements at the outputs of the interferometer. Setups of this type, with static voltages, have been considered both in experiment [Neder et al., 2007b] and theory [Neder and Marquardt, 2007; Levkivskyi and Sukhorukov, 2009]. However, so far the conductor has been operated as a which-path detector for the interferometer [Neder et al., 2007a; Dressel et al., 2012; Weisz et al., 2014]. Here, by contrast, we exchange the roles and instead use the interferometer as a detector of the FCS in the conductor.

4.2. Mach-Zehnder interferometer

4.2.1. Basic principle

The interferometer is implemented with edge states of a two-dimensional electron gas in the integer quantum Hall regime [Ji et al., 2003; Neder et al., 2007c,b,a; Roulleau et al.,

2008; Litvin et al., 2010; Helzel et al., 2015]. Incoming electrons are coherently split at the first QPC and recombined at the second. Single electrons are emitted into the interferometer by applying periodic voltage pulses to one of the inputs [Hofer and Flindt, 2014; Gaury and Waintal, 2014; Lebedev et al., 2005; Hassler et al., 2007; Keeling et al., 2006]. The pulses are sufficiently separated so that only one electron at a time traverses the interferometer. (In an alternative implementation, one may consider the injection of charges from a mesoscopic capacitor.) The electronic state inside the interferometer is a coherent superposition of the electron being in the upper $(|u\rangle)$ or lower $(|l\rangle)$ arm,

$$|\Psi\rangle = t_1 |l\rangle + e^{i\phi} r_1 |u\rangle. \tag{4.1}$$

Here, t_1 and r_1 are the transmission and reflection amplitudes of the first QPC and $\phi = 2\pi\Phi/\Phi_0$ is the ratio of the magnetic flux Φ enclosed by the arms over the flux quantum Φ_0 . This state resembles the spin in the proposal of Levitov et al. [1996]. For electrons injected into the interferometer with period \mathcal{T} , the current in the upper output reads

$$\langle \hat{I} \rangle = (e/\mathcal{T})|t_1t_2 + r_1r_2e^{i\phi}|^2,$$
 (4.2)

where t_2 and r_2 are the transmission and reflection amplitudes of the second QPC. Eq. (4.1) describes a pure state. More generally, for instance due to a finite temperature or external noise causing fluctuations of ϕ , the electron must be described by a density matrix $\hat{\rho}$. Importantly, a measurement of the average current yields an ensemble average over the phase ϕ [Samuelsson and Büttiker, 2006].

4.2.2. FCS measurement

The Mach-Zehnder interferometer is coupled to a nearby conductor whose current fluctuations we wish to measure. The electrical fluctuations are described by the moment generating function (MGF)

$$\chi(\lambda) = \sum_{n} P(n)e^{in\lambda} = \langle e^{in\lambda} \rangle. \tag{4.3}$$

The average is defined with respect to the probability P(n) of n charges being transmitted through the conductor and λ is the counting field. The conductor is driven by periodic pulses such that the MGF after many periods $(N \gg 1)$ factorizes as $\chi(\lambda) = [\chi_{\rm ext}(\lambda)]^N$, where $\chi_{\rm ext}(\lambda)$ characterizes the *extensive* FCS per period [Ivanov et al., 1997]. We focus on the measurement of $\chi_{\rm ext}(\lambda)$ and omit the subscript "ext" in the following.

The conductor is coupled to the upper arm of the interferometer. Such a setup has been experimentally realized [Neder et al., 2007c,a; Roulleau et al., 2008], albeit with statically biased contacts. By contrast, here we drive both the conductor and the interferometer with periodic voltage pulses. The frequency of the two pulse sequences is the same, but we allow for a time delay τ between them. With this setup, an electron in the upper arm picks up the additional phase $\delta \phi = n\lambda$ due to n electrons passing by in the conductor per period. This is substantiated in our analysis in Sec. 4.3, where we also show that

4. Interferometric measurements of full counting statistics

the dimensionless coupling λ indeed can be identified with the counting field. At zero temperature, the density matrix of the interferometer reads

$$\hat{\rho} = \begin{pmatrix} |t_1|^2 & t_1 r_1^* e^{i\phi} \chi(\lambda) \\ t_1^* r_1 e^{-i\phi} [\chi(\lambda)]^* & |r_1|^2 \end{pmatrix}, \tag{4.4}$$

having used

$$\langle e^{i\delta\phi}\rangle = \langle e^{in\lambda}\rangle = \chi(\lambda).$$
 (4.5)

The off-diagonal element of $\hat{\rho}$ is thus determined by the MGF of the conductor. Eq. (4.4) generalizes Eq. (4.1) to mixed states.

The MGF can now be extracted from the current in the upper output. The current $\langle \hat{I} \rangle = \text{tr}[\hat{\rho}\hat{I}]$ reads

$$\langle \hat{I} \rangle = (e/\mathcal{T})(T_1 T_2 + R_1 R_2 + 2 \operatorname{Re}\{t_1^* t_2^* r_1 r_2 e^{i\phi} \chi(\lambda)\}),$$
 (4.6)

where $T_j = |t_j|^2$ and $R_j = |r_j|^2$ are the transmissions and reflections of the two QPCs (j = 1, 2). At half transmission, we get

$$\langle \hat{I} \rangle = (e/\mathcal{T})(1 + \text{Re}\{e^{i\phi}\chi(\lambda)\})/2. \tag{4.7}$$

Moreover, by changing the magnetic flux, we find

$$\langle \hat{I} \rangle_{\phi=0} = (e/\mathcal{T})(1 + \text{Re}\{\chi(\lambda)\})/2,$$

$$\langle \hat{I}_1 \rangle_{\phi=3\pi/2} = (e/\mathcal{T})(1 + \text{Im}\{\chi(\lambda)\})/2.$$
 (4.8)

These expressions lead us to the MGF

$$\chi(\lambda) = \frac{2\mathcal{T}}{e} \left[\left(\langle \hat{I} \rangle_{\phi=0} - \frac{e}{2\mathcal{T}} \right) + i \left(\langle \hat{I} \rangle_{\phi=3\pi/2} - \frac{e}{2\mathcal{T}} \right) \right]. \tag{4.9}$$

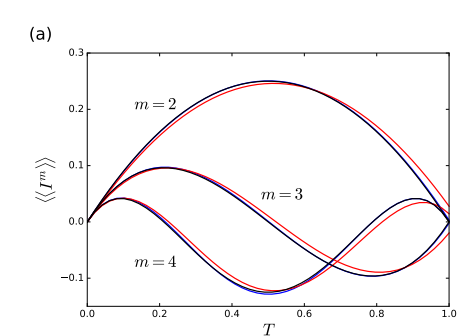
Remarkably, the MGF can be obtained from average current measurements. This is the first central result of our work. As we go on to show, the counting field λ can be controlled by varying the time delay τ between the pulse sequences. We can then perform a full tomography of $\chi(\lambda)$ and thereby evaluate the FCS of charge transfer.

4.3. Detailed analysis

We now embark on a detailed analysis of the coupling between the interferometer and the conductor. The interaction between the two edge states is described by the Hamiltonian [Vyshnevyy et al., 2013]

$$\hat{H}_{\lambda_0} = \lambda_0 \frac{\hbar v_F}{2a} \hat{N}_C \hat{N}_I. \tag{4.10}$$

Here, λ_0 is a dimensionless coupling, v_F is the Fermi velocity, and a is a characteristic length scale over which electrons in the two edge states interact. The operators $\hat{N}_C = \int \mathrm{d}x \kappa_C(x) : \hat{\Psi}_C^{\dagger}(x) \hat{\Psi}_C(x) :$ and $\hat{N}_I = \int \mathrm{d}y \kappa_I(y) : \hat{\Psi}_I^{\dagger}(y) \hat{\Psi}_I(y) :$ count the number of excess electrons in the interacting regions of the conductor and the interferometer, weighted



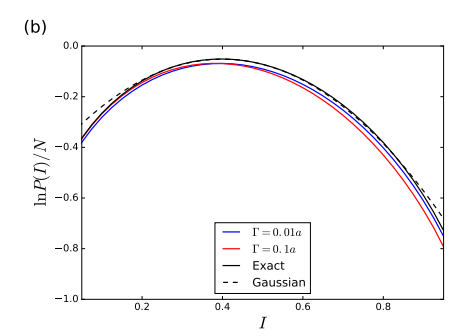


Figure 4.2.: Interferometric measurement of the full counting statistics in a QPC. (a) Cumulants of the current as functions of the QPC transmission T. We show results for different pulse widths Γ in terms of the length a of the interaction region. The exact results for a binomial process are $\langle\langle I^2 \rangle\rangle = T(1-T)$, $\langle\langle I^3 \rangle\rangle = T(1-T)(1-2T)$, $\langle\langle I^4 \rangle\rangle = T(1-T)(1-6T+6T^2)$, having set e=1 and T=1 here and in the figure. (b) Full distribution of the current I=en/N with T=0.4 and N=40. For a large number of periods, $N\gg 1$, the distribution takes on the large-deviation form $\ln[P(I)]/N=\mathcal{G}(I)$ with the rate function $\mathcal{G}(I)$ being independent of N. For a binomial process we find $\ln[P(I)]/N=\ln[(1-T)/(1-I)]+I(\ln[T/(1-T)]-\ln[I/(1-I)])+\mathcal{O}(N^{-1})$. [Dasenbrook and Flindt, 2016a].

by the coordinate kernels $\kappa_C(x)$ and $\kappa_I(y)$. Normal-ordering with respect to the Fermi sea is denoted as : \cdots :, and $\hat{\Psi}_C(x)$ and $\hat{\Psi}_I(y)$ are field operators for electrons in the conductor and in the interferometer.

The MGF in the off-diagonal element of the density matrix in Eq. (4.4) can now be expressed as [Levitov et al., 1996; Belzig and Nazarov, 2001]

$$\chi(\lambda_0) = \left\langle \operatorname{tr} \left(\widetilde{T} \left\{ e^{-i \int_{t_0}^t dt' \hat{H}_{\lambda_0}(t')} \right\} T \left\{ e^{i \int_{t_0}^t dt' \hat{H}_{-\lambda_0}(t')} \right\} \hat{\rho} \right) \right\rangle, \tag{4.11}$$

having set $\hbar = 1$ and $\hat{H}_{\lambda_0}(t)$ is in the Heisenberg representation governed by the full Hamiltonian $\hat{H} = \hat{H}_0 + \hat{H}_{\lambda_0}$ with \hat{H}_0 describing the uncoupled systems. The initial density matrix of the electron in the interferometer is denoted as $\hat{\rho} = \hat{\rho}(t_0)$ and the trace is taken over the spatial coordinates. The average is defined with respect to the electrons in the conductor. Time and anti-time ordering are denoted as T and \tilde{T} , respectively.

The considerations above are general. To make further progress, we take for the kernels the specific form [Vyshnevyy et al., 2013]

$$\kappa_C(x) = \kappa_I(x) = e^{-|x|/a}. \tag{4.12}$$

If a is much smaller than the length of the interferometer, the current measured at the output is determined by the limit $t \to \infty$ in Eq. (4.11). With a linear dispersion relation for electrons close to the Fermi level and a pure initial state of the electron in

4. Interferometric measurements of full counting statistics

the interferometer, we find

$$\chi(\lambda_0) = \left\langle \int dy e^{i\lambda_0 \int dx : \hat{\Psi}_C^{\dagger}(x) \hat{\Psi}_C(x) : \Phi(x,y)} |f(y)|^2 \right\rangle, \tag{4.13}$$

where f(y) is the wave function of the electron injected into the interferometer and the function

$$\Phi(x,y) = e^{-\frac{|x-y|}{a}} \left(1 + \frac{|x-y|}{a} \right)$$
 (4.14)

follows from the definition of the coordinate kernels.

We now derive Eq. (4.13). The interferometer electron possesses both a pseudo-spin degree of freedom, corresponding to the path that it takes, and a spatial degree of freedom, corresponding to its position within the arms. In Eq. (4.11), the average is taken over the spatial degrees of freedom of the interferometer electron as well as over the conductor. The density matrix of the interferometer electron factorizes as $\rho = \hat{\rho}_S \otimes \hat{\rho}_L$ at all times, where $\hat{\rho}_S$ describes the pseudo-spin and $\hat{\rho}_L$ describes the spatial degrees of freedom. This is due to the fact that propagation along the arms is independent of the arm index.

The particle density operators in Eq. (4.10) commute at different times. We therefore obtain

$$\chi(\lambda_0) = \left\langle \operatorname{tr} e^{2i\hat{H}_{\lambda_0} t} \hat{\rho}_L \right\rangle, \tag{4.15}$$

where the factor 2 accounts for the forward- and backward propagation on the Keldysh contour (with opposite coupling constants), the average $\langle ... \rangle$ is taken over the degrees of freedom of the conductor and the trace is taken over the internal degrees of freedom of the electron in the interferometer, i. e. its coordinate.

To evaluate the trace in Eq. (4.15), we first write the density matrix of the electron in real-space as

$$\hat{\rho}_L = \iint dx dy f(x) f^*(y) |y\rangle\langle x|, \qquad (4.16)$$

where f(x) is the electronic wave function.

Next, we consider the action of the exponential of a general operator \hat{A} that commutes with the interferometer electron density : $\hat{\Psi}_I^{\dagger}(x)\hat{\Psi}_I(x)$: on this density matrix. The Hamiltonian \hat{H}_{λ_0} is such an operator. We therefore expand the exponential

$$e^{\hat{A}\int du\kappa(u):\hat{\Psi}_{I}^{\dagger}(u)\hat{\Psi}_{I}(u):}|x\rangle\langle y| = |x\rangle\langle y| + \hat{A}\kappa(x)|x\rangle\langle y| + \frac{1}{2}\hat{A}^{2}\kappa^{2}(x)|x\rangle\langle y| + \dots$$
(4.17)

We recall that $|x\rangle$ is a single-particle state such that

$$\hat{\Psi}_I^{\dagger}(u)\hat{\Psi}_I(u)|x\rangle = \delta(x-u)|x\rangle. \tag{4.18}$$

We can then conclude that

$$e^{\hat{A}\int \mathrm{d}u\kappa(u):\hat{\Psi}_I^{\dagger}(u)\hat{\Psi}_I(u):} |x\rangle\langle y| = e^{\hat{A}\kappa(x)} |x\rangle\langle y|. \tag{4.19}$$

Using this result we can evaluate the trace in Eq. (4.15) as

$$\chi(\lambda) = \left\langle \int dy e^{it\lambda_0 \int dx \kappa(x) : \hat{\Psi}_C^{\dagger}(x) \hat{\Psi}_C(x) : \kappa(y)} |f(y)|^2 \right\rangle. \tag{4.20}$$

Close to the Fermi level the dispersion relation is linear. The time-dependence of the field operators is then $\hat{\Psi}(x,t) = \hat{\Psi}(x_t)$, having introduced the shorthand notation $x_t = x - v_F t$, where v_F is the Fermi velocity. The operator now has to be averaged over the initial state in Eq. (4.16). This procedure yields

$$\chi(\lambda, t) = \left\langle \int \mathrm{d}y e^{i\lambda_0 \int_0^t \mathrm{d}t' \int \mathrm{d}x : \hat{\Psi}_1^{\dagger}(x) \hat{\Psi}_1(x) : \kappa(x_{-t'}) \kappa(y_{-t'})} |f(y)|^2 \right\rangle. \tag{4.21}$$

Using the specific kernel $\kappa(x)$ given by Eq. (4.12), we then obtain Eqs. (4.13) and (4.14). We first consider the injection of electron wave packets with small widths compared to a, so that we can approximate $|f(y)|^2 \simeq \delta(y)$ and $: \Psi_C^{\dagger}(x)\Psi_C(x) : \simeq \delta(x + v_F\tau)\hat{n}(x)$, where $\hat{n}(x)$ is the number operator for excess electrons in the conductor at position x and τ is the time delay between the injection of electrons into the conductor and the interferometer. Equation (4.13) then yields

$$\chi(\lambda) = \left\langle e^{i\hat{n}\lambda(\tau)} \right\rangle,\tag{4.22}$$

with

$$\lambda(\tau) = \lambda_0 e^{-v_F \tau/a} \left(1 + \frac{v_F \tau}{a} \right). \tag{4.23}$$

Equation (4.23) is the second important result of this chapter. It shows that the effective counting field λ can be controlled by changing the time delay τ . Negative values of the counting field can be realized by injecting hole-like excitations into the interferometer. The specific functional form of Eq. (4.23) is determined by the coordinate kernels in Eq. (4.12) and, in reality, the dependence on τ may be different. Experimentally, one may then obtain $\lambda(\tau)$ using a conductor with a known FCS, e. g. a fully open QPC, for calibration.

In general, the wave functions have a finite width. Evaluating Eq. (4.13) with the same wave functions f(x) in the conductor and the interferometer, we find

$$\chi_{\text{meas}}(\lambda) = \int dy |f(y)|^2 \chi(\widetilde{\lambda}(y,\lambda))$$
(4.24)

with

$$\widetilde{\lambda}(y,\lambda) = \lambda \int dx \Phi(x,y) |f(x)|^2$$
(4.25)

and λ given by Eq. (4.23). Thus, for finite widths a measurement yields an average of MGFs for different effective couplings. However, if the pulses applied to the interferometer are sharper than the length of the interaction regions, we can incorporate the finite width of the electrons in the conductor into a rescaling of the effective counting field λ , which again can be obtained by proper calibration.

4.4. Applications

4.4.1. Driven quantum point contact

To illustrate our measurement scheme, we consider a QPC driven by Lorentzian voltage pulses of unit charge as realized in recent experiments [Dubois et al., 2013a; Jullien et al., 2014]. The QPC transmits electrons with probability T, and the exact MGF reads

$$\chi(\lambda) = 1 + T(e^{i\lambda} - 1). \tag{4.26}$$

The measured MGF is given by Eq. (4.24) with a Lorentzian wave packet

$$|f(y)|^2 = \frac{2\Gamma}{y^2 + \Gamma^2}$$
 (4.27)

of width Γ . We now obtain the cumulants of the current as

$$\langle \langle I^m \rangle \rangle = \frac{e^m}{\mathcal{T}} \partial_{i\lambda}^m \ln\{\chi_{\text{meas}}(\lambda)\}|_{\lambda \to 0},$$
 (4.28)

where λ is the rescaled counting field. In Fig. 4.2a we show results for the cumulants as functions of the QPC transmission. For narrow wave packets, we find good agreement with analytic results for a binomial process.

Next, we turn to the full distribution of transferred charge after N periods, given by the inversion formula

$$P(n) = \frac{1}{2\pi} \int_{-\pi}^{\pi} d\lambda e^{N[\ln\{\chi_{\text{meas}}(\lambda)\} - i\lambda n/N]}.$$
 (4.29)

For a large number of periods, $N \gg 1$, the distribution of the current $I = en/(N\mathcal{T})$ takes on the large-deviation form $P(I) \simeq e^{\mathcal{G}(I)N}$ following from a saddle-point approximation of the integral in Eq. (4.29). Here, the rate function $\mathcal{G}(I)$ describes the exponentially rare current fluctuations, beyond what is captured by the central-limit theorem. In Fig. 4.2b, we again find good agreement with the analytic result for a binomial distribution.

4.4.2. Entanglement entropy

Finally, as a further application of our scheme, we consider measuring the entanglement entropy generated by partitioning electrons on a QPC. Recently, it has been realized that the entanglement entropy between two electronic reservoirs connected by a QPC is closely linked to the FCS [Klich and Levitov, 2009; Song et al., 2011, 2012; Petrescu et al., 2014; Thomas and Flindt, 2015]. Specifically, the entanglement entropy generated per period can be approximated from the first four current cumulants as [Song et al., 2011, 2012]

$$S \simeq \alpha_2 \langle \langle I^2 \rangle \rangle + \alpha_4 \langle \langle I^4 \rangle \rangle,$$
 (4.30)

where the coefficients

$$\alpha_m = 2\sum_{k=m-1}^4 \frac{S_1(k, m-1)}{e^m k! k} \tag{4.31}$$

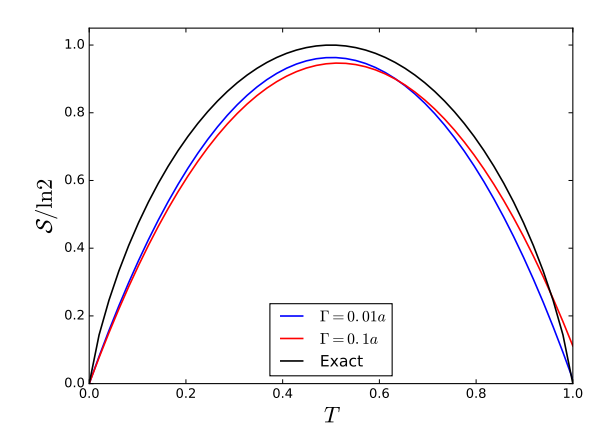


Figure 4.3.: The entanglement entropy generated per period obtained from Eq. (4.30). The exact result for the entanglement entropy reads $S = (T-1)\ln(1-T) - T\ln T$. The maximum value $S = \ln 2$ is obtained for T = 1/2. [Dasenbrook and Flindt, 2016a].

are given by the unsigned Stirling numbers of the first kind $S_1(k, m)$. Figure 4.3 shows that the entanglement entropy obtained from the cumulants in Fig. 4.2a is in good agreement with the exact result. This demonstrates that the entanglement entropy in a fermionic quantum many-body system may be within experimental reach.

4.5. Dephasing

We now breifly comment on the effects of unwanted environmental dephasing on our measurement scheme. Our scheme is based on the reduced visibility of the current oscillations in the Mach-Zehnder interferometer due to the dephasing induced by electrons in the conductor. In realistic systems, however, the visibility will already be reduced due to other dephasing mechanisms such as finite temperatures, the coupling to bulk electrons, co-propagating edge states, or electrons in the Fermi sea [Levkivskyi and Sukhorukov, 2008]. These effects are encoded in an additional fluctuating phase $\delta\theta$ [Ji et al., 2003; Roulleau et al., 2009; Bieri et al., 2009]. For a Gaussian distribution of width σ , the measured MGF simply gets rescaled as $\chi_{\rm meas}(\lambda) \to e^{-\sigma^2}\chi_{\rm meas}(\lambda)$, and the width can be determined from a visibility measurement without electrons injected into the conductor. For non-Gaussian fluctuations [Neder and Marquardt, 2007; Helzel et al., 2015], the total measured MGF takes the form $\chi_{\rm meas}(\lambda) \to \chi_{\rm meas}(\lambda)\chi_{\rm env}(\lambda_0)$ for some fixed coupling λ_0 to the environment, such that the environmental contribution $\chi_{\rm env}(\lambda_0)$ again can be factored out. Here we assume that the noise sources are uncorrelated.

4.6. Conclusions

Electronic Mach-Zehnder interferometers can function as detectors of current fluctuations in mesoscopic conductors. Equation (4.9) expresses the full counting statistics exclusively in terms of average currents measured at the outputs of the interferometer. Equation (4.23) shows that the counting field can be controlled by varying the time delay between separate voltage signals. These findings make it possible to measure the current cumulants as well as the full distribution of current fluctuations as illustrated in Fig. 4.2. Our scheme is robust against moderate dephasing and finite temperature effects. As an application we have shown that our scheme enables measurements of the entanglement entropy in fermionic many-body systems. Extensions of our work may facilitate the detection of short-time quantities such as the electronic waiting time distribution discussed in the previous chapters.

Part II.

Entanglement in mesoscopic conductors

5. Dynamical entanglement of neutral leviton pairs

5.1. Introduction

Entanglement is one of the most fascinating phenomena in quantum physics, and it can lead to many useful effects such as nonlocality (the observation of correlations that are inexplicable in a locally realistic model of the world, such as classical physics) [Brunner et al., 2014], teleportation [Beenakker and Kindermann, 2004] or dense coding (the ability to transmit two bits of classical information using a quantum two-level system and some pre-shared entanglement), among others [Horodecki et al., 2009].

A pure quantum state is considered entangled across a given bipartition of the Hilbert space,

$$\mathcal{H} = \mathcal{H}_A \otimes \mathcal{H}_B, \tag{5.1}$$

if it cannot be written as a direct product of states from \mathcal{H}_A and \mathcal{H}_B :

$$|\Psi\rangle \neq |\phi\rangle_A |\phi\rangle_B,$$
 (5.2)

where $|\phi\rangle_A \in \mathcal{H}_A$ and $|\phi\rangle_B \in \mathcal{H}_B$. A mixed state is entangled if it cannot be written as a convex decomposition into pure separable (non-entangled) states:

$$\rho \neq \sum_{n} p_n |\phi_n\rangle \langle \phi_n|, \qquad (5.3)$$

with all $|\phi_n\rangle$ separable. In general, to determine whether a given mixed state is entangled can be a hard problem, even mathematically. Furthermore, when implementing an experiment that generates entangled states, it is desirable to use a measurement strategy that clearly discriminates entangled states (possibly showing non-classical correlations) from non-entangled states. This can be difficult if the kinds of measurement one can perform are restricted by some fundamental principle or just some practical concerns, or if external noise causes dephasing and loss of coherence.

In quantum optics, entangled states of few photons are now routinely generated and used to test the foundations of quantum mechanics. Similarly, entanglement has been successfully realized and detected in systems of cold atoms [Bloch, 2008] and NV-centres in diamond, such as in the recent loophole-free demonstration of nonlocality [Hensen et al., 2015]. Given the level of control down to the single-electron level that has been achieved in mesoscopic conductors, it would of course be desirable to generate and detect entangled states of electrons in these systems. To this end, several strategies have been

proposed, using the spin- and orbital degree of freedom of the electrons. By contrast, an experimental verification of controlled electronic entanglement is still missing.

In this and the following chapter, our focus will be on a conceptually somewhat different type of entanglement, called occupation number entanglement. In this case, the different basis states may differ in their particle number. The detection of entanglement using this number degree of freedom is not as obvious as for other types of entanglement, and for this reason, occupation number entanglement has so far received only limited attention. However, as we will show, even the experimental prospects for demonstrating this kind of entanglement may look promising, if the setups and observables are chosen in a careful way.

5.2. Electron-hole entanglement

Entangled modes with different photon numbers can be generated by sending single photons onto a beam splitter [Björk et al., 2001; van Enk, 2005]. Due to particle number superselection rules this type of entanglement has often been considered inaccessible [Wiseman and Vaccaro, 2003]. Further investigations have however clarified that entangled states of different photon numbers provide a resource that is as useful as polarisation-entangled photons [Lombardi et al., 2002; Bartlett et al., 2007; Salart et al., 2010; Takeda et al., 2015]. Advancing similar techniques to entangle states of different electron numbers is clearly desirable, however, the task is challenging. For example, a suitable witness to detect the electronic entanglement must be identified. As such, earlier proposals have instead focused on the orbital entanglement of several electron-hole pairs [Beenakker et al., 2003; Samuelsson et al., 2004; Samuelsson and Büttiker, 2005; Sherkunov et al., 2012] or pairs of electrons [Samuelsson et al., 2003; Sim and Sukhorukov, 2006; Samuelsson et al., 2009b].

Electron-hole pairs naturally occur in mesoscopic conductors as a result of time-dependent perturbations [Vanević et al., 2007]. These pairs can be split at electronic beam splitters, resulting in an electron-hole state delocalized over two different modes:

$$\left|\Psi\right\rangle = \frac{1}{2}\left(\left|0\right\rangle_{A}\left|2\right\rangle_{B} + \left|2\right\rangle_{A}\left|0\right\rangle_{B} + \left|+\right\rangle_{A}\left|-\right\rangle_{B} + \left|-\right\rangle_{A}\left|+\right\rangle_{B}\right),\tag{5.4}$$

where the $|0/2/+/-\rangle_{\alpha}$ denote 0 or 2 particles, or the hole (+) or the electron (-) in mode $\alpha = A, B$. In this notation, one might naturally consider treating the the electron-hole degree of freedom (+ or -) as a pseudo-spin: The hole could be identified with a spin-up particle, and the electron with a spin-down particle. Then, post-selecting the last two terms out of the state in Eq. (5.4), one obtains the analogue of a maximally entangled spin-singlet.

We call the entanglement using the electron-hole "pseudo-spin" degree of freedom electron-hole entanglement, and it is one example of entanglement using the electron occupation number: The two pseudo-spin states that encode the quantum information differ by a particle number of two. To detect the entanglement and see any non-classical correlations, we have to be able to partially rotate one of the basis states on the Bloch

sphere, which is made difficult by the charge superselection rule [Bartlett et al., 2007]. Note that in this case, this superselection rule might be lifted by providing a common phase reference between modes A and B in the form of a superconductor [Beenakker, 2014]. A different way to detect the entanglement is to perform a nonlocal measurement.

In this chapter we present an experimental recipe for the detection of electron-hole entanglement in an electronic conductor. Specifically, we demonstrate that noise measurements at the outputs of an electronic Mach-Zehnder interferometer, despite the fermionic superselection rules, can provide a robust witness of electron-hole entanglement. This is an example of a non-local measurement, since the split state is recombined at a beam splitter before the measurement.

For the generation of electron-hole entanglement, a state with one positively-charged leviton and one negatively-charged leviton is produced at a quantum point contact (QPC) and is delocalised across the two arms of the interferometer. Due to particle number conservation the electron-hole entanglement in the state cannot easily be used to violate a Bell inequality [Brunner et al., 2014]. We circumvent this problem by recombining the state at a second QPC. As we show, an entanglement witness can be constructed from cross-correlation measurements at the output arms. We evaluate the entanglement witness using Floquet theory and find that the electron-hole entanglement can be detected for realistic system parameters, including finite electronic temperatures and dephasing corresponding to recent experiments [Ji et al., 2003; Neder et al., 2007c; Roulleau et al., 2007; Litvin et al., 2008; Huynh et al., 2012].

In chapter 6, we go one step further and show that even the state of just a single electron split between two electronic modes is entangled. This case is conceptually even more interesting, since in this case the parity superselection rule has to be circumvented, which is considered to be more fundamental than charge superselection [Friis, 2016].

5.3. Setup

5.3.1. Mach-Zehnder interferometer

The interferometer consists of a Corbino disk in the quantum Hall regime with electronic motion along edge states from left to right as in Fig. 5.1. The upper and lower arms of the interferometer form a loop that encloses the magnetic flux ϕ . In addition, electrons above the Fermi level in the upper arm can enter a small cavity which encloses the flux ϕ_c . Two QPCs act as electronic beam splitters. Contrary to recent experiments, all contacts are grounded. Instead, we modulate the transmission probability of the first QPC periodically in time in such a way that clean electron-hole excitations are generated out of the otherwise undisturbed Fermi sea at the location of the QPC. Each electron-hole pair delocalises across the arms of the interferometer, leading to a superposition of a negatively-charged leviton being in the upper arm and a positively-charged leviton in the lower arm and vice versa. As we go on to show, the resulting electron-hole entanglement can be detected by measuring the cross-correlations of the currents in the output arms after the second QPC.

5. Dynamical entanglement of neutral leviton pairs

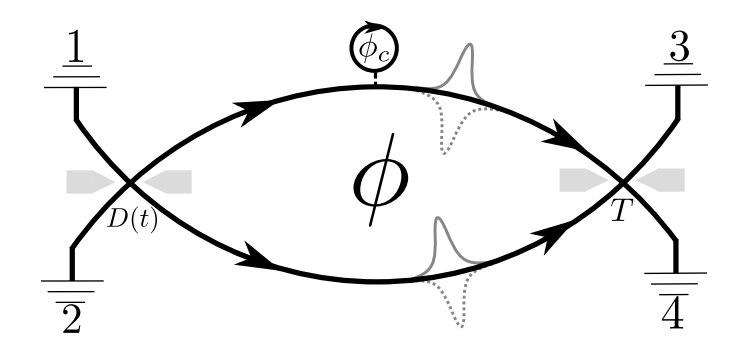


Figure 5.1.: Dynamic Mach-Zehnder interferometer. Entangled states of neutral leviton pairs are generated by modulating the transmission $D(t) = |d(t)|^2$ of the first QPC periodically in time. The levitons travel along edge states to the second QPC with transmission T and the entanglement is detected by measuring the current cross-correlations at the output arms. The interferometer encloses the magnetic flux ϕ . Negatively-charged levitons in the upper part can enter a small cavity with magnetic flux ϕ_c and pick up an additional phase. ([Dasenbrook and Flindt, 2015], (C) 2015 American Physical Society.)

5.3.2. Dynamical entanglement generation

We start with the generation of clean electron-hole pairs at a QPC. This problem is closely related to the creation of levitons by applying Lorentzian-shaped voltage pulses to a contact [Ivanov et al., 1997; Levitov et al., 1996; Keeling et al., 2006; Dubois et al., 2013a]. As predicted by Levitov and co-workers and recently realised experimentally [Dubois et al., 2013b; Jullien et al., 2014], pulses of the form

$$V(t) = -\frac{\hbar}{e} \sum_{n=-\infty}^{\infty} \frac{2\eta}{(t+n\mathcal{T})^2 + \eta^2},$$
(5.5)

lead to the emission of levitons from the contact on top of the otherwise undisturbed Fermi sea (with a hole-like leviton going into the contact). The width of the pulses is η and \mathcal{T} the period of the driving. Levitons are created as each electron leaving the contact picks up the phase factor $e^{i\varphi(t)}$ with the phase given as

$$\varphi(t) = -\frac{e}{\hbar} \int_0^t dt' V(t'). \tag{5.6}$$

See also Appendix A for a discussion of the Floquet scattering matrix for the creation of levitons. The phase changes sign $\varphi(t) \to -\varphi(t)$ upon inverting the voltage $V(t) \to -V(t)$, leading to the emission of a hole-like leviton from the contact.

Remarkably, a similar strategy can be used to generate superpositions of electron-like and hole-like levitons by modulating the transmission of a QPC periodically in time [Sherkunov et al., 2009; Zhang et al., 2009]. To see this, we consider the time-dependent

scattering matrix of the first QPC in Fig. 5.1,

$$S(t) = \begin{bmatrix} r(t) & d(t) \\ -d(t) & r(t) \end{bmatrix}, \tag{5.7}$$

where the reflection and transmission amplitudes, chosen to be real below, fulfil $|r(t)|^2 + |d(t)|^2 = 1$. Switching to the eigenbasis of S(t), particles in the two incoming eigenchannels will be completely reflected with the reflection amplitudes $r(t) \pm id(t)$ given by the eigenvalues of S(t). We now choose the transmission and reflection as

$$d(t) = \sin \varphi(t),$$

$$r(t) = \cos \varphi(t)$$
(5.8)

with $\varphi(t)$ given by Eq. (5.6). The reflection amplitudes in the eigenbasis then become $r(t)\pm id(t)=e^{\pm i\varphi(t)}$, implying that an electron-like leviton is reflected in one eigenchannel and a hole-like leviton in the other. Returning to the physical channels of the QPC, the outgoing state after the small cavity in Fig. 5.1 becomes

$$|\Psi\rangle = \frac{1}{2} \left(e^{i\vartheta} \hat{b}_{u-}^{\dagger} \hat{b}_{u+}^{\dagger} - \hat{b}_{l-}^{\dagger} \hat{b}_{l+}^{\dagger} + i \left\{ e^{i\vartheta} \hat{b}_{u-}^{\dagger} \hat{b}_{l+}^{\dagger} + \hat{b}_{u+}^{\dagger} \hat{b}_{l-}^{\dagger} \right\} \right) |0\rangle , \qquad (5.9)$$

where $|0\rangle$ is the filled Fermi sea at zero temperature and the Fermi energy is zero. The operators $\hat{b}_{i-}^{\dagger} = \sum_{E>0} e^{-\eta E} \hat{b}_{i}^{\dagger}(E)$ and $\hat{b}_{i+}^{\dagger} = \sum_{E<0} e^{\eta E} \hat{b}_{i}(E)$ create electron-like and hole-like levitons in the upper (i=u) or lower (i=l) arms of the interferometer, and $\hat{b}_{i}^{\dagger}(E)$ creates electrons at energy E in either of the two arms. We assume for now that the effect of the small cavity can be encoded in a tunable phase $\vartheta = \vartheta(\phi_c)$ picked up by electron-like levitons in the upper arm. Below, we return to a more detailed description of the cavity [see Eq. (5.26)]. As Eq. (5.9) cannot be written as a product of b_u^{\dagger} and b_l^{\dagger} operators, the state is entangled. Furthermore, the projection of the state on the subspace with one particle per arm (in curly brackets) is maximally entangled in the electron-hole degree of freedom. This is the entanglement we wish to detect. We note that the state in Eq. (5.9) can also be generated by emitting levitons from different inputs onto the QPC tuned to half transmission using quantum capacitors with a linear drive [Büttiker et al., 1993; Keeling et al., 2008].

5.4. Entanglement witness

It is difficult to formulate a Bell inequality for the entanglement between modes of different particle numbers. (It would require measurements in a basis of non-definite particle number and for electrons a superconductor, for instance, would be needed [Beenakker, 2014]). Furthermore, the violation of Bell inequalities often relies on very high visibilities and is therefore currently out of reach for mesoscopic conductors. To circumvent these problems, we instead construct an entanglement witness based on current cross-correlation measurements at the output arms after the second QPC, similar to what has been considered in the context of spin entanglement [Burkard and Loss, 2003; Giovannetti

5. Dynamical entanglement of neutral leviton pairs

et al., 2006]. To develop our witness, we consider a general two-leviton state incident on the second QPC

$$|\Upsilon\rangle = \sum_{\substack{\alpha,\beta=\pm\\i,j=u,l}} \Upsilon_{\alpha\beta}^{ij} \hat{b}_{i\alpha}^{\dagger} \hat{b}_{j\beta}^{\dagger} |0\rangle$$
 (5.10)

with the normalisation condition $\sum_{\alpha\beta ij} |\Upsilon^{ij}_{\alpha\beta}|^2 = 1$. Equation (5.9) is a particular example of such a state.

If the projection on the single-particle sector is separable, the matrix Υ^{ul} has rank one [Amico et al., 2008]. Calculating the cross-correlator

$$S_{34}(\phi) = \langle \hat{I}_3 \hat{I}_4 \rangle \tag{5.11}$$

measured after the second QPC, we can then show that the function

$$f(\phi) \equiv S_{34}(\phi) - S_0(1 - 2TR) \tag{5.12}$$

is always zero or negative. Here,

$$S_0 = \sum_{\alpha\beta} \alpha\beta |\Upsilon^{ul}_{\alpha\beta}|^2 \tag{5.13}$$

is the noise at zero transmission and $\phi=2\pi\Phi/\Phi_0$ is the Aharonov-Bohm phase with Φ being the magnetic flux enclosed by the interferometer and $\Phi_0=h/e$ the magnetic flux quantum.

We now derive this entanglement witness. The general input state is given by Eq. (5.10). The cross-correlator $S_{34}(\phi)$ measured after the second QPC, with transmission probability T and reflection R, can be written as $S_{34}(\phi) = S_{34}^{(1)}(\phi) + S_{34}^{(2)}(\phi)$, where

$$S_{34}^{(1)}(\phi) = S_0(1 - 2TR) - 2TR \sum_{\alpha\beta} \Upsilon_{\alpha\beta}^{ul*} \Upsilon_{\beta\alpha}^{ul} e^{i(\beta - \alpha)\phi}$$

$$(5.14)$$

is the contribution from the single-particle subspace [terms with $i \neq j$ in Eq. (5.10)] and

$$S_{34}^{(2)}(\phi) = -2TR \left| \Upsilon_{+-}^{uu} - \Upsilon_{-+}^{ll} \right|^2$$
 (5.15)

is the two-particle contribution. The single-particle term contains the Aharonov-Bohm phase $\phi = 2\pi\Phi/\Phi_0$, where Φ is the magnetic flux enclosed by the interferometer and $\Phi_0 = h/e$ is the magnetic flux quantum.

Now, we consider the function

$$f(\phi) \equiv S_{34}(\phi) - S_0(1 - 2TR)$$

$$= -2TR \left[\sum_{\alpha\beta} \Upsilon^{ul*}_{\alpha\beta} \Upsilon^{ul}_{\beta\alpha} e^{i(\beta - \alpha)\phi} + \left| \Upsilon^{uu}_{+-} - \Upsilon^{ll}_{-+} \right|^2 \right]. \tag{5.16}$$

If the projection of the state Eq. (5.10) onto the subspace with one particle per arm is separable, Υ^{ul} is a matrix of rank one, so it can be factorised as $\Upsilon^{ul}_{\alpha\beta} = v_{\alpha}^{(1)} v_{\beta}^{(2)}$. Then, $f(\phi)$ can be written as

$$f(\phi) = -2TR \left[\left| \sum_{\alpha} v_{\alpha}^{(1)*} v_{\alpha}^{(2)} e^{-i\alpha\phi} \right|^{2} + \left| \Upsilon_{+-}^{uu} - \Upsilon_{-+}^{ll} \right|^{2} \right].$$
 (5.17)

Clearly, in this case $f(\phi) \leq 0$, proving that the condition

$$f(\phi) > 0 \tag{5.18}$$

acts as a witness for entanglement on the single-particle subsector.

Moreover, for a general separable density matrix [Horodecki et al., 2009]

$$\hat{\rho} = \sum_{n} p_n |\Upsilon_n\rangle \langle \Upsilon_n| \tag{5.19}$$

with each $|\Upsilon_n\rangle$ of the form (5.10) and separable, the noise is the average noise of each separable state weighted by the probabilities p_n . Therefore, the condition $f(\phi) > 0$ provides a witness of electron-hole entanglement also at finite temperatures. The witness is not optimal, since negative two-particle contributions to the noise [terms with i = j = u or i = j = l in Eq. (5.10)] can make it harder to detect the entanglement, even if it is maximal [Horodecki et al., 2009]. Importantly, our witness relies on reconnecting the two arms at the second QPC, making the measurement nonlocal. This is the key ingredient that allows us to circumvent the superselection rules for particle number.

Evaluating the witness for the state in Eq. (5.9), we first find a pure interference current determined by the enclosed fluxes,

$$\langle \hat{I}_3 \rangle = -\langle \hat{I}_4 \rangle = e(\Omega/\pi)\sqrt{TR}\cos[\vartheta(\phi_c)/2]\sin[\phi + \vartheta(\phi_c)/2],$$
 (5.20)

where $\Omega = 2\pi/\mathcal{T}$ is the frequency of the driving. For the current cross-correlator, we find

$$S_{34} = -\frac{e^2\Omega}{4\pi} \left[1 - 2TR\left\{1 - \cos(2\phi)\right\}\right] + \langle \hat{I}_3 \rangle \langle \hat{I}_4 \rangle. \tag{5.21}$$

Both the current and the noise are independent of the pulse width η , which determines the spatial extent of the levitons. Now, tuning the phase $\vartheta(\phi_c)$ to π and choosing T = R = 1/2, the average currents vanish and the witness becomes

$$f(\phi) = -e^2 \Omega/(8\pi) \cos(2\phi),$$
 (5.22)

which clearly can be positive, signalling electron-hole entanglement.

5.5. Floquet scattering theory

The noise in Eq. (5.21) corresponds to the ideal case of the entangled state in Eq. (5.9). We now proceed with a full Floquet calculation [Moskalets and Büttiker, 2002; Moskalets, 2011] of the entanglement witness for the interferometer in Fig. 5.1, including finite electronic temperatures and a detailed description of the small cavity. In this case, the outgoing state is not known and we need to evaluate the witness to detect the entanglement. As we will see, electron-hole entanglement is detectable under realistic experimental conditions.

5.5.1. Realistic description

The current operator in contact i can be written as

$$\hat{I}_i = \frac{e}{h} \int_{-\infty}^{\infty} dE \left(\hat{c}_i^{\dagger}(E) \hat{c}_i(E) - \hat{a}_i^{\dagger}(E) \hat{a}_i(E) \right)$$
(5.23)

in terms of the operators for particles at energy E incoming from and outgoing to reservoir i, respectively. As usual, the operators for outgoing particles can be expressed as

$$\hat{c}_i(E) = \sum_{j} \sum_{n=-\infty}^{\infty} \mathcal{S}_{ij}(E, E_n) \hat{a}_j(E_n), \qquad (5.24)$$

where S is the Floquet scattering matrix and $\hat{a}_j(E)$ are operators for incoming particles from reservoir j.

The Floquet amplitudes for incoming particles at energy E to scatter into the outgoing reservoirs with energy $E_n = E + n\hbar\Omega$, having absorbed (n > 0) or emitted (n < 0) |n| energy quanta of size $\hbar\Omega$, read

$$S_{31}(E_n, E) = -\sqrt{T} S_F^d(n) + \sqrt{R} e^{i\phi} S_c(E_n) S_F^r(n),$$

$$S_{32}(E_n, E) = \sqrt{T} S_F^r(n) - \sqrt{R} e^{i\phi} S_c(E_n) S_F^d(n),$$

$$S_{41}(E_n, E) = \sqrt{R} S_F^d(n) + \sqrt{T} e^{i\phi} S_c(E_n) S_F^r(n),$$

$$S_{42}(E_n, E) = -\sqrt{R} S_F^r(n) - \sqrt{T} e^{i\phi} S_c(E_n) S_F^d(n).$$
(5.25)

Here, the Floquet amplitudes of the first QPC, $S_F^s(n) = \int_0^{\mathcal{T}} \mathrm{d}t s(t) e^{in\Omega t}/\mathcal{T}$, with s=d,r given in Eq. (5.8), are $S_F^d(n\neq 0) = -\sinh(2\pi\eta)e^{-2\pi|n|\eta}$, $S_F^d(n=0) = e^{-2\pi\eta}$ and $S_F^r(n) = \mathrm{sgn}(n)\sinh(2\pi\eta)e^{-2\pi|n|\eta}$. In addition, the scattering matrix of the small cavity reads

$$S_c(E) = r_c(E) + t_c^2(E) \frac{e^{i(\phi_c + E\tau/\hbar + \pi)}}{1 + r_c(E)e^{i(\phi_c + E\tau/\hbar + \pi)}},$$
(5.26)

where τ is the time it takes to complete one loop inside the cavity and

$$t_c(E) = \frac{1}{e^{-\mathcal{B}E} + 1} \tag{5.27}$$

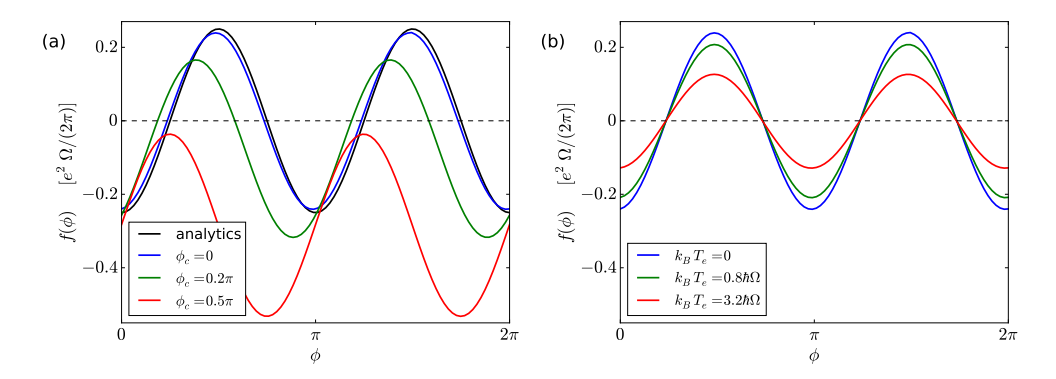


Figure 5.2.: Entanglement witness. (a) The witness $f(\phi)$ as a function of the Aharonov-Bohm phase ϕ with different values of the flux ϕ_c enclosed by the small cavity. The electronic temperature is zero. Positive values of f (above the dashed line) signal electron-hole entanglement. With $\phi_c = 0$, the Floquet calculation is close to the analytic result $-\cos(2\phi)/4$ (black line) corresponding to the maximally entangled state in Eq. (5.9). The parameters of the cavity are $\tau = \mathcal{T}/50$ and $\mathcal{B} = 5\mathcal{T}/\hbar$. (b) The witness $f(\phi)$ as a function of ϕ with $\phi_c = 0$ and different electronic temperatures T_e . An increased temperature merely decreases the amplitude of the oscillations, so that the entanglement is still detectable at finite temperatures. ([Dasenbrook and Flindt, 2015], (C) 2015 American Physical Society.)

is the transmission amplitude into the cavity with the cut-off \mathcal{B} being tunable by a magnetic field [Fertig and Halperin, 1987; Büttiker, 1990a]. The reflection amplitude is $r_c(E) = \sqrt{1 - t_c^2(E)}$. With a sharp cut-off $\mathcal{B} \gg \mathcal{T}/h$ and a short loop-time $\tau \ll \mathcal{T}$, we recover the state in Eq. (5.9) with $\vartheta(\phi_c) \simeq \phi_c + \pi$.

Figure 5.2 shows the entanglement witness calculated using Floquet scattering theory [Moskalets and Büttiker, 2002; Moskalets, 2011]. We vary the Aharonov-Bohm phase ϕ and show in panel (a) results for different values of the flux ϕ_c enclosed by the cavity. The electronic temperature is zero. The entanglement cannot be detected in all situations. However, by tuning ϕ_c we come close to the analytic result (black line) corresponding to the maximally entangled state in Eq. (5.9). The system then maximally violates the inequality $f(\phi) \leq 0$ in the sense that the witness has the same weight above and below the f = 0 line as a function of ϕ . Under this condition, the witness is thus expected to be very robust against a decreased visibility, in contrast to entanglement detection based on Bell inequalities [Samuelsson et al., 2009b].

In panel (b) we fix the optimal value of $\phi_c = 0$ and consider the effect of a finite electronic temperature. With increasing temperature, the amplitude of the oscillations decreases and the entanglement gets harder to detect. Still, even with temperatures that are higher than the driving frequency, the witness can become positive and entanglement can be detected. Since there is no direct scattering path between the two output reservoirs, thermal noise is not visible in the witness [Hofer and Flindt, 2014]. The re-

5. Dynamical entanglement of neutral leviton pairs

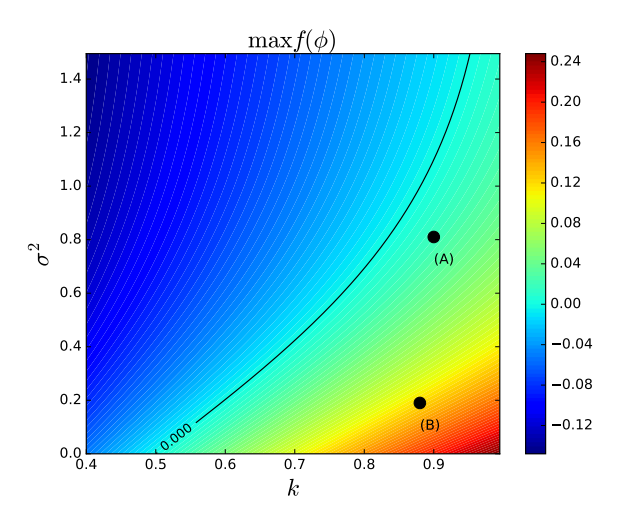


Figure 5.3.: Influence of dephasing. The maximum value of the entanglement witness $f(\phi)$ as a function of the decoherence parameter k and the variance of the phase σ^2 . The contour line separates the region of detectable electron-hole entanglement, where the witness is positive, from the region where the entanglement cannot be detected. The black dots mark the experimental parameters from Ji et al. [2003] (A) and Neder et al. [2007c] (B), which lie in the region of detectable entanglement. ([Dasenbrook and Flindt, 2015], (C) 2015 American Physical Society.)

sults in Fig. 5.2 are promising for the detection of electron-hole entanglement in driven mesoscopic conductors.

5.5.2. Dephasing

Finally, to estimate the influence of dephasing and phase averaging, we return to the analytic result for the noise in Eq. (5.21). Focusing on the optimal value $\vartheta = \pi$, the noise can be written as

$$S_{34} = -e^2 \Omega/(4\pi) [1 - 2kTR\{1 - \exp(-2\sigma^2)\cos(2\phi)\}]$$
 (5.28)

in terms of the phenomenological parameters k [Ji et al., 2003] and σ^2 [Roulleau et al., 2007] which describe the coherence of the wave function across the interferometer (k = 1 meaning full coherence and k = 0 no coherence, e. g. as a result of a finite electronic temperature or interactions) and the variance of the total Aharonov-Bohm phase leading to phase-averaging. In Fig. 5.3 we show the maximal value of the witness $f(\phi)$ as a function of k and σ^2 . We find that the witness is robust against moderate dephasing mechanisms and that entanglement is detectable for parameters corresponding to the experiments reported by Ji et al. [2003]; Neder et al. [2007c]. This is in contrast to the detection of orbital entanglement based on a Bell inequality [Samuelsson et al., 2009b].

5.6. Conclusions

We have proposed and analysed a dynamical scheme to generate and detect entanglement in the electron-hole degree of freedom of leviton pairs. Measuring the cross-correlations at the output arms of a mesoscopic Mach-Zehnder interferometer, entanglement can be detected despite superselection rules. The entanglement witness is robust against moderate dephasing mechanisms and entanglement can be detected using current technologies.

6. Single-electron entanglement and nonlocality

6.1. Introduction

It is a question that has been much debated whether a state of a single particle in a superposition of two spatially separate modes should be considered entangled [Tan et al., 1991; Hardy, 1994; Greenberger et al., 1995; Vaidman, 1995; Hardy, 1995; Wiseman and Vaccaro, 2003; Bartlett et al., 2007]. For photons (and other bosons) it is by now well established that the answer is yes, and that the entanglement is in fact useful in quantum communication applications [van Enk, 2005; Sangouard and Zbinden, 2012]. For electrons (and other fermions), the situation is different because of the charge superselection rule, and the question still causes controversy [Lebedev et al., 2004; Wiseman et al., 2004; Samuelsson et al., 2005; Giovannetti et al., 2007; Sherkunov et al., 2009].

Here, we revisit this question motivated by the recent development of dynamic single-particle sources in electron quantum optics. We demonstrate rigorously that the answer for electrons is affirmative based on the situation sketched in Fig. 6.1(a): Two independent sources each produce a single electron which is delocalised with one part transmitted to location A and the other to B. Using only local operations (LOs) and measurements at each location, a Bell inequality between A and B is violated deterministically, i. e. without post-selection. This necessarily implies that there is entanglement between A and B. Since the sources are independent this in turn implies that the state emitted by a single source is entangled between regions A and B. Specifically, we show that such a situation can be realised in an electronic Hanbury Brown-Twiss interferometer driven by Lorentzian voltage pulses as illustrated in Fig. 6.1(b). Notably, the single-electron entanglement can be observed from current cross-correlation measurements at the outputs of the interferometer.

6.2. Single-particle entanglement

We start with a brief introduction to single-particle entanglement. A single particle in a superposition of two different locations can be described by the state

$$|\Psi\rangle = \frac{1}{\sqrt{2}} \left(|0\rangle_A |1\rangle_B + |1\rangle_A |0\rangle_B \right), \tag{6.1}$$

where the numbers in the kets indicate the particle numbers in the spatially separated modes. The basic question is whether such a state is entangled. One can ask the question

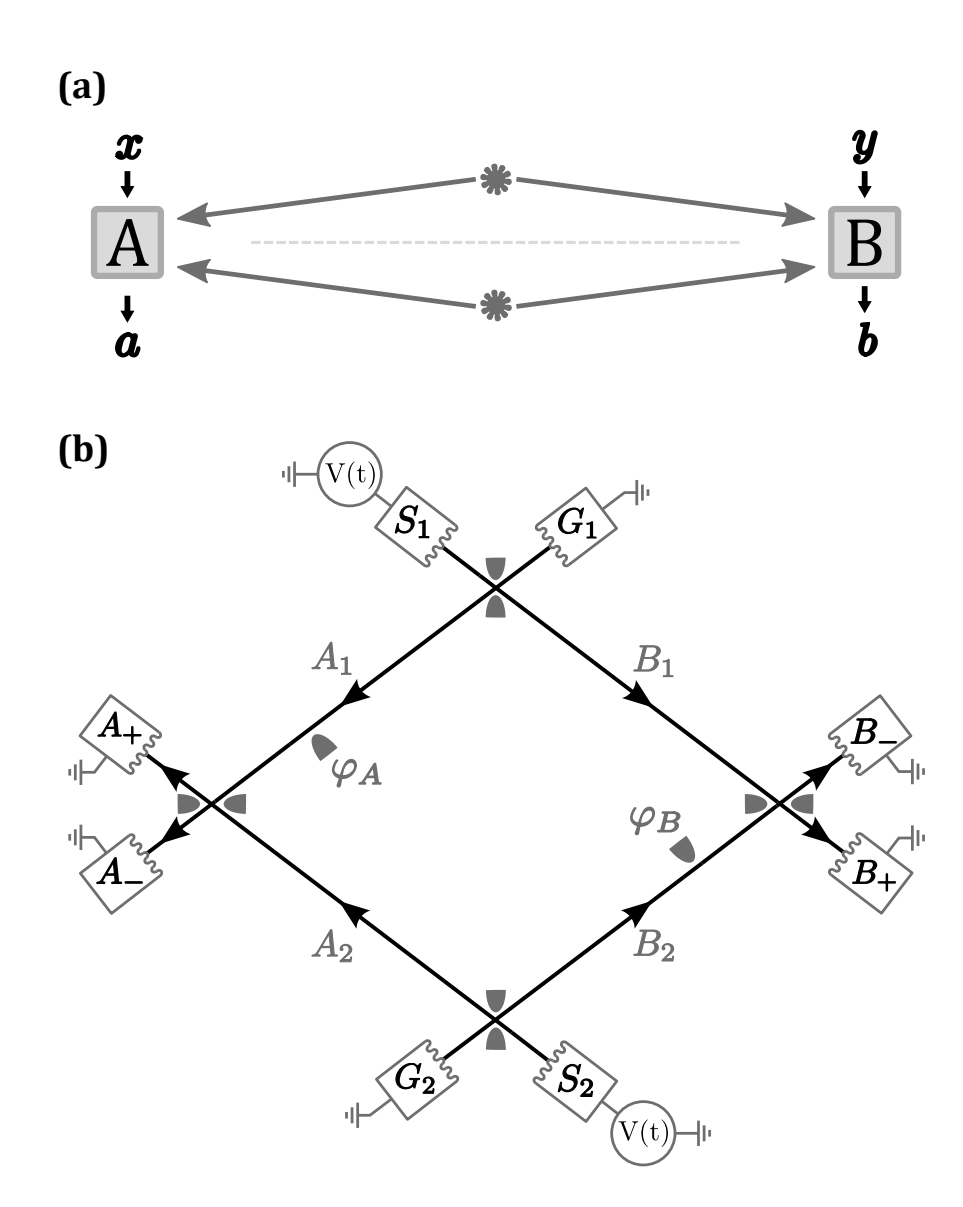


Figure 6.1.: Schematic setup. (a) Two independent single-electron sources emit delocalised electrons towards the locations A and B. A Bell test is performed using local operations and measurements at A and B. If the resulting data p(ab|xy) violates a Bell inequality, A and B necessarily share entanglement. Hence, the sources must emit entangled states. (b) Electronic Hanbury Brown-Twiss interferometer realising the idea in (a) for an experimental demonstration of single-electron entanglement. [Dasenbrook et al., 2016].

both for bosons and for fermions, in particular for photons and electrons. To answer affirmatively, the entanglement must be experimentally detectable.

Entanglement should be verified directly from measurements on each spatial mode in Eq. (6.1), e. g. by testing the observations against a Bell inequality [Bell, 1964; Brunner et al., 2014]. If arbitrary measurements were possible, Eq. (6.1) should indeed be considered entangled since it for example violates the Clauser-Horne-Shimony-Holt (CHSH) Bell inequality [Clauser et al., 1969]. However, the possible measurements may be limited because the state (6.1) is a single-particle state. Violating the CHSH inequality requires measurements which are not diagonal in the occupation number basis, i. e. they should contain projections onto superpositions of states with different particle numbers such as $(|0\rangle + |1\rangle)/\sqrt{2}$. One may therefore expect a fundamental difference between photons and electrons because global charge conservation forbids such superpositions for electrons [Schuch et al., 2004; Bartlett et al., 2007].

For photons it is by now established that the state (6.1) is entangled and in fact useful for applications in quantum communication [Sangouard et al., 2011; Sangouard and Zbinden, 2012]. Experimental demonstrations of single-photon entanglement have been reported using homodyne [Babichev et al., 2004; Fuwa et al., 2015] and weak displacement measurements [Hessmo et al., 2004; Monteiro et al., 2015]. These measurements require the use of coherent states of light (laser light), which introduces additional particles. These particles provide a reference frame between the observers [Bartlett et al., 2007; Bohr Brask et al., 2013]. Alternatively, single-photon entanglement can be converted into entanglement between two atoms [van Enk, 2005]. In Eq. (6.1), the numbers 0, 1 then represent internal atomic states and entanglement can be verified straightforwardly. Importantly, since the conversion process involves only LOs, one concludes that the original single-photon state (6.1) must have been entangled. These procedures, however, cannot be straightforwardly applied to fermions (for example, there is no equivalent of coherent states for fermions). Hence, a more careful analysis is necessary as we show in the following.

6.3. Setup for the demonstration of single-electron entanglement

We consider the experiment pictured in Fig. 6.1(b) and now argue that single-electron entanglement is observable. To keep the analysis simple, we work at zero temperature and assume that the sources create single electronic excitations above the Fermi sea which can be detected one by one. These assumptions do not contradict any fundamental principle such as charge conservation. We consider the possibility of an experimental implementation with current technology later on.

Single electrons are excited above the Fermi sea at the sources S_1 and S_2 , and are coherently split and interfered on electronic beamsplitters – quantum point contacts (QPCs) tuned to half transmission. Tunable phases φ_A and φ_B can be applied in one arm on either side of the interferometer. The phases can be tuned using side gates or by changing the magnetic flux Φ through the device. In the latter case, we have

 $2\pi\Phi/\Phi_0 = \varphi_A + \varphi_B$, where $\Phi_0 = h/e$ is the magnetic flux quantum.

Labelling the modes as indicated in the figure, in second quantized notation the top beam splitter implements the transformation

$$\begin{split} a_{S_1}^\dagger &\to (a_{A_1}^\dagger + a_{B_1}^\dagger)/\sqrt{2}, \\ a_{G_1}^\dagger &\to (a_{A_1}^\dagger - a_{B_1}^\dagger)/\sqrt{2} \end{split} \tag{6.2}$$

and similarly for the others. Here, we have introduced the fermionic creation and annihilation operators a_{α}^{\dagger} and a_{α} for electrons above the Fermi sea in mode α . Considering just the top source (S_1) , the state created after the beam splitter is thus

$$\frac{1}{\sqrt{2}}(a_{A_1}^{\dagger} + a_{B_1}^{\dagger}) |0\rangle, \qquad (6.3)$$

where the state $|0\rangle$ represents the undisturbed Fermi sea. This is the electronic version of Eq. (6.1), and we use the interferometer to demonstrate that the state indeed is entangled between the regions A and B.

The joint initial state of the two sources is $a_{S_1}^{\dagger} a_{S_2}^{\dagger} |0\rangle$, and the state evolution up to the output of the interferometer is then

$$\begin{split} a_{S_{1}}^{\dagger} a_{S_{2}}^{\dagger} & | 0 \rangle \rightarrow \frac{1}{2} (a_{A_{1}}^{\dagger} e^{i\varphi_{A}} + a_{B_{1}}^{\dagger}) (a_{A_{2}}^{\dagger} + a_{B_{2}}^{\dagger} e^{i\varphi_{B}}) | 0 \rangle \\ \rightarrow \frac{1}{4} \left[a_{A_{+}}^{\dagger} a_{B_{+}}^{\dagger} (e^{i\varphi} - 1) + a_{A_{+}}^{\dagger} a_{B_{-}}^{\dagger} (e^{i\varphi} + 1) + a_{A_{-}}^{\dagger} a_{B_{-}}^{\dagger} (e^{i\varphi} - 1) + a_{A_{-}}^{\dagger} a_{B_{-}}^{\dagger} (e^{i\varphi} - 1) + a_{A_{-}}^{\dagger} a_{A_{-}}^{\dagger} a_{A_{-}}^{\dagger} + 2e^{i\varphi_{B}} a_{B_{+}}^{\dagger} a_{B_{-}}^{\dagger} \right] | 0 \rangle \,, \end{split}$$
(6.4)

where $\varphi = \varphi_A + \varphi_B$ and we have used the fermionic anti-commutation relations $\{a_{A_1}^{\dagger}, a_{B_1}^{\dagger}\} = 0$, etc. We omit terms where two electrons go to the same output since these are ruled out by the Pauli exclusion principle and vanish due to the fermionic anti-commutation relations, e. g. $2(a_{A_1}^{\dagger})^2 = \{a_{A_1}^{\dagger}, a_{A_1}^{\dagger}\} = 0$.

Assuming that single-electron detection is possible, the state (6.4) can be seen to violate the CHSH inequality using the following strategy: The phases φ_A^x and φ_B^y are determined by the inputs x, y = 0, 1, and the binary outputs $a, b = \pm 1$ are determined by outputting ± 1 when one click is observed in detector A_{\pm} (similarly for B). In cases where both or none of the detectors click, the outputs are defined to be +1 and -1 respectively. We denote the probability for outputs a, b given inputs x, y by P(ab|xy). The correlator defined as

$$E_{xy} = \sum_{a,b} abP(ab|xy) \tag{6.5}$$

is then given by

$$E_{xy} = -\frac{1 + \cos(\varphi_A^x + \varphi_B^y)}{2}. (6.6)$$

If the experiment can be explained by a local hidden variable model, then the CHSH inequality holds [Clauser et al., 1969]

$$S = |E_{00} + E_{01} + E_{10} - E_{11}| \le 2. (6.7)$$

Now, with the choice $\varphi_A^0 = 0$, $\varphi_A^1 = \pi/2$, $\varphi_B^0 = -3\pi/4$, and $\varphi_B^1 = 3\pi/4$, we find

$$S = 1 + \sqrt{2} > 2. \tag{6.8}$$

Thus, the CHSH inequality is clearly violated. Since the state (6.4) violates a Bell inequality between A and B, it must necessarily be entangled. Furthermore, it was created by LOs on two copies of the state (6.3) coming from two independent sources. Since any product of separable states is separable, it follows that the state (6.3) must itself be entangled. We thus conclude that the state of a single electron split between two modes is entangled.

It should be pointed out that the setup in Fig. 6.1(b) is similar to the Hanbury Brown-Twiss interferometer for electrons, as theoretically proposed by Samuelsson et al. [2004] and experimentally realised by Neder et al. [2007c] using edge states of a two-dimensional electron gas in the integer quantum hall regime. However, in these works maximal CHSH inequality violation $(S=2\sqrt{2})$ is achieved by post-selection on the subspace of one electron on each side of the interferometer (effectively post-selecting a maximally entangled state), which is interpreted as two-electron orbital entanglement. Here, by contrast, our scheme involves no post-selection and we do not achieve maximal CHSH violation, but in turn we can demonstrate single-electron entanglement.

It should also be noted that the possibility of using two copies of a single electron entangled state in order to distil one entangled two-electron state has been discussed by Wiseman and Vaccaro [2003]; Vaccaro et al. [2003]. There, the idea is that each observer performs a non-demolition measurement of the local electron number and then post-selects on the cases where a single electron is detected on each side. Alternatively, the distilled entanglement can be transferred to a pair of additional target particles [Ashhab et al., 2007], in which case however single-electron nonlocality cannot be unambiguously concluded. Again, as argued above, our setup involves no post-selection and is thus conceptually different. Moreover, the setup does not require non-demolition measurements.

The scheme described so far is a thought experiment, demonstrating that single-electron entanglement in theory is observable. In principle, nothing prevents its realisation. Single-electron sources [Fève et al., 2007; Dubois et al., 2013b; Jullien et al., 2014] and electronic beam splitters have been experimentally realised and the first steps towards single-electron detectors [Thalineau et al., 2014; Fletcher et al., 2013] have recently been taken. Still, realising our thought experiment is at present challenging, mainly because of the requirement to detect single electrons. To relax this constraint, we discuss in the next section an experiment which only relies on measurements of the average current and the zero-frequency current-correlators. These are standard measurements which would also demonstrate single-electron entanglement, albeit under slightly stronger assumptions about the experimental implementation.

6.4. Floquet scattering description

We consider again the setup in Fig. 6.1(b), but now discuss a detection scheme which is feasible using existing technology. Specifically, we consider measurements of zero-frequency currents and current correlators as an alternative to single-electron detection. We give a detailed description of the single-electron sources and the interferometer based on Floquet scattering theory [Pedersen and Büttiker, 1998; Moskalets and Büttiker, 2002; Moskalets, 2011; Dubois et al., 2013a]. This allows us to investigate realistic operating conditions such as finite electronic temperatures and dephasing. As we will see, it is possible to demonstrate single-electron entanglement under one additional assumption, namely that the measurement of the mean current and the zero-frequency current correlators amounts to taking ensemble averages over the state in each period of the driving. This is a reasonable assumption if the period of the driving is so long that only one electron from each source is traversing the interferometer at any given time.

For the single-electron sources, we consider the application of Lorentzian-shaped voltage pulses to the contacts [Levitov et al., 1996; Keeling et al., 2006; Dubois et al., 2013b; Jullien et al., 2014]. A driven mesoscopic capacitor [Fève et al., 2007] can be used instead. Electrons leaving a contact pick up a time-dependent phase given by Eq. (3.37). At zero temperature, this results in the excitation of exactly one electron out of the Fermi sea (and one hole going into the contact) without any additional electron-hole pairs, as explained before. In Eq. (3.37), the temporal width of the pulse is denoted as Γ and \mathcal{T} is the period of the driving.

6.4.1. Scattering matrix

Floquet scattering theory provides us with a convenient theoretical framework to describe the periodically driven interferometer [Pedersen and Büttiker, 1998; Moskalets and Büttiker, 2002; Moskalets, 2011; Dubois et al., 2013a]. By Fourier transforming Eq. (3.37), we obtain the Floquet scattering matrix of the driven contacts as in Eq. (A.5) in Appendix A.

The scattering matrix of the interferometer can be found as follows. Since there are eight terminals in total (four inputs and four outputs), the scattering matrix of the interferometer is an 8×8 matrix. However, due to the chirality of the edge states, electrons leaving an input contact can only travel to an output. This allows us to work with an effective 4×4 scattering matrix connecting every possible input to every possible output. Including the phases φ_A and φ_B , that the particles pick up when travelling from input 1 to location A or from input 2 to B, the scattering matrix reads

$$\mathcal{S} = \begin{pmatrix} r_1 r_A e^{i\varphi_A} & r_1 t_A e^{i\varphi_A} & t_1 t_B & t_1 r_B \\ t_1 r_A e^{i\varphi_A} & t_1 t_A e^{i\varphi_A} & -r_1 t_B & -r_1 r_B \\ t_2 t_A & -t_2 r_A & -r_2 r_B e^{i\varphi_B} & r_2 t_B e^{i\varphi_B} \\ -r_2 t_A & r_2 r_A & -t_2 r_B e^{i\varphi_B} & t_2 t_B e^{i\varphi_B} \end{pmatrix}.$$

Here, $t_{1(2)}$ refers to the transmission amplitude of the QPCs after source 1(2) and $t_{A(B)}$ is the amplitude for the QPC located at A(B). The r's are the corresponding reflection

amplitudes. The rows number the possible inputs S_1 , G_1 , S_2 and G_2 (in this order) and the columns the possible outputs A+, A-, B+ and B-. We have chosen all amplitudes to be real and inserted factors of -1 for half of the reflection amplitudes to ensure the unitarity of the scattering matrix. Below, we consider only half-transparent beam splitters and thus set all amplitudes to $\pm 1/\sqrt{2}$.

To obtain the combined Floquet scattering matrix of the interferometer and the singleelectron sources, we multiply every matrix element of the stationary S-matrix corresponding to a voltage-biased input (i. e. the first and third rows) by $S_{RL}(n)$ from Eq. (A.5) and every element corresponding to a grounded input (i. e. the second and fourth rows) by δ_{n0} . In doing so, we assume that the two electron sources are perfectly synchronised and all arms of the interferometer have the same length. The resulting Floquet scattering matrix $S_F(E_n, E) \equiv S_F(n)$ is the basis of all calculations below.

The current operator in output α is given by [Blanter and Büttiker, 2000]

$$I_{\alpha} = \frac{e}{h} \int_{-\infty}^{\infty} \left\{ c_{\alpha}^{\dagger}(E) c_{\alpha}(E) - b_{\alpha}^{\dagger}(E) b_{\alpha}(E) \right\} dE, \tag{6.9}$$

where the operators $c_{\alpha}(E)$ ($b_{\alpha}(E)$) annihilate an incoming (outgoing) electron in lead α at energy E. Outgoing electrons from the leads are distributed according to the Fermi-Dirac distribution function

$$\langle b_{\alpha}^{\dagger}(E)b_{\beta}(E')\rangle = \delta_{\alpha\beta}\delta(E - E')\frac{1}{e^{E/(k_BT)} + 1},\tag{6.10}$$

where T is the electronic temperature and we have set the Fermi level in all reservoirs to $E_F = 0$. The scattered electrons are not in thermal equilibrium. We find their distribution by relating the incoming electrons to the outgoing ones via the Floquet scattering matrix as [Moskalets, 2011]

$$c_{\alpha}(E) = \sum_{n=-\infty}^{\infty} \sum_{\beta} [S_F(E, E_n)]_{\alpha\beta} b_{\beta}(E_n). \tag{6.11}$$

6.4.2. Zero temperature

At zero temperature, the average currents and the zero-frequency current correlators can be calculated analytically using Eqs. (6.9) and (6.11). For example, the average current at output A+ reads

$$\langle I_{A+} \rangle = \frac{e}{\mathcal{T}} \left(T_2 T_A + T_1 R_A \right), \tag{6.12}$$

where $T_i = |t_i|^2$ and $R_i = |r_i|^2$ (i = 1, 2, A, B). The zero-frequency current cross-correlator is defined as

$$P_{\alpha\beta} = \langle I_{\alpha}I_{\beta}\rangle - \langle I_{\alpha}\rangle \langle I_{\beta}\rangle. \tag{6.13}$$

For the cross-correlator between the A+ and B+ outputs we obtain

$$P_{A+B+} = -\frac{e^2}{\mathcal{T}} \left| t_2 t_A r_2 t_B e^{i\varphi_B} + t_1 r_A r_1 r_B e^{-i\varphi_A} \right|^2.$$
 (6.14)

6. Single-electron entanglement and nonlocality

Note that the average currents are insensitive to the phases φ_A and φ_B , whereas the current cross-correlators depend on their sum $\varphi_A + \varphi_B$. This is known as the two-particle Aharonov-Bohm effect [Samuelsson et al., 2004].

We now formulate the CHSH inequality [Clauser et al., 1969] for our system. The leviton annihilation operator is [Keeling et al., 2006]

$$a_{\alpha} = \sqrt{2\Gamma} \sum_{E>0} e^{-\Gamma E/\hbar} b_{\alpha}(E). \tag{6.15}$$

At zero temperature, we can express the operator of the number of levitons emitted from lead α per period in terms of the current operator as

$$a_{\alpha}^{\dagger} a_{\alpha} = \frac{\mathcal{T}}{e} I_{\alpha}. \tag{6.16}$$

This allows us to relate the current operator for a given detector at A or B to an operator on the modes on side A or B before the final beam splitter and the phase shift, cf. Fig. 6.1(b). Taking for instance the detector A_+ and transforming Eq. (6.16) through the beam splitter and the phase shift, we get

$$a_{A_{+}}^{\dagger} a_{A_{+}} \to \frac{1}{2} (e^{-i\varphi_{A}} a_{A_{1}}^{\dagger} + a_{A_{2}}^{\dagger}) (e^{i\varphi_{A}} a_{A_{1}} + a_{A_{2}})$$

$$= \frac{1}{2} (a_{A_{1}}^{\dagger} a_{A_{1}} + a_{A_{2}}^{\dagger} a_{A_{2}}) + \frac{1}{2} (e^{-i\varphi_{A}} a_{A_{1}}^{\dagger} a_{A_{2}} + e^{i\varphi_{A}} a_{A_{2}}^{\dagger} a_{A_{1}}).$$

$$(6.17)$$

To gain an intuitive understanding of this operator, we consider its restriction to the single-electron subspace, i. e. the case where there is exactly one electron on side A of the interferometer. In this case, the first term in (6.17) is just 1/2. The Hilbert space is two-dimensional and the states $a_{A_1}^{\dagger} |0\rangle$, $a_{A_2}^{\dagger} |0\rangle$ form a basis. In this basis, the second term in (6.17) is $(\cos(\varphi_A)\sigma_x + \sin(\varphi_A)\sigma_y)/2$, with σ_x , σ_y , σ_z being the usual Pauli matrices. Thus, in the single-electron subspace we have

$$I_{A_{+}} = \frac{e}{2\mathcal{T}} \left(1 + \sigma_{\varphi_{A}}^{A} \right), \tag{6.18}$$

where $\sigma_{\varphi_A}^A = \cos(\varphi_A)\sigma_x^A + \sin(\varphi_A)\sigma_y^A$ is the rotated Pauli matrix in the x-y plane, acting on side A. From this we see that, in the single-electron subspace, measuring I_{A_+} is equivalent to measuring $\sigma_{\varphi_A}^A$. Similar expressions can be obtained for the currents at the other detectors, and thus, by measuring the currents at the four outputs, we can measure any combination of Pauli operators in the two-qubit subspace with a single electron on each side of the interferometer.

With this in mind, we define the observables

$$X_A^{\varphi_A} = \frac{2\mathcal{T}}{e} I_{A_+}^{\varphi_A} - 1, \qquad X_B^{\varphi_B} = \frac{2\mathcal{T}}{e} I_{B_+}^{\varphi_B} - 1,$$
 (6.19)

where the current for a given phase setting φ is denoted as I_{α}^{φ} . In the subspace with one electron on each side of the interferometer, these correspond to measuring (rotated)

Pauli operators. Events where two or no electrons arrive on the same side will give contributions of +1 or -1 respectively, cf. Eq. (6.16), independent of the phase settings, analogously to the output strategy in the previous section. At zero temperature the correlator becomes

$$\langle X_A^{\varphi_A} X_B^{\varphi_B} \rangle = -\frac{1 + \cos(\varphi_A + \varphi_B)}{2},\tag{6.20}$$

showing that the joint statistics is the same as in Sec. 6.2, where single-electron detection was assumed. Here, however, we interpret the current expectation values entering in the correlator, such as $\langle I_{A_+}^{\varphi_A} \rangle$, as the result of time-integrated measurements. We thus assume that a measurement of the time-integrated current and the zero-frequency current correlators amounts to taking ensemble averages over the state in each period of the driving. The statistics obtained from the time-integrated current measurement is then the same as what one would obtain by averaging over several periods of the driving with single-electron detection. Under this assumption, we can again consider the CHSH inequality

$$S = \left| \left\langle X_A^{\varphi_A^0} X_B^{\varphi_B^0} + X_A^{\varphi_A^0} X_B^{\varphi_B^1} + X_A^{\varphi_A^1} X_B^{\varphi_B^0} - X_A^{\varphi_A^1} X_B^{\varphi_B^1} \right\rangle \right| \le 2, \tag{6.21}$$

It is easy to see that the choice $\varphi_A^0 = 0$, $\varphi_A^1 = \pi/2$, $\varphi_B^0 = -3\pi/4$, $\varphi_B^1 = 3\pi/4$ leads to a violation, giving

$$S = 1 + \sqrt{2} > 2. \tag{6.22}$$

This finally shows us that this scheme makes it possible to observe single-electron entanglement using zero-frequency measurements only.

We note that our results for the current and the zero-frequency noise do not depend on the pulse width Γ . As such, our measurement strategy based on Eq. (6.19) would also work with constant voltages as realised in the experiment by Neder et al. [2007c] and the CHSH violation of Eq. (6.22) would be obtained. However, to unambiguously demonstrate single-electron entanglement, in line with the thought experiment described in Sec. 6.2, it is important that only one electron from each source is traversing the interferometer at any given time. We therefore need to work with a long period and well-separated pulses, as opposed to constant voltages.

It is instructive to compare our proposal to the previous work of Samuelsson et al. [2004]. Although the two setups are similar, the detection scheme discussed here is different. This significantly changes the interpretation of the observations. The measurement scheme suggested by Samuelsson et al. [2004] is formulated in terms of coincidence rates [Samuelsson et al., 2009a]. The corresponding observable is then sensitive only to the part of the state with a single electron on each side of the interferometer. Thus, the measurement effectively corresponds to performing post-selection, discarding the part of the state where two electrons are on the same side. In this case, the CHSH inequality is maximally violated $(S = 2\sqrt{2})$, as the post-selected state is a maximally entangled two-qubit state. The Bell inequality is then violated because of the two-electron orbital entanglement. By contrast, our measurement strategy is sensitive to the entire state (including terms with two electrons on the same side) and does not imply any effective

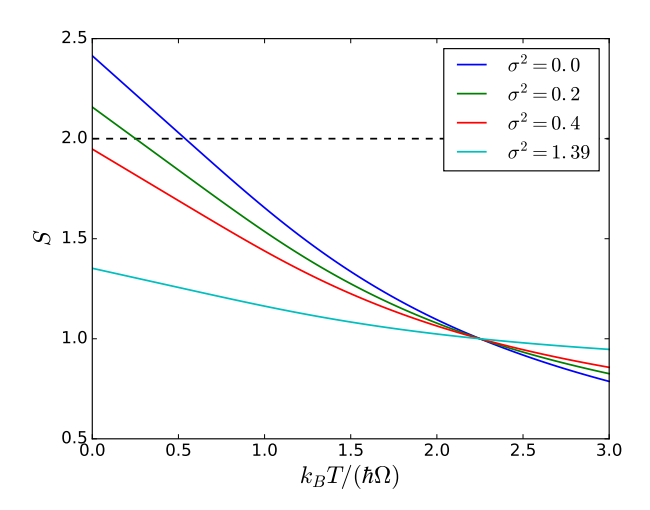


Figure 6.2.: Maximal value of the CHSH parameter as a function of temperature. The Bell angles are $\varphi_A = 0$, $\varphi_A' = \pi/2$, $\varphi_B = -\pi/4$ and $\varphi_B' = 5\pi/4$. The dephasing parameter σ^2 is the variance of the distribution of the sum of the phases $\varphi_A + \varphi_B$. The dashed line indicates the CHSH bound. [Dasenbrook et al., 2016].

post-selection. For this reason we reach a lower CHSH violation, $S=1+\sqrt{2}$. However, we observe in turn single-electron entanglement.

6.4.3. Finite temperature and dephasing

At finite temperatures, additional excitations in terms of electron-hole pairs are expected. Consequently, Eq. (6.16) does not hold any longer. The operators in Eq. (6.19) are thus not strictly bounded between -1 and +1, although values outside this range should be rare at low temperatures. Since the CHSH parameter S is a monotonically decreasing function of temperature, a violation of the CHSH inequality at finite temperatures indicates that the corresponding zero temperature state is unambiguously entangled. We will thus continue to use Eq. (6.21) to detect single-particle entanglement and come back to this issue in Sec. 6.5.

At finite temperatures, the average current and the zero-frequency current correlators can be calculated numerically. Fig. 6.2 shows the maximal value of the CHSH parameter (using the same phase settings as above) as a function of the electronic temperature. In the absence of any additional dephasing mechanisms (blue curve), the CHSH inequality can be violated up to a temperature of $k_BT \approx 0.5\hbar\Omega$. For a typical driving frequency of 5 GHz [Dubois et al., 2013b; Jullien et al., 2014], this corresponds to a temperature of about 120 mK, which is well within experimental reach.

Due to interactions with the electrons in the underlying Fermi sea as well as with nearby conductors, the injected single-electron states may experience decoherence and dephasing. Here we do not give a microscopic model for theses interactions, but instead we introduce a phenomenological dephasing parameter σ^2 which denotes the variance of the total phase $\varphi_A + \varphi_B$ in a model that leads to Gaussian phase averaging. Previous experiments have shown that this is the dominant effect of the interaction of electronic interferometers with their environments [Ji et al., 2003; Roulleau et al., 2007]. At zero temperature, the correlator in Eq. (6.20) then becomes

$$\langle X_A^{\varphi_A} X_B^{\varphi_B} \rangle = -\frac{1 + e^{-\sigma^2} \cos(\varphi_A + \varphi_B)}{2},\tag{6.23}$$

making a Bell violation possible up to $\sigma^2 \lesssim 0.35$. At finite temperatures, an analogous expression can be found [Samuelsson et al., 2009a] and the dephasing has a similar qualitative effect. Fig. 6.2 shows that for small values of the dephasing parameter, a CHSH violation is still possible at low enough temperatures, while for $\sigma^2 \gtrsim 0.35$, the entanglement cannot be detected any longer. We note that the visibility of the current correlators observed in the experiment by Neder et al. [2007c] is too low to violate Eq. (6.21) in this setup. It corresponds to a dephasing parameter of $\sigma^2 \approx 1.39$ (light blue line in Fig. 6.2). Nevertheless, by a careful design of the interferometer the dephasing may be further reduced, bringing the measurement described here within experimental reach.

6.5. Single-electron entanglement at finite temperature

At zero temperature, it is clear that violating the CHSH inequality constructed out of current and noise measurements demonstrates entanglement, since the measured correlators are clearly ensemble averages over individual runs with either qubits on both sides or two particles on one side. For these particular states, the considered operators output the values ± 1 . However, at finite temperature, the situation is less clear, since in individual driving periods, sometimes more than one particle might be found in the same arm due to thermal excitations, such that the total charge transferred is more than one or less than minus one. The aim is to show that even in this case, the experiment can be interpreted as being composed of individual runs, in each of which only a dichotomic variable with outcomes ± 1 is measured.

To this end, we first note that we only ever measure two-particle observables, i. e. observables that are at most quadratic in the creation and annihilation operators. All outcomes of these observables are given in terms of some reduced two-particle density matrix (2PDM), and so we can always interpret measurements as ensemble averages over single runs of measurements on only two electrons. If we detect any entanglement, it is entanglement of this 2PDM.

Note that there are many ways to define reduced 2PDMs in mesoscopic conductors connected to leads [Samuelsson et al., 2009a], some of which can be reconstructed to-mographically by current and noise measurements [Samuelsson and Büttiker, 2006]. We here consider the two-leviton reduced density matrix defined by

$$[\rho_r]_{ij}^{kl} = \left\langle A_i^{\dagger} A_k^{\dagger} A_j A_l \right\rangle, \tag{6.24}$$

where the leviton creation operator is defined as [Keeling et al., 2006]

$$A_i = \sqrt{2\tau} \sum_{E>0} e^{-\tau/\hbar E} b_i(E).$$
 (6.25)

In Eq. (6.25), τ is the width of the injected pulses, and in Eq. (6.24), the average is over the full electronic state of the interferometer at arbitrary temperature.

At zero temperature and for the case that only single-charge levitons are periodically injected at a frequency f, the current operator can be written as

$$I_{\alpha} = ef A_{\alpha}^{\dagger} A_{\alpha}. \tag{6.26}$$

Then, currents and current correlators are completely determined by the reduced 2PDM in Eq. (6.24). For average currents, this is even true at arbitrary temperatures. For the current cross-correlators, however, the situation at finite temperatures is less clear. In general, for a measurement of correlations between two different terminals, temperature provides a factor ≤ 1 to the zero-temperature result [Dubois et al., 2013a].

However, we will now show that the correlations measured at finite temperatures are bounded from above by those resulting from the reduced 2PDM Eq. (6.24) if the overlap between successive levitons is negligible. Therefore, even though we are strictly measuring correlations between incoming and outgoing electrons at all energies, we can infer statements about entanglement of the reduced 2PDM.

To this end, we directly calculate leviton densities and density correlators at finite temperatures and compare them with average currents and zero-frequency current correlations functions. We first evaluate the expectation value¹

$$\left\langle A_i^{\dagger} A_i \right\rangle = 2\tau \iint_0^{\infty} e^{-\tau(E+E')} \left\langle c_i^{\dagger}(E) c_i(E') \right\rangle dE dE'$$
 (6.27)

in a state with one leviton added to the finite temperature Fermi sea, i. e. directly after the contact. By this we mean that we assume exactly one Lorentzian voltage pulse has been applied. Using the Floquet scattering matrix, we map the c operators to the outgoing a operators, which are in thermal equilibrium:

$$\left\langle A_i^{\dagger} A_i \right\rangle = 2\tau \iint_0^{\infty} dE dE' e^{-\tau(E+E')} \iint_{-\infty}^{\infty} d\omega d\omega' S_F^*(-\omega) S_F(-\omega') \left\langle a_i^{\dagger}(E_{\omega}) a_i(E'_{\omega'}) \right\rangle. \tag{6.28}$$

In Eq. (6.28), $E_{\omega} = E + \omega$. In the limit of a single pulse, i. e. an infinite period, the scattering matrix for the creation of a leviton is [Keeling et al., 2006]

$$S_F(\omega) = \delta(\omega) - 2\tau e^{-\tau\omega}\Theta(\omega). \tag{6.29}$$

¹In this calculation, $\hbar = 1$.

²Strictly speaking, this is not a Floquet scattering matrix since we are not dealing with a periodic process. We model this by a periodic process where the period goes to infinity, therefore the energy absorbed / emitted due to scattering is continuous and not discrete as in the case of a periodically time-dependent scatterer.

Using $\langle a_i^{\dagger}(E_{\omega})a_i(E'_{\omega'})\rangle = \delta(E_{\omega}-E'_{\omega'})f(E_{\omega})$, where f(E) is the Fermi-Dirac distribution function, we can simplify this to

$$\left\langle A_i^{\dagger} A_i \right\rangle = (2\tau)^2 \int_0^{\infty} dE \int_{-\infty}^{-E} d\omega e^{2\tau\omega} f(E_{\omega}) = 2\tau \int_0^{\infty} dE e^{-2\tau E} f(-E). \tag{6.30}$$

Similarly, we can also evaluate

$$\left\langle A_i A_i^{\dagger} \right\rangle = 2\tau \int_0^{\infty} dE e^{-2\tau E} (1 - f(-E)).$$
 (6.31)

If no leviton is created and the contact i is instead grounded, these averages become

$$\left\langle A_i^{\dagger} A_i \right\rangle = 2\tau \int_0^{\infty} dE e^{-2\tau E} f(E)$$

$$\left\langle A_i A_i^{\dagger} \right\rangle = 2\tau \int_0^{\infty} dE e^{-2\tau E} (1 - f(E)). \tag{6.32}$$

Using the relation f(-E) = 1 - f(E), we immediately see that the two correlators are just exchanged for a grounded reservoir. Furthermore, we have

$$\left\langle A_i^{\dagger} A_i \right\rangle = 1 - \left\langle A_i A_i^{\dagger} \right\rangle. \tag{6.33}$$

At zero temperature, Eqs. (6.30) and (6.31) evaluate to one and zero, respectively. At finite temperatures, the integral can be performed numerically. Alternatively, we can expand the integrand in powers of T in an analogous way to the Sommerfeld expansion. For example, in Eq. (6.31), we can make a change of variables $xk_BT = E$:

$$\left\langle A_i A_i^{\dagger} \right\rangle = 2\tau k_B T \int_0^{\infty} \frac{e^{-2\tau x k_B T}}{e^x + 1} dx.$$
 (6.34)

Expanding the numerator to linear order in T, we thus immediately obtain

$$\left\langle A_i A_i^{\dagger} \right\rangle = 2\tau k_B T \left(\int_0^{\infty} \frac{\mathrm{d}x}{e^x + 1} - \int_0^{\infty} \frac{2\tau k_B T x}{e^x + 1} \mathrm{d}x \right) + \mathcal{O}(T^3)$$

$$= 2\tau k_B T \log 2 - (2\tau k_B T)^2 \frac{\pi^2}{12} + \mathcal{O}(T^3). \tag{6.35}$$

The low-T expansion for the other correlator can then be obtained by Eq. (6.33).

Equations (6.30)-(6.32) now allow us to calculate average leviton densities and density correlation functions at the outputs of our full scattering setup. Relating incoming leviton operators to outgoing ones using the S-matrix of the static interferometer and using Wick's theorem, we obtain

$$\left\langle B_i^{\dagger} B_i \right\rangle = \sum_{j} |S_{ij}|^2 \left\langle A_j^{\dagger} A_j \right\rangle \tag{6.36}$$

$$\left\langle B_{i}^{\dagger}B_{i}B_{j}^{\dagger}B_{j}\right\rangle = \sum_{kl} |S_{ik}|^{2}|S_{jl}|^{2} \left\langle A_{k}^{\dagger}A_{k}\right\rangle \left\langle A_{l}^{\dagger}A_{l}\right\rangle + \sum_{kl} S_{ik}^{*}S_{jk}S_{il}S_{jk}^{*} \left\langle A_{k}^{\dagger}A_{k}\right\rangle \left\langle A_{l}A_{l}^{\dagger}\right\rangle. \tag{6.37}$$

6. Single-electron entanglement and nonlocality

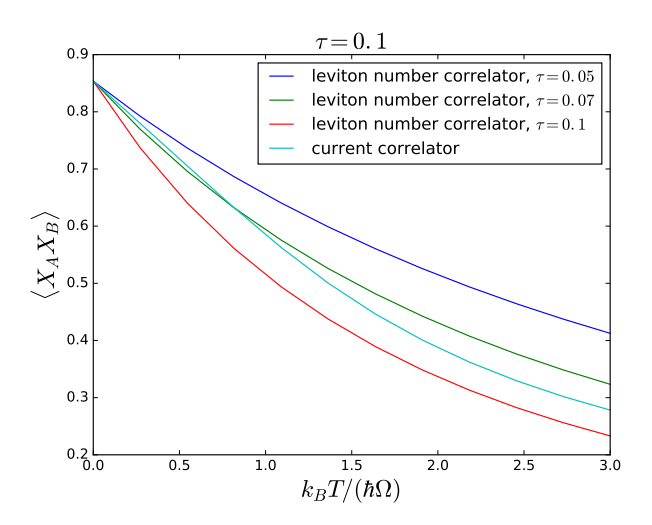


Figure 6.3.: Correlators of the X-observables in the Hanbury Brown-Twiss setup using levitons of different temporal widths, and the result based on zero-frequency current and noise for comparison. Below a certain width, the measurement based on currents gives a lower bound for the correlations based on the reduced two-leviton DM. In this case, entanglement of the 2PDM can be detected.

At zero temperature, these expressions coincide with the average current and the reducible zero-frequency current correlation functions due to Eq. (6.26).

In formulating a CHSH inequality without post-selection using current and noise measurements, we considered the observables

$$X_A^{\varphi_A} = 2B_{A+}^{\dagger} B_{A+} - 1, \tag{6.38}$$

and similarly for the operator on side B. Instead of the leviton densities $B_{A+}^{\dagger}B_{A+}$, what is measured instead is the average current at output A+. Therefore, we have to make sure that we do not overestimate the entanglement in the reduced two-leviton DM by measuring correlators based on currents instead of the operators in Eq. (6.38) at finite temperatures.

Fig. 6.3 shows the behaviour of the correlator $\langle X_A^{\varphi_A} X_B^{\varphi_B} \rangle$ obtained using the leviton correlators at different pulse widths as well as using the zero-frequency currents (which are independent of the pulse width). The angles $\varphi_A = 0$, $\varphi_B = -\pi/2$ have been chosen. We see that if the pulse width is smaller than about $\tau \approx 0.06$, the correlations based on the current operator are always a lower bound for the real leviton correlations. In this case, entanglement of the 2PDM in Eq. (6.24) can be faithfully detected. If levitons are injected periodically, the relevant quantity is $\eta = \tau/\mathcal{T}$, where \mathcal{T} is the period of the driving. This has to be compared to the injection of a single leviton with width τ . Therefore, the value of τ in these results should be seen as the necessary ratio of the width over the period in such a system. Thus, our requirement for small τ translates to

having vanishing overlap between successive pulses. This is not an experimental difficulty [Dubois et al., 2013b] and ties in well with the conceptual argument for single-electron entanglement.

We note that in the case that the CHSH inequality is constructed only out of reducible current-current correlators, and not currents, as in the proposal by Samuelsson et al. [2004], the requirement on the pulse width is the opposite: wide pulses should be used for the current correlator to be a lower bound for the excess particle number correlator. This is in agreement with the findings by Samuelsson et al. [2009a].

Next, we show that entanglement of the reduced two-leviton DM ρ_r implies entanglement of the full density matrix ρ (the one that the average is taken over on the right hand side of Eq. (6.24)). To this end, we assume that ρ is separable,

$$\rho = \sum_{n} p_n \rho_n^{(A)} \otimes \rho_n^{(B)} \tag{6.39}$$

and show that separability of ρ_r follows. In Eq. (6.39), $\rho_n^{(A/B)}$ are states fully localised on side A/B (they can be assumed pure for simplicity), and p_n are probabilities fulfilling $\sum_n p_n = 1$. Plugging this into Eq. (6.24), we can write its right hand side as

$$\left\langle A_i^{\dagger} A_k^{\dagger} A_j A_l \right\rangle = \sum_n p_n \left\langle A_i^{\dagger} A_k^{\dagger} A_j A_l \right\rangle_n, \tag{6.40}$$

where the index n denotes taking the average over the state $\rho_n^{(A)} \otimes \rho_n^{(B)}$. Then, we use Wick's theorem to expand this as

$$\begin{split} \left\langle A_{i}^{\dagger}A_{k}^{\dagger}A_{j}A_{l}\right\rangle_{n} &= \left\langle A_{i}^{\dagger}A_{j}\right\rangle_{A,n} \left\langle A_{k}^{\dagger}A_{l}\right\rangle_{A,n} + \left\langle A_{i}^{\dagger}A_{j}\right\rangle_{A,n} \left\langle A_{k}^{\dagger}A_{l}\right\rangle_{B,n} + \\ &\left\langle A_{i}^{\dagger}A_{j}\right\rangle_{B,n} \left\langle A_{k}^{\dagger}A_{l}\right\rangle_{A,n} + \left\langle A_{i}^{\dagger}A_{j}\right\rangle_{B,n} \left\langle A_{k}^{\dagger}A_{l}\right\rangle_{B,n} + \\ &\left\langle A_{i}^{\dagger}A_{l}\right\rangle_{A,n} \left\langle A_{k}^{\dagger}A_{j}\right\rangle_{A,n} + \left\langle A_{i}^{\dagger}A_{l}\right\rangle_{A,n} \left\langle A_{k}^{\dagger}A_{j}\right\rangle_{B,n} + \\ &\left\langle A_{i}^{\dagger}A_{l}\right\rangle_{B,n} \left\langle A_{k}^{\dagger}A_{j}\right\rangle_{A,n} + \left\langle A_{i}^{\dagger}A_{l}\right\rangle_{B,n} \left\langle A_{k}^{\dagger}A_{j}\right\rangle_{B,n} . \end{split} \tag{6.41}$$

Separability of ρ implies that $\langle A_i^{\dagger} A_j \rangle_n = 0$ unless $i, j \in A$ or $i, j \in B$. All the terms in Eq. (6.41) describe separable density matrices: The resulting matrices are outer products of single-particle density matrices that are either fully localised on side A or side B. For example, the second term might be written as the outer product of two matrices, $M^{(A)} \otimes M^{(B)}$, with elements $[M^{(A)}]_{ij} = \langle A_i^{\dagger} A_j \rangle_{A,n}$ and $[M^{(B)}]_{kl} = \langle A_k^{\dagger} A_l \rangle_{B,n}$. Therefore, we have written the two-leviton DM as a convex combination of outer products of density matrices localised on side A or side B. It is therefore separable.

Reversing this argument, if we detect entanglement of ρ_r (e. g. by a measurement of leviton density operators or current operators), it follows that the full state ρ of our system must be entangled.

6.6. Conclusion

We have provided a simple argument that shows that the single-electron split-mode state is entangled, and furthermore, nonlocal. To this end, we have considered a Hanbury-Brown Twiss interferometer where a Bell inequality can be violated using two independent copies of this state. Using an argument from entanglement theory, we conclude that each copy of this state must have been entangled. We also presented a way to relate the electron detection statistics required for the formulation of the CHSH inequality to experimentally measurable zero-frequency currents and current-correlators. We have shown that the CHSH inequality can be violated and thus single-electron be demonstrated using current experimental technologies if the dephasing is not too strong.

We have calculated the required current correlators at finite temperatures using Floquet theory. Furthermore, we have shown that the argument remains valid in the presence of thermal electron-hole excitations if the injected single-electron wave-functions have negligible overlap.

Conclusions

In this thesis, current fluctuations and entanglement in quantum-coherent conductors have been investigated. In the first part, the focus was on the electronic waiting time distribution and the extensive full counting statistics in periodically driven quantum conductors. We have derived the Floquet scattering formalism for WTDs and calculated them for a quantum point contact driven by voltage pulses, as well as for a driven mesoscopic capacitor. We then generalized the theory to account for many channels and correlations between subsequent waiting times and presented a theory for an electron waiting time clock capable of measuring waiting time distributions for electrons above the Fermi level. Finally, we presented a proposal for measuring the extensive full counting statistics (the FCS per period) using a periodically driven Mach-Zehnder interferometer coupled to a nearby conductor.

The second part was dedicated to occupation number entanglement in mesoscopic conductors. We introduced a setup for creating and detecting on-demand entanglement in the electron-hole degree of freedom of electronic excitations. We then presented a simple argument showing that even the state of a single-electronic excitation in a superposition of two electronic modes must be considered entangled, and investigated a setup based on an electronic Hanbury Brown-Twiss interferometer demonstrating single-electron entanglement.

The work presented here ties in with the general field of electron quantum optics. Using edge channels in topological insulators such as two-dimensional electron gases in the quantum Hall regime, electronic excitations can be guided between beam splitters. Additional tunable phases can be applied using gates and magnetic fields, and interference experiments can be carried out. Combined with dynamic single-electron emitters, analogues of many experiments from the quantum optical toolbox can now be realized in electronic conductors. The characterization of these dynamically driven systems requires new observables such as the electronic waiting time distribution, and the controlled creation and detection of entanglement benefits from an adaptation of Bell inequalities and entanglement witnesses into the electronic domain. Furthermore, conceptual questions such as the possibility of single-particle entanglement require different treatments in the electronic and optical settings.

Evidently, this work can only scratch the surface of what there is to investigate on these topics. For example, it would be interesting to find stronger connections between the different chapters of this thesis. While some connections between current fluctuations and entanglement are well-known (for example, the CHSH inequality in chapter 6 and the witness in chapter 5 have both been formulated in terms of current correlation functions), it would be desirable to find more general and deeper relationships between properties of fluctuating currents and non-classical correlations.

The WTD carries complementary information to the full counting statistics and characterizes transport processes on short time scales. As it constitutes the probability distribution for time durations between classical detection events, every properly normalized and positive waiting time distribution can always be simulated by a classical stochastic process. However, taking into account correlations between waiting times such as in chapter 2, the situation becomes less clear. It would be interesting to find out if there are some correlated waiting time distributions which can never correspond to a classical process. To this end, possible connections to Leggett-Garg inequalities could be investigated [Emary, 2012; Emary et al., 2013].

Also on the side of the entanglement detection, many things remain to be investigated and improved. The violation of Bell inequalities in electronic conductors remains experimentally challenging due to the strong effects of environmental dephasing and interactions between or within edge channels. While we have investigated an entanglement witness for the particular case of electron-hole entanglement as a promising alternative, this witness relies on recombining the parts of the system that are entangled, and therefore constitutes a nonlocal measurement. To formulate more general entanglement witnesses requires a detailed analysis of the relevant subspaces of the total Hilbert space, which is complicated by the fact that in electronic systems, there are always spurious excitations, e. g. due to finite temperatures or interactions, that enlarge the relevant Hilbert space even though the entanglement that we want to consider can be formulated mathematically as the entanglement between two qubits. Therefore, it is desirable to investigate further what observables can be used to certify the presence of entanglement unambiguously, but with a tolerance to noise that is as high as possible.

To this end, short-time observables such as the finite frequency noise or the electron waiting time distribution might play a role. Another route would be to derive bounds for the noise correlators in terms of two-particle correlation functions such as the two-leviton density matrix, as done in section 6.5, but for more general input states that allow for the discrimination of entangled states from separable states.

The differences between photons and electrons are not just superficial. Therefore, a straightforward extension of ideas from quantum optics to the domain of electron quantum optics is often not possible. Most importantly, electrons are charged particles that interact strongly via the Coulomb interaction, whereas interactions between photons do not play a role at the energy scales typically considered. Here, we have often neglected electron-electron interactions or only included them on a phenomenological level, such as by introducing the dephasing parameters in chapters 5 and 6. This approach works well for some purposes, but to make further experimental and theoretical progress, a more detailed microscopic understanding of the interaction is necessary. It is desirable to extend the simple models considered in this thesis to include some explicit model for electron-electron interactions. In quantum Hall edge channels, a bosonization approach is often successful [Sukhorukov and Cheianov, 2007; Levkivskyi and Sukhorukov, 2009]. Most devices to date operate at a filling factor of 2, where interactions between copropagating edge channels lead to profound effects. The separation of injected wave packets into charge and neutral modes is theoretically predicted and experimentally validated [Levkivskyi and Sukhorukov, 2008; Bocquillon et al., 2013b].

For these reasons, it is to be expected that the realization of electron quantum optical experiments faces many challenges that are different from their photonic counterparts. The importance of interactions and the fact that electrons are fermions certainly complicate things, and the demonstrations of entanglement and effects useful for quantum information processing or quantum communication are somewhat less advanced compared to what has been achieved in optical setups. On the plus side however, the richer physics might also turn out to be advantageous, and lead to fundamentally different ideas for technological applications. A promising perspective is provided by the small size of these systems, which make them amenable to integration into micro- and nano-circuits. Thus, the possibilities for scaling up and combining many small devices into technological innovations seem more obvious when compared to macroscopic optical setups. For these reasons, it is definitely worth exploring the physics of electron quantum optical systems further and broaden our understanding of quantum transport, dephasing, electron interactions, statistics and entanglement in periodically driven mesoscopic conductors.

A. Levitons

Here we briefly discuss the Floquet scattering theory for the periodic creation of levitons [Ivanov et al., 1997; Levitov et al., 1996; Keeling et al., 2006; Dubois et al., 2013a]. Applying a series of periodic Lorentzian voltage pulses of unit charge to one of the reservoirs leads to the creation of one clean electron excitation per period — a leviton — without accompanying electron-hole pairs.

The voltage consists of a series of Lorentzian-shaped pulses

$$V(t) = \frac{\hbar}{e} \sum_{n=-\infty}^{\infty} \frac{2\tau_p}{(t - n\mathcal{T})^2 + \Gamma^2}$$
 (A.1)

as illustrated in Fig. 1.2. The width of the pulses is Γ and the period is \mathcal{T} . The same outgoing state can also be created by a mesoscopic capacitor with a slow linear driving protocol [Keeling et al., 2008; Hofer and Büttiker, 2013; Inhofer and Bercioux, 2013; Battista and Samuelsson, 2012; Ol'khovskaya et al., 2008; Haack et al., 2013].

Importantly, a time-dependent voltage has the effect of adding a phase to the single-particle states in the contact [Pedersen and Büttiker, 1998]. We can treat this additional phase as a scattering phase which is picked up after the particles leave the contact but before they arrive at the scatterer, i. e.

$$S_{V_i}(t) = e^{-i\frac{e}{\hbar} \int_{t_0}^t dt' V_i(t')}.$$
 (A.2)

Here t_0 is the time when the voltage is switched on. In this way, the contacts can be treated as equilibrium reservoirs at the same chemical potential and all the effects due to the time-dependent driving are captured by the phase Eq. (A.2).

We treat the adiabatic regime, where the time scale over which the voltage is modulated is much longer than the time it takes an electron to pass through the scattering region. The Floquet scattering matrix S can then be related to the "frozen" scattering matrix $S^f(t)$ at time t as [Moskalets and Büttiker, 2002; Moskalets, 2011]

$$S_{\alpha\beta}(E_n, E) = \int_0^{\mathcal{T}} dt e^{in\Omega t} S_{\alpha\beta}^f(E, t) / \mathcal{T}.$$
(A.3)

The frozen transmission amplitude is energy-independent and reads

$$S_{RL}^{f}(E,t) = \sqrt{T} \frac{\sin[\pi(t/\mathcal{T} + i\eta)]}{\sin[\pi(t/\mathcal{T} - i\eta)]}$$
(A.4)

with $\eta = \Gamma/\mathcal{T}$, see e. g. Dubois et al. [2013a]. Here, we have introduced an additional QPC with transmission probability T placed after the voltage-biased contact. For the

A. Levitons

Floquet scattering amplitude, we find

$$S_{RL}(E_n, E) = \sqrt{T} \begin{cases} -2e^{-n\Omega\Gamma} \sinh(\Omega\Gamma) & n > 0 \\ e^{-\Omega\Gamma} & n = 0 \\ 0 & n < 0 \end{cases}$$
 (A.5)

For well-separated pulses, $\eta \ll 1$, the scattering amplitude reduces to [Dubois et al., 2013a]

$$S_{RL}(E_n, E) \simeq 4\pi\sqrt{T}\eta e^{-2\pi\eta n}\Theta(n).$$
 (A.6)

For pulses with a large overlap, $\eta \gg 1$, the scattering amplitude $S_{RL}(E_n, E) \simeq \sqrt{T} \delta_{n,1}$ is that of a QPC with transmission T and static voltage $V_{\rm dc} = \hbar \Omega/e$, see also Eq. (1.22).

This Floquet scattering matrix relates particles incident on the scatterer to equilibrium particles through Eq. (1.15). Together with the scattering matrix of the scatterer itself, it yields the Floquet scattering matrix used for the calculation of the idle time probability in Eqs. (1.17) and (C.4). For the Hong-Ou-Mandel calculations, the time delay between the sources can be tuned by changing the parameter t_0 in one of the matrix elements in the channel space.

B. Determinant formula for the ITP

In this appendix, we show how to derive the determinant formula for the idle time probability

$$\Pi(\tau, t_0) = \det(1 - \mathbf{Q}_{\tau, t_0}) \tag{B.1}$$

with the matrix elements

$$\mathbf{Q}_{\tau,t_0}(E,E') = \sum_{m=-\lfloor E/\hbar\Omega\rfloor}^{\infty} \sum_{RL}^{\infty} (E_m, E) \mathcal{S}_{RL}(E'_n, E')$$

$$= -\lfloor E'/\hbar\Omega\rfloor$$

$$\times K_{\tau,t_0}(E_m, E'_n) \Theta(-E) \Theta(-E')$$
(B.2)

from the expression

$$\Pi(\tau, t_0) = \left\langle : e^{-\widehat{Q}_{\tau}} : \right\rangle_{t_0 + \tau}. \tag{B.3}$$

We first show that for a general single-particle operator

$$\hat{Q} = \sum_{m,n} q_{mn} \hat{a}_m^{\dagger} \hat{a}_n, \tag{B.4}$$

where the \hat{a}_{m}^{\dagger} , \hat{a}_{n} are operators creating / annihilating particles in given basis states labelled by m, n, and a Slater determinant of the form

$$|\Psi\rangle = \prod_{n=1}^{N} \hat{a}_n^{\dagger} |0\rangle , \qquad (B.5)$$

the average of the normal-ordered exponential can be expressed as

$$\langle \Psi | : \exp(-\hat{Q}) : | \Psi \rangle = \det(\mathbf{1} - Q).$$
 (B.6)

Here, Q is the matrix with elements $[Q]_{mn} = q_{mn}$.

To this end, we first make a change of basis such that the matrix \tilde{Q} corresponding to the operator \hat{Q} in this basis is diagonal. The determinant in Eq. (B.6) can then be written as a simple product and expanded in orders k:

$$\det(\mathbf{1} - \widetilde{Q}) = \prod_{n=1}^{N} (1 - \widetilde{q}_n) = \sum_{k=0}^{N} (-1)^k \sum_{\sigma \in \mathcal{P}_k(\mathbb{N}_N)} \prod_{i \in \sigma} \widetilde{q}_i.$$
 (B.7)

In this notation, we define $\mathcal{P}_k(\mathbb{N}_N)$ to be the set of all subsets with k elements of the set of the first N natural numbers, \mathbb{N}_N . In other words, at order k, we pick k different elements out of the N \widetilde{q}_i 's and multiply them with each other.

B. Determinant formula for the ITP

Likewise, the l.h.s. of Eq. (B.6) can be expanded:

$$\left\langle : \exp\left(-\hat{Q}\right) : \right\rangle = \sum_{k=0}^{N} \frac{(-1)^k}{k!} \left\langle : \left(\sum_{i=1}^{N} \widetilde{q}_i \hat{c}_i^{\dagger} \hat{c}_i\right)^k : \right\rangle, \tag{B.8}$$

where the operators \hat{c}_i^{\dagger} , \hat{c}_i follow from the operators \hat{a}_i^{\dagger} , \hat{a}_i by going over to the diagonal basis.

The equality of Eqs. (B.7) and (B.8) can now be established order by order using mathematical induction. We immediately see that for k=0, both terms are simply 1. We now assume the equality of the terms for a given k. Defining the k-th order term in Eq. (B.8) to be $\langle \hat{E}_k \rangle$ for brevity, the term of order k+1 then reads

$$\langle \hat{E}_{k+1} \rangle = -\sum_{l=1}^{N} \frac{\widetilde{q}_l}{k+1} \left\langle \hat{c}_l^{\dagger} \hat{E}_k \hat{c}_l \right\rangle,$$
 (B.9)

where we used that the operator \hat{E}_k is already normal-ordered by definition. By the induction hypothesis, the expectation value of \hat{E}_k in a Slater determinant is given by the k-th order term in Eq. (B.7). Seeing that the operator \hat{c}_l just removes the particle labelled l from the Slater determinant, we have

$$\langle \hat{E}_{k+1} \rangle = \sum_{l=1}^{N} \frac{\widetilde{q}_l}{k+1} (-1)^{k+1} \sum_{\sigma \in \mathcal{P}_k(\mathbb{N}_N \setminus \{l\})} \prod_{i \in \sigma} \widetilde{q}_i.$$
 (B.10)

Instead of summing over all $\sigma \in \mathcal{P}_k(\mathbb{N}_N \setminus \{l\})$ and multiplying by \widetilde{q}_l , we can instead sum directly over all $\sigma \in \mathcal{P}_{k+1}(\mathbb{N}_N)$. The summation over l then just provides an additional factor k+1, allowing us to arrive at

$$\langle \hat{E}_{k+1} \rangle = (-1)^{k+1} \sum_{\sigma \in \mathcal{P}_{k+1}(\mathbb{N}_N)} \prod_{i \in \sigma} \widetilde{q}_i,$$
 (B.11)

which is just the k + 1-st order term of Eq. (B.7). Thus, this completes the proof of Eq. (B.6).

We now use this general result to derive Eq. (B.1). The role of the labels m, n indexing the single-particle states is now played by the energy indices E, E' (after a suitable regularisation, see e. g. Hassler et al. [2008]; Bornemann [2010]) and the lead indices α, β . The incoming state is a Slater determinant of all single-particle states filled up to the Fermi energy:

$$|\Psi_{\rm in}(t)\rangle = \prod_{\alpha=L,R} \prod_{E<0} e^{-itE} \hat{a}_{\alpha}^{\dagger}(E) |0\rangle.$$
 (B.12)

We now consider the operator

$$Q_{\tau} = \sum_{E,E'} q_{E,E'}(\tau) \hat{b}_{R}^{\dagger}(E) \hat{b}_{R}(E')$$
(B.13)

counting particles in the right-lead, with its matrix elements in the basis of outgoing right-moving states

$$q_{E,E'}(\tau) = \Theta(E)\Theta(E') \int_{x_0}^{x_0 + v_F \tau} \phi_{R,E'}^*(x) \phi_{R,E}(x) dx.$$
 (B.14)

We write it in terms of the *incoming* operators $\hat{a}^{\dagger}_{\alpha}(E)$, $\hat{a}_{\beta}(E')$ using the Floquet S-matrix:

$$\hat{b}_{\alpha}(E) = \sum_{\beta} \sum_{E_n} \mathcal{S}_{\alpha\beta}(E, E_n) \hat{a}_{\beta}(E_n). \tag{B.15}$$

The Θ -functions in Eq. (B.14) make sure that only particles above the Fermi level are counted. This can be achieved e. g. using an appropriate energy filter (see the discussion of the electron waiting time clock in chapter 3), or by emitting the particles into an energy window with some separation to the Fermi sea [Fletcher et al., 2013]. Absorbing the time-dependence of the Slater determinant Eq. (B.12) into the operator Q_{τ} and taking the average at a time $t_0 + \tau$ as in Eq. (B.3), the matrix elements in terms of the incoming states are then given by Eq. (B.2). We focus here on situations where all particles scattered into the right lead originate from the left lead, as is the case for the directed processes at zero temperature involving a voltage bias or a single-electron emitter.

Using the result Eq. (B.6), we thus see that the ITP is given by Eq. (B.1).

C. Evaluation of the generalised ITP

To compute the generalised ITP in Eq. (2.18), we map the outgoing operators onto the incoming ones using the Floquet scattering matrix [Moskalets and Büttiker, 2002; Moskalets, 2011]

$$\hat{b}_{\alpha}(E) = \sum_{n=-\infty}^{\infty} \sum_{\beta=1}^{N_i} S_{F,\alpha\beta}(E, E_n) \hat{a}_{\beta}(E_n), \tag{C.1}$$

where Ω is the frequency of the external driving and we have defined the energies

$$E_n = E + n\hbar\Omega,\tag{C.2}$$

for integer n. Since the incoming equilibrium particles are described by a Slater determinant, we may evaluate the quantum statistical average in Eq. (2.18) and we thereby obtain a determinant formula of the form

$$\Pi(t_1^s, t_1^e; \dots; t_{N_o}^s, t_{N_o}^e) = \det(\mathbb{I} - \mathcal{Q}(t_1^s, t_1^e; \dots; t_{N_o}^s, t_{N_o}^e)).$$

Here \mathbb{I} is the identity matrix and \mathcal{Q} contains the single-particle matrix elements of the operator $\sum_{\alpha} \widehat{Q}_{\alpha}$.

The matrix Q has a block form with elements in the (incoming) channel space

$$[\mathcal{Q}(t_1^s, t_1^e, \dots, t_{N_o}^s, t_{N_o}^e)]_{\alpha\beta} = \mathbf{K}_{\alpha\beta}$$
 (C.3)

with the $\mathbf{K}_{\alpha\beta}$ being matrices in energy space. In the general case of a time-dependent scatterer with many channels described by the Floquet scattering matrix in Eq. (C.1), these matrices have the elements

$$[\mathbf{K}_{\alpha\beta}]_{E,E'} = \sum_{\gamma=1}^{N_o} \sum_{m=-\lfloor E/\hbar\Omega \rfloor}^{\infty} S_{F,\gamma\alpha}^{\dagger}(E_m, E) S_{F,\gamma\beta}(E'_n, E')$$

$$= \sum_{m=-\lfloor E'/\hbar\Omega \rfloor}^{\infty} S_{F,\gamma\alpha}^{\dagger}(E_m, E) S_{F,\gamma\beta}(E'_n, E')$$

$$\times \Theta(-E) \Theta(-E') [K(t_{\gamma}^s, t_{\gamma}^e)]_{E=-E'},$$
(C.4)

where we have defined

$$[K(t_{\gamma}^s, t_{\gamma}^e)]_E = \frac{\kappa}{\pi} e^{-iE(t_{\gamma}^s + t_{\gamma}^e)/2} \frac{\sin(E(t_{\gamma}^e - t_{\gamma}^s)/2)}{E}.$$
 (C.5)

In addition, the floor function is denoted as $\lfloor \cdot \rfloor$ and we have discretized [Hassler et al., 2008; Albert et al., 2012; Haack et al., 2014] the transport window $[E_F, E_F + eV]$ into compartments of width $\kappa = eV/\mathcal{N}$, where \mathcal{N} is the number of particles. We always consider the limit $\mathcal{N} \to \infty$. The matrix has a block form with respect to the incoming channels, while we sum over the indices of the outgoing channels. The result in Eq. (C.4) generalises the expressions Eqs. (B.1)-(B.2) to many channels.

D. Numerical evaluation of Fredholm determinants

We here briefly sketch the numerical method used to evaluate Fredholm determinants, such as the ones appearing in Eqs. (1.12), (1.16), (B.1). We use the efficient and simple method recently proposed by Bornemann [2010].

A compact operator Q on a Hilbert space \mathcal{H} is said to be *trace class* if its trace can be defined [Reed and Simon, 1980]. More precisely, given any orthonormal basis $\{e_k\}_k$ of \mathcal{H} , the series

$$\operatorname{tr} Q = \sum_{k} \langle e_{k} | Q | e_{k} \rangle \tag{D.1}$$

should converge. For a trace class operator, one can define the determinant

$$f(z) := \det(1 + zQ) \tag{D.2}$$

for $z \in \mathbb{C}$. Eq. (1.12) is an example of such a Fredholm determinant for z = -1.

We now specify to the concrete case of operators that can be written as integral transforms on $L^2(\mathbb{R})$,

$$(Qf)(x) = \int_{a}^{b} Q(y, x)f(y)dy.$$
 (D.3)

The operator Q_{τ} in Eq. (1.12) falls into this category with a = 0, b = eV and the kernel Q(y, x) given by Eq. (1.14).

Now, given a quadrature rule for integrations on the interval [a, b],

$$\int_{a}^{b} f(x) dx \approx \sum_{j=1}^{m} w_{j} f(x_{j})$$
(D.4)

with weights w_j and a set of samples $\{x_j\}_j$, the determinant Eq. (D.2) is approximated

$$f(z) = \det(M(z)), \tag{D.5}$$

where the matrix M(z) has elements

$$[M(z)]_{ij} = \delta_{ij} + zw_j Q(x_i, x_j). \tag{D.6}$$

For analytic kernels $Q(x_i, x_j)$, Bornemann [2010] has proven exponential convergence rates for this method. In practice, for our waiting time calculations, we have indeed found very fast convergence, with a fourth order Gaussian quadrature rule already sufficient for a static QPC. For driven systems, this number should be multiplied by the number of relevant Floquet scattering amplitudes. In this case, we apply the discretization Eq. (D.6) in every matrix block m, n corresponding to a certain choice of Floquet energies E_m, E_n .

E. Full scattering matrix of the electron waiting time clock

In this appendix, we give the full scattering matrix of the electron waiting time clock, including all scattering amplitudes corresponding to electrons taking more than one turn in the capacitor.

If electrons can complete several loops inside the capacitor, the moment generating function reads

$$\chi(\lambda, \tau) = \det \left(\mathcal{S}_{\text{sys}}^{\dagger} \left(P_R + P_T \mathcal{S}_{-\lambda}^{(l)\dagger} P_T + P_T \mathcal{M}_{-\lambda}^{\dagger} P_T \right) \right. \\ \left. \times \left(P_R + P_T \mathcal{S}_{\lambda}^{(l)} P_T + P_T \mathcal{M}_{\lambda} P_T \right) \mathcal{S}_{\text{sys}} \right), \tag{E.1}$$

having introduced the matrix

$$\mathcal{M}_{\lambda} = \mathcal{S}_{\lambda}^{(l)} P_R \left(1 - P_R \mathcal{S}_{\lambda}^{(l)} P_R \right)^{-1} P_R \mathcal{S}_{\lambda}^{(l)}$$
 (E.2)

which describes processes where electrons complete more than one loop. By further manipulations, the moment generating function can be brought on the form

$$\chi(\lambda, \tau) = \det\left(1 + \mathcal{S}_{\text{sys}}^{\dagger} P_T \left[\left(\mathcal{K}_{\tau}^{\dagger} + \mathcal{K}_{\tau} \right) \left(e^{i\lambda/2} - 1 \right) + \mathcal{K}_{\tau}^{\dagger} P_T \mathcal{K}_{\tau} \left(e^{i\lambda/2} - 1 \right)^2 + \mathcal{R}_{\tau}^{\lambda} \right] P_T \mathcal{S}_{\text{sys}} \right)$$
(E.3)

with

$$\mathcal{R}_{\tau}^{\lambda} = \mathcal{M}_{-\lambda}^{\dagger} P_{T} \mathcal{M}_{\lambda} + \left(\mathcal{L}^{\dagger} \mathcal{M}_{\lambda} + \mathcal{M}_{-\lambda}^{\dagger} \mathcal{L} \right) + \mathcal{L}^{\dagger} \mathcal{K}_{\tau}^{-\lambda \dagger} P_{T} \mathcal{M}_{\lambda} + \mathcal{M}_{-\lambda}^{\dagger} P_{T} \mathcal{K}_{\tau}^{\lambda} \mathcal{L}, \tag{E.4}$$

where the matrix elements of \mathcal{L} read

$$[\mathcal{L}]_{E,E'} = e^{i(E' + e\delta V_g)\tau_D} \delta(E - E' - e\delta V_g). \tag{E.5}$$

In this case, the function in Eq. (E.3) contains terms that are proportional to $\exp(i\lambda/2)$. This is due to the commutator $[P_T, \mathcal{K}_\tau]$ being non-zero.

Bibliography

- A. G. Abanov and D. A. Ivanov. Allowed Charge Transfers between Coherent Conductors Driven by a Time-Dependent Scatterer. Phys. Rev. Lett. 100, 086602 [2008].
- A. G. Abanov and D. A. Ivanov. Factorization of quantum charge transport for noninteracting fermions. Phys. Rev. B 79, 205315 [2009].
- Y. Aharonov and D. Bohm. Significance of Electromagnetic Potentials in the Quantum Theory. Phys. Rev. 115, 485 [1959].
- M. Albert and P. Devillard. Waiting time distribution for trains of quantized electron pulses. Phys. Rev. B 90, 035431 [2014].
- M. Albert, C. Flindt, and M. Büttiker. Accuracy of the quantum capacitor as a single-electron source. Phys. Rev. B 82, 041407 [2010].
- M. Albert, C. Flindt, and M. Büttiker. Distributions of Waiting Times of Dynamic Single-Electron Emitters. Phys. Rev. Lett. 107, 086805 [2011].
- M. Albert, G. Haack, C. Flindt, and M. Büttiker. *Electron Waiting Times in Mesoscopic Conductors*. Phys. Rev. Lett. 108, 186806 [2012].
- A. Altland and B. D. Simons. *Condensed matter field theory* (Cambridge University Press, 2010).
- L. Amico, R. Fazio, A. Osterloh, and V. Vedral. Entanglement in many-body systems. Rev. Mod. Phys. 80, 517 [2008].
- S. Ashhab, K. Maruyama, and F. Nori. Detecting mode entanglement: The role of coherent states, superselection rules, and particle statistics. Phys. Rev. A 76, 052113 [2007].
- S. A. Babichev, J. Appel, and A. I. Lvovsky. *Homodyne Tomography Characterization and Nonlocality of a Dual-Mode Optical Qubit.* Phys. Rev. Lett. 92, 193601 [2004].
- S. D. Bartlett, T. Rudolph, and R. W. Spekkens. Reference frames, superselection rules, and quantum information. Rev. Mod. Phys. 79, 555 [2007].
- F. Battista and P. Samuelsson. Spectral distribution and wave function of electrons emitted from a single-particle source in the quantum Hall regime. Phys. Rev. B 85, 075428 [2012].

- V. Beaud, G. M. Graf, A. V. Lebedev, and G. B. Lesovik. Statistics of Charge Transport and Modified Time Ordering. J. Stat. Phys. 153, 177 [2013].
- A. Bednorz and W. Belzig. Quasiprobabilistic Interpretation of Weak Measurements in Mesoscopic Junctions. Phys. Rev. Lett. 105, 106803 [2010].
- C. W. J. Beenakker. Annihilation of Colliding Bogoliubov Quasiparticles Reveals their Majorana Nature. Phys. Rev. Lett. 112, 070604 [2014].
- C. W. J. Beenakker, C. Emary, M. Kindermann, and J. L. van Velsen. Proposal for Production and Detection of Entangled Electron-Hole Pairs in a Degenerate Electron Gas. Phys. Rev. Lett. 91, 147901 [2003].
- C. W. J. Beenakker and M. Kindermann. Quantum Teleportation by Particle-Hole Annihilation in the Fermi Sea. Phys. Rev. Lett. 92, 056801 [2004].
- J. Bell. On the Einstein Podolsky Rosen Paradox. Physics 1, 195 [1964].
- W. Belzig and Y. V. Nazarov. Full Counting Statistics of Electron Transfer between Superconductors. Phys. Rev. Lett. 87, 197006 [2001].
- C. H. Bennett and D. P. DiVincenzo. Quantum information and computation. Nature 404, 247 [2000].
- E. Bieri, M. Weiss, O. Göktas, M. Hauser, C. Schönenberger, and S. Oberholzer. Finite-bias visibility dependence in an electronic Mach-Zehnder interferometer. Phys. Rev. B 79, 245324 [2009].
- G. Björk, P. Jonsson, and L. L. Sánchez-Soto. Single-particle nonlocality and entanglement with the vacuum. Phys. Rev. A 64, 042106 [2001].
- Y. M. Blanter and M. Büttiker. *Shot noise in mesoscopic conductors*. Phys. Rep. 336, 1 [2000].
- I. Bloch. Quantum coherence and entanglement with ultracold atoms in optical lattices. Nature 453, 1016 [2008].
- E. Bocquillon, V. Freulon, J.-M. Berroir, P. Degiovanni, B. Plaçais, A. Cavanna, Y. Jin, and G. Fève. Coherence and Indistinguishability of Single Electrons Emitted by Independent Sources. Science 339, 1054 [2013a].
- E. Bocquillon, V. Freulon, P. Degiovanni, B. Placais, A. Cavanna, Y. Jin, G. Fève, et al. Separation of neutral and charge modes in one-dimensional chiral edge channels. Nat. Commun. 4, 1839 [2013b].
- E. Bocquillon, V. Freulon, F. D. Parmentier, J.-M. Berroir, B. Plaçais, C. Wahl, J. Rech, T. Jonckheere, T. Martin, C. Grenier, D. Ferraro, P. Degiovanni, and G. Fève. *Electron quantum optics in ballistic chiral conductors*. Ann. Phys. 526, 1 [2014].

- E. Bocquillon, F. D. Parmentier, C. Grenier, J.-M. Berroir, P. Degiovanni, D. C. Glattli, B. Plaçais, A. Cavanna, Y. Jin, and G. Fève. *Electron Quantum Optics: Partitioning Electrons One by One*. Phys. Rev. Lett. 108, 196803 [2012].
- J. Bohr Brask, R. Chaves, and N. Brunner. Testing nonlocality of a single photon without a shared reference frame. Phys. Rev. A 88, 012111 [2013].
- Y. Bomze, G. Gershon, D. Shovkun, L. Levitov, and M. Reznikov. Measurement of Counting Statistics of Electron Transport in a Tunnel Junction. Phys. Rev. Lett. 95, 176601 [2005].
- F. Bornemann. On the numerical evaluation of Fredholm determinants. Math. Comp. 79, 871 [2010].
- T. Brandes. Waiting times and noise in single particle transport. Ann. Phys. 17, 477 [2008].
- N. Brunner, D. Cavalcanti, S. Pironio, V. Scarani, and S. Wehner. Bell nonlocality. Rev. Mod. Phys. 86, 419 [2014].
- G. Burkard and D. Loss. Lower Bound for Electron Spin Entanglement from Beam Splitter Current Correlations. Phys. Rev. Lett. 91, 087903 [2003].
- G. Burkard, D. Loss, and E. V. Sukhorukov. *Noise of entangled electrons: Bunching and antibunching.* Phys. Rev. B 61, R16303 [2000].
- M. Büttiker. Absence of backscattering in the quantum Hall effect in multiprobe conductors. Phys. Rev. B 38, 9375 [1988].
- M. Büttiker. Quantized transmission of a saddle-point constriction. Phys. Rev. B 41, 7906 [1990a].
- M. Büttiker. Scattering theory of thermal and excess noise in open conductors. Phys. Rev. Lett. 65, 2901 [1990b].
- M. Büttiker. Scattering Theory of Thermal and Excess Noise in Open Conductors. Phys. Rev. Lett. 65, 2901 [1990c].
- M. Büttiker, Y. Imry, and M. Y. Azbel. Quantum oscillations in one-dimensional normal-metal rings. Phys. Rev. A 30, 1982 [1984].
- M. Büttiker, H. Thomas, and A. Prêtre. *Mesoscopic capacitors*. Phys. Lett. A 180, 364 [1993].
- H. J. Carmichael, S. Singh, R. Vyas, and P. R. Rice. *Photoelectron waiting times and atomic state reduction in resonance fluorescence*. Phys. Rev. A 39, 1200 [1989].
- H. J. Carmichael and D. F. Walls. Proposal for the measurement of the resonant Stark effect by photon correlation techniques. Journal of Physics B: Atomic and Molecular Physics 9, L43 [1976].

- J. F. Clauser, M. A. Horne, A. Shimony, and R. A. Holt. Proposed Experiment to Test Local Hidden-Variable Theories. Phys. Rev. Lett. 23, 880 [1969].
- A. A. Clerk. Full counting statistics of energy fluctuations in a driven quantum resonator. Phys. Rev. A 84, 043824 [2011].
- C. Cohen-Tannoudji and J. Dalibard. Single-Atom Laser Spectroscopy. Looking for Dark Periods in Fluorescence Light. EPL (Europhysics Letters) 1, 441 [1986].
- D. R. Cox. Renewal Theory (Chapman and Hall, London, 1962).
- M. Čubrović, J. Zaanen, and K. Schalm. String Theory, Quantum Phase Transitions, and the Emergent Fermi Liquid. Science 325, 439 [2009].
- S. Das Sarma, S. Adam, E. H. Hwang, and E. Rossi. *Electronic transport in two-dimensional graphene*. Rev. Mod. Phys. 83, 407 [2011].
- D. Dasenbrook, J. Bowles, J. B. Brask, P. P. Hofer, C. Flindt, and N. Brunner. *Single-electron entanglement and nonlocality*. New J. Phys. 18, 043036 [2016].
- D. Dasenbrook and C. Flindt. Dynamical generation and detection of entanglement in neutral leviton pairs. Phys. Rev. B 92, 161412(R) [2015].
- D. Dasenbrook and C. Flindt. Dynamical Scheme for Interferometric Measurements of Full Counting Statistics [2016a]. ArXiv:1605.01926.
- D. Dasenbrook and C. Flindt. Quantum theory of an electron waiting time clock. Phys. Rev. B 93, 245409 [2016b].
- D. Dasenbrook, C. Flindt, and M. Büttiker. Floquet Theory of Electron Waiting Times in Quantum-Coherent Conductors. Phys. Rev. Lett. 112, 146801 [2014].
- D. Dasenbrook, P. P. Hofer, and C. Flindt. *Electron waiting times in coherent conductors are correlated.* Phys. Rev. B 91, 195420 [2015].
- S. Datta. Electronic transport in mesoscopic systems (Cambridge university press, 1997).
- A. Di Lorenzo and Y. V. Nazarov. Full Counting Statistics with Spin-Sensitive Detectors Reveals Spin Singlets. Phys. Rev. Lett. 94, 210601 [2005].
- J. Dressel, Y. Choi, and A. N. Jordan. Measuring which-path information with coupled electronic Mach-Zehnder interferometers. Phys. Rev. B 85, 045320 [2012].
- J. Dubois, T. Jullien, C. Grenier, P. Degiovanni, P. Roulleau, and D. C. Glattli. Integer and fractional charge Lorentzian voltage pulses analyzed in the framework of photonassisted shot noise. Phys. Rev. B 88, 085301 [2013a].
- J. Dubois, T. Jullien, P. Roulleau, F. Portier, P. Roche, A. Cavanna, Y. Jin, W. Wegschneider, and D. C. Glattli. *Minimal-excitation states for electron quantum optics using levitons*. Nature 502, 659 [2013b].

- C. Emary. Leggett-Garg inequalities for the statistics of electron transport. Phys. Rev. B 86, 085418 [2012].
- C. Emary, N. Lambert, and F. Nori. Leggett-Garg inequalities. Rep. Prog. Phys. 77, 016001 [2013].
- M. Esposito, U. Harbola, and S. Mukamel. Nonequilibrium fluctuations, fluctuation theorems, and counting statistics in quantum systems. Rev. Mod. Phys. 81, 1665 [2009].
- H. A. Fertig and B. I. Halperin. Transmission coefficient of an electron through a saddle-point potential in a magnetic field. Phys. Rev. B 36, 7969 [1987].
- G. Fève, A. Mahe, J.-M. Berroir, T. Kontos, B. Placais, D. Glattli, A. Cavanna, B. Etienne, and Y. Jin. An on-demand coherent single-electron source. Science 316, 1169 [2007].
- J. D. Fletcher, P. See, H. Howe, M. Pepper, S. P. Giblin, J. P. Griffiths, G. A. C. Jones, I. Farrer, D. A. Ritchie, T. J. B. M. Janssen, and M. Kataoka. *Clock-Controlled Emission of Single-Electron Wave Packets in a Solid-State Circuit*. Phys. Rev. Lett. 111, 216807 [2013].
- C. Flindt, C. Fricke, F. Hohls, T. Novotný, K. Netočný, T. Brandes, and R. J. Haug. Universal oscillations in counting statistics. Proc. Natl. Acad. Sci. USA 106, 10116 [2009].
- H. Förster and M. Büttiker. Fluctuation Relations Without Microreversibility in Nonlinear Transport. Phys. Rev. Lett. 101, 136805 [2008].
- N. Friis. Reasonable fermionic quantum information theories require relativity. New J. Phys. 18, 033014 [2016].
- T. Fujisawa, T. Hayashi, R. Tomita, and Y. Hirayama. *Bidirectional Counting of Single Electrons*. Science 312, 1634 [2006].
- M. Fuwa, S. Takeda, M. Zwierz, H. M. Wiseman, and A. Furusawa. Experimental proof of nonlocal wavefunction collapse for a single particle using homodyne measurements. Nat. Commun. 6 [2015].
- J. Gabelli, G. Fève, J.-M. Berroir, B. Plaçais, A. Cavanna, B. Etienne, Y. Jin, and D. C. Glattli. Violation of Kirchhoff's Laws for a Coherent RC Circuit. Science 313, 499 [2006].
- J. Gabelli and B. Reulet. Full counting statistics of avalanche transport: An experiment. Phys. Rev. B 80, 161203 [2009].
- B. Gaury and X. Waintal. Dynamical control of interference using voltage pulses in the quantum regime. Nat. Commun. 5, 3844 [2014].

- U. Gavish, Y. Levinson, and Y. Imry. Shot-Noise in Transport and Beam Experiments. Phys. Rev. Lett. 87, 216807 [2001].
- Y. Gefen, Y. Imry, and M. Y. Azbel. Quantum Oscillations and the Aharonov-Bohm Effect for Parallel Resistors. Phys. Rev. Lett. 52, 129 [1984].
- G. Gershon, Y. Bomze, E. V. Sukhorukov, and M. Reznikov. *Detection of Non-Gaussian Fluctuations in a Quantum Point Contact*. Phys. Rev. Lett. 101, 016803 [2008].
- V. Giovannetti, D. Frustaglia, F. Taddei, and R. Fazio. Electronic Hong-Ou-Mandel interferometer for multimode entanglement detection. Phys. Rev. B 74, 115315 [2006].
- V. Giovannetti, D. Frustaglia, F. Taddei, and R. Fazio. *Characterizing electron entanglement in multiterminal mesoscopic conductors*. Phys. Rev. B 75, 241305 [2007].
- N. V. Gnezdilov, B. van Heck, M. Diez, J. A. Hutasoit, and C. W. J. Beenakker. Topologically protected charge transfer along the edge of a chiral p-wave superconductor. Phys. Rev. B 92, 121406 [2015].
- D. M. Greenberger, M. A. Horne, and A. Zeilinger. *Nonlocality of a Single Photon?* Phys. Rev. Lett. 75, 2064 [1995].
- S. Gustavsson, R. Leturcq, B. Simovic, R. Schleser, T. Ihn, P. Studerus, K. Ensslin, D. C. Driscoll, and A. C. Gossard. Counting Statistics of Single-Electron Transport in a Quantum Dot. Phys. Rev. Lett. 96, 076605 [2006].
- S. Gustavsson, R. Leturcq, M. Studer, I. Shorubalko, T. Ihn, K. Ensslin, D. C. Driscoll, and A. C. Gossard. *Electron counting in quantum dots*. Surf. Sci. Rep. 64, 191 [2009].
- D. B. Gutman, Y. Gefen, and A. D. Mirlin. Full Counting Statistics of a Luttinger Liquid Conductor. Phys. Rev. Lett. 105, 256802 [2010].
- G. Haack, M. Albert, and C. Flindt. Distributions of electron waiting times in quantum-coherent conductors. Phys. Rev. B 90, 205429 [2014].
- G. Haack, M. Moskalets, and M. Büttiker. *Glauber coherence of single-electron sources*. Phys. Rev. B 87, 201302 [2013].
- B. I. Halperin. Quantized Hall conductance, current-carrying edge states, and the existence of extended states in a two-dimensional disordered potential. Phys. Rev. B 25, 2185 [1982].
- L. Hardy. Nonlocality of a Single Photon Revisited. Phys. Rev. Lett. 73, 2279 [1994].
- L. Hardy. *Hardy Replies:*. Phys. Rev. Lett. 75, 2065 [1995].
- M. Z. Hasan and C. L. Kane. *Colloquium : Topological insulators*. Rev. Mod. Phys. 82, 3045 [2010].

- F. Hassler, G. B. Lesovik, and G. Blatter. Effects of Exchange Symmetry on Full Counting Statistics. Phys. Rev. Lett. 99, 076804 [2007].
- F. Hassler, M. V. Suslov, G. M. Graf, M. V. Lebedev, G. B. Lesovik, and G. Blatter. Wave-packet formalism of full counting statistics. Phys. Rev. B 78, 165330 [2008].
- A. Helzel, L. V. Litvin, I. P. Levkivskyi, E. V. Sukhorukov, W. Wegscheider, and C. Strunk. Counting statistics and dephasing transition in an electronic Mach-Zehnder interferometer. Phys. Rev. B 91, 245419 [2015].
- M. Henny, S. Oberholzer, C. Strunk, T. Heinzel, K. Ensslin, M. Holland, and C. Schönenberger. *The Fermionic Hanbury Brown and Twiss Experiment*. Science 284, 296 [1999].
- B. Hensen, H. Bernien, A. Dréau, A. Reiserer, N. Kalb, M. Blok, J. Ruitenberg, R. Vermeulen, R. Schouten, C. Abellán, W. Amaya, V. Pruneri, M. W. Mitchell, M. Markham, D. J. Twitchen, D. Elkouss, S. Wehner, T. H. Taminiau, and R. Hanson. Loophole-free Bell inequality violation using electron spins separated by 1.3 kilometres. Nature 526, 682 [2015].
- D. Herman, T. T. Ong, G. Usaj, H. Mathur, and H. U. Baranger. Level spacings in random matrix theory and Coulomb blockade peaks in quantum dots. Phys. Rev. B 76, 195448 [2007].
- L. G. Herrmann, F. Portier, P. Roche, A. L. Yeyati, T. Kontos, and C. Strunk. *Carbon Nanotubes as Cooper-Pair Beam Splitters*. Phys. Rev. Lett. 104, 026801 [2010].
- B. Hessmo, P. Usachev, H. Heydari, and G. Björk. Experimental Demonstration of Single Photon Nonlocality. Phys. Rev. Lett. 92, 180401 [2004].
- P. P. Hofer and M. Büttiker. Emission of time-bin entangled particles into helical edge states. Phys. Rev. B 88, 241308(R) [2013].
- P. P. Hofer and A. A. Clerk. Negative Full Counting Statistics Arise from Interference Effects. Phys. Rev. Lett. 116, 013603 [2016].
- P. P. Hofer, D. Dasenbrook, and C. Flindt. *Electron waiting times for the mesoscopic capacitor*. Physica E 82, 3 [2015].
- P. P. Hofer and C. Flindt. *Mach-Zehnder interferometry with periodic voltage pulses*. Phys. Rev. B 90, 235416 [2014].
- L. Hofstetter, S. Csonka, J. Nygård, and C. Schönenberger. Cooper pair splitter realized in a two-quantum-dot Y-junction. Nature 461, 960 [2009].
- R. Horodecki, P. Horodecki, M. Horodecki, and K. Horodecki. Quantum entanglement. Rev. Mod. Phys. 81, 865 [2009].

- P.-A. Huynh, F. Portier, H. le Sueur, G. Faini, U. Gennser, D. Mailly, F. Pierre, W. Wegscheider, and P. Roche. Quantum Coherence Engineering in the Integer Quantum Hall Regime. Phys. Rev. Lett. 108, 256802 [2012].
- A. Inhofer and D. Bercioux. Proposal for an on-demand source of polarized electrons into the edges of a topological insulator. Phys. Rev. B 88, 235412 [2013].
- D. A. Ivanov, H. W. Lee, and L. S. Levitov. *Coherent states of alternating current*. Phys. Rev. B 56, 6839 [1997].
- Y. Ji, Y. Chung, D. Sprinzak, M. Heiblum, D. Mahalu, and H. Shtrikman. An electronic Mach-Zehnder interferometer. Nature 422, 415 [2003].
- T. Jonckheere, J. Rech, C. Wahl, and T. Martin. Electron and hole Hong-Ou-Mandel interferometry. Phys. Rev. B 86, 125425 [2012].
- T. Jullien, P. Roulleau, B. Roche, A. Cavanna, Y. Jin, and D. C. Glattli. Quantum tomography of an electron. Nature 514, 603 [2014].
- D. Kambly, C. Flindt, and M. Büttiker. Factorial cumulants reveal interactions in counting statistics. Phys. Rev. B 83, 075432 [2011].
- A. Kamenev. Field Theory of Non-Equilibrium Systems (Cambridge University Press, 2011).
- S. Kawabata. Test of Bell's Inequality using the Spin Filter Effect in Ferromagnetic Semiconductor Microstructures. J. Phys. Soc. Japan 70, 1210 [2001].
- J. Keeling, I. Klich, and L. S. Levitov. *Minimal Excitation States of Electrons in One-Dimensional Wires*. Phys. Rev. Lett. 97, 116403 [2006].
- J. Keeling, A. V. Shytov, and L. S. Levitov. *Coherent Particle Transfer in an On-Demand Single-Electron Source*. Phys. Rev. Lett. 101, 196404 [2008].
- H. J. Kimble and L. Mandel. Theory of resonance fluorescence. Phys. Rev. A 13, 2123 [1976].
- I. Klich and L. S. Levitov. Quantum Noise as an Entanglement Meter. Phys. Rev. Lett. 102, 100502 [2009].
- A. Komnik and G. W. Langhanke. Full counting statistics of persistent current. Phys. Rev. B 90, 165107 [2014].
- A. Komnik and H. Saleur. Full Counting Statistics of Chiral Luttinger Liquids with Impurities. Phys. Rev. Lett. 96, 216406 [2006].
- B. Küng, C. Rössler, M. Beck, M. Marthaler, D. S. Golubev, Y. Utsumi, T. Ihn, and K. Ensslin. *Irreversibility on the Level of Single-Electron Tunneling*. Phys. Rev. X 2, 011001 [2012].

- R. B. Laughlin. Quantized Hall conductivity in two dimensions. Phys. Rev. B 23, 5632 [1981].
- A. V. Lebedev, G. Blatter, C. W. J. Beenakker, and G. B. Lesovik. *Entanglement in mesoscopic structures: Role of projection*. Phys. Rev. B 69, 235312 [2004].
- A. V. Lebedev, G. B. Lesovik, and G. Blatter. Generating spin-entangled electron pairs in normal conductors using voltage pulses. Phys. Rev. B 72, 245314 [2005].
- A. V. Lebedev, G. B. Lesovik, and G. Blatter. *Optimal noninvasive measurement of full counting statistics by a single qubit.* Phys. Rev. B 93, 115140 [2016].
- G. Lesovik, T. Martin, and G. Blatter. Electronic entanglement in the vicinity of a superconductor. Eur. Phys. J. B 24, 287 [2001].
- G. B. Lesovik, F. Hassler, and G. Blatter. *Using Qubits to Measure Fidelity in Mesoscopic Systems*. Phys. Rev. Lett. 96, 106801 [2006].
- G. B. Lesovik and I. A. Sadovskyy. Scattering matrix approach to the description of quantum electron transport. Physics-Uspekhi 54, 1007 [2011].
- L. S. Levitov, H. Lee, and G. B. Lesovik. *Electron counting statistics and coherent states of electric current*. J. Math. Phys. 37, 4845 [1996].
- I. P. Levkivskyi and E. V. Sukhorukov. Dephasing in the electronic Mach-Zehnder interferometer at filling factor $\nu = 2$. Phys. Rev. B 78, 045322 [2008].
- I. P. Levkivskyi and E. V. Sukhorukov. Noise-Induced Phase Transition in the Electronic Mach-Zehnder Interferometer. Phys. Rev. Lett. 103, 036801 [2009].
- Z. Li, C. Lam, and J. You. Probing Majorana bound states via counting statistics of a single electron transistor. Scientific Reports 5, 11416 [2015].
- L. V. Litvin, A. Helzel, H.-P. Tranitz, W. Wegscheider, and C. Strunk. *Edge-channel interference controlled by Landau level filling*. Phys. Rev. B 78, 075303 [2008].
- L. V. Litvin, A. Helzel, H.-P. Tranitz, W. Wegscheider, and C. Strunk. Phase of the transmission amplitude for a quantum dot embedded in the arm of an electronic Mach-Zehnder interferometer. Phys. Rev. B 81, 205425 [2010].
- D. E. Liu, A. Levchenko, and R. M. Lutchyn. *Majorana zero modes choose Euler numbers as revealed by full counting statistics*. Phys. Rev. B 92, 205422 [2015].
- E. Lombardi, F. Sciarrino, S. Popescu, and F. De Martini. *Teleportation of a Vacuum-One-Photon Qubit.* Phys. Rev. Lett. 88, 070402 [2002].
- A. Mahé, F. D. Parmentier, E. Bocquillon, J.-M. Berroir, D. C. Glattli, T. Kontos, B. Plaçais, G. Fève, A. Cavanna, and Y. Jin. Current correlations of an on-demand single-electron emitter. Phys. Rev. B 82, 201309 [2010].

- V. F. Maisi, D. Kambly, C. Flindt, and J. P. Pekola. Full Counting Statistics of Andreev Tunneling. Phys. Rev. Lett. 112, 036801 [2014].
- Y. Makhlin and A. D. Mirlin. Counting Statistics for Arbitrary Cycles in Quantum Pumps. Phys. Rev. Lett. 87, 276803 [2001].
- T. Martin and R. Landauer. Wave-packet approach to noise in multichannel mesoscopic systems. Phys. Rev. B 45, 1742 [1992].
- F. Monteiro, V. C. Vivoli, T. Guerreiro, A. Martin, J.-D. Bancal, H. Zbinden, R. T. Thew, and N. Sangouard. Revealing Genuine Optical-Path Entanglement. Phys. Rev. Lett. 114, 170504 [2015].
- M. Moskalets. Scattering Matrix Approach to Non-Stationary Quantum Transport (Imperial College Press, 2011).
- M. Moskalets. Noise of a single-electron emitter. Phys. Rev. B 88, 035433 [2013].
- M. Moskalets and M. Büttiker. Floquet scattering theory of quantum pumps. Phys. Rev. B 66, 205320 [2002].
- M. Moskalets and M. Büttiker. *Time-resolved noise of adiabatic quantum pumps*. Phys. Rev. B 75, 035315 [2007].
- M. Moskalets, G. Haack, and M. Büttiker. Single-electron source: Adiabatic versus nona-diabatic emission. Phys. Rev. B 87, 125429 [2013].
- M. Moskalets, P. Samuelsson, and M. Büttiker. Quantized Dynamics of a Coherent Capacitor. Phys. Rev. Lett. 100, 086601 [2008].
- B. A. Muzykantskii and Y. Adamov. Scattering approach to counting statistics in quantum pumps. Phys. Rev. B 68, 155304 [2003].
- K. E. Nagaev, O. S. Ayvazyan, N. Y. Sergeeva, and M. Büttiker. Magnetic-Field-Induced Non-Gaussian Fluctuations in Macroscopic Equilibrium Systems. Phys. Rev. Lett. 105, 146802 [2010].
- Y. V. Nazarov and M. Kindermann. Full counting statistics of a general quantum mechanical variable. Eur. Phys. J. B 35, 413 [2003].
- I. Neder, M. Heiblum, D. Mahalu, and V. Umansky. Entanglement, Dephasing, and Phase Recovery via Cross-Correlation Measurements of Electrons. Phys. Rev. Lett. 98, 036803 [2007a].
- I. Neder and F. Marquardt. Coherence oscillations in dephasing by non-Gaussian shot noise. New J. Phys. 9, 112 [2007].
- I. Neder, F. Marquardt, M. Heiblum, D. Mahalu, and V. Umansky. *Controlled dephasing of electrons by non-gaussian shot noise*. Nat. Phys. 3, 534 [2007b].

- I. Neder, N. Ofek, Y. Chung, M. Heiblum, D. Mahalu, and V. Umansky. Interference between two indistinguishable electrons from independent sources. Nature 448, 333 [2007c].
- W. D. Oliver, J. Kim, R. C. Liu, and Y. Yamamoto. Hanbury Brown and Twiss-Type Experiment with Electrons. Science 284, 299 [1999].
- S. Ol'khovskaya, J. Splettstoesser, M. Moskalets, and M. Büttiker. *Shot Noise of a Mesoscopic Two-Particle Collider*. Phys. Rev. Lett. 101, 166802 [2008].
- F. D. Parmentier, E. Bocquillon, J.-M. Berroir, D. C. Glattli, B. Plaçais, G. Fève, M. Albert, C. Flindt, and M. Büttiker. Current noise spectrum of a single-particle emitter: Theory and experiment. Phys. Rev. B 85, 165438 [2012].
- M. H. Pedersen and M. Büttiker. Scattering theory of photon-assisted electron transport. Phys. Rev. B 58, 12993 [1998].
- A. Petrescu, H. F. Song, S. Rachel, Z. Ristivojevic, C. Flindt, N. Laflorencie, I. Klich, N. Regnault, and K. Le Hur. Fluctuations and entanglement spectrum in quantum Hall states. J. Stat. Mech. p. P10005 [2014].
- A. Prêtre, H. Thomas, and M. Büttiker. Dynamic admittance of mesoscopic conductors: Discrete-potential model. Phys. Rev. B 54, 8130 [1996].
- J. Rammer and A. Shelankov. Counting quantum fluctuations of particle density. Ann. Phys. 524, 163 [2012].
- P. Recher, E. V. Sukhorukov, and D. Loss. Andreev tunneling, Coulomb blockade, and resonant transport of nonlocal spin-entangled electrons. Phys. Rev. B 63, 165314 [2001].
- M. Reed and B. Simon. Functional Analysis, vol. I (Academic Press (London), 1980).
- B. Reulet, J. Senzier, and D. E. Prober. Environmental Effects in the Third Moment of Voltage Fluctuations in a Tunnel Junction. Phys. Rev. Lett. 91, 196601 [2003].
- G. Rosenberg and M. Franz. Witten effect in a crystalline topological insulator. Phys. Rev. B 82, 035105 [2010].
- P. Roulleau, F. Portier, D. C. Glattli, P. Roche, A. Cavanna, G. Faini, U. Gennser, and D. Mailly. Finite bias visibility of the electronic Mach-Zehnder interferometer. Phys. Rev. B 76, 161309 [2007].
- P. Roulleau, F. Portier, P. Roche, A. Cavanna, G. Faini, U. Gennser, and D. Mailly. Direct Measurement of the Coherence Length of Edge States in the Integer Quantum Hall Regime. Phys. Rev. Lett. 100, 126802 [2008].
- P. Roulleau, F. Portier, P. Roche, A. Cavanna, G. Faini, U. Gennser, and D. Mailly. *Tuning Decoherence with a Voltage Probe.* Phys. Rev. Lett. 102, 236802 [2009].

- O.-P. Saira, Y. Yoon, T. Tanttu, M. Möttönen, D. V. Averin, and J. P. Pekola. Test of the Jarzynski and Crooks Fluctuation Relations in an Electronic System. Phys. Rev. Lett. 109, 180601 [2012].
- S. Saito, J. Endo, T. Kodama, A. Tonomura, A. Fukuhara, and K. Ohbayashi. *Electron counting theory*. Phys. Lett. A 162, 442 [1992].
- D. Salart, O. Landry, N. Sangouard, N. Gisin, H. Herrmann, B. Sanguinetti, C. Simon, W. Sohler, R. T. Thew, A. Thomas, and H. Zbinden. *Purification of Single-Photon Entanglement*. Phys. Rev. Lett. 104, 180504 [2010].
- P. Samuelsson and M. Büttiker. *Dynamic generation of orbital quasiparticle entanglement in mesoscopic conductors*. Phys. Rev. B 71, 245317 [2005].
- P. Samuelsson and M. Büttiker. Quantum state tomography with quantum shot noise. Phys. Rev. B 73, 041305 [2006].
- P. Samuelsson, I. Neder, and M. Büttiker. Entanglement at finite temperatures in the electronic two-particle interferometer. Physica Scripta 2009, 014023 [2009a].
- P. Samuelsson, I. Neder, and M. Büttiker. Reduced and Projected Two-Particle Entanglement at Finite Temperatures. Phys. Rev. Lett. 102, 106804 [2009b].
- P. Samuelsson, E. V. Sukhorukov, and M. Büttiker. Orbital Entanglement and Violation of Bell Inequalities in Mesoscopic Conductors. Phys. Rev. Lett. 91, 157002 [2003].
- P. Samuelsson, E. V. Sukhorukov, and M. Büttiker. Two-Particle Aharonov-Bohm Effect and Entanglement in the Electronic Hanbury Brown-Twiss Setup. Phys. Rev. Lett. 92, 026805 [2004].
- P. Samuelsson, E. V. Sukhorukov, and M. Büttiker. Quasi-particle entanglement: redefinition of the vacuum and reduced density matrix approach. New J. Phys. 7, 176 [2005].
- N. Sangouard, C. Simon, H. de Riedmatten, and N. Gisin. Quantum repeaters based on atomic ensembles and linear optics. Rev. Mod. Phys. 83, 33 [2011].
- N. Sangouard and H. Zbinden. What are single photons good for? J. Mod. Opt. 59, 1458 [2012].
- J. Schindele, A. Baumgartner, and C. Schönenberger. Near-Unity Cooper Pair Splitting Efficiency. Phys. Rev. Lett. 109, 157002 [2012].
- K. Schönhammer. Full counting statistics for noninteracting fermions: Exact results and the Levitov-Lesovik formula. Phys. Rev. B 75, 205329 [2007].
- E. Schrödinger. Discussion of Probability Relations between Separated Systems. Mathematical Proceedings of the Cambridge Philosophical Society 31, 555 [1935].

- N. Schuch, F. Verstraete, and J. I. Cirac. Nonlocal Resources in the Presence of Superselection Rules. Phys. Rev. Lett. 92, 087904 [2004].
- A. Shelankov and J. Rammer. Charge transfer counting statistics revisited. Europhys. Lett.) 63, 485 [2003].
- Y. Sherkunov, N. d'Ambrumenil, P. Samuelsson, and M. Büttiker. *Optimal pumping of orbital entanglement with single-particle emitters*. Phys. Rev. B 85, 081108 [2012].
- Y. Sherkunov, J. Zhang, N. d'Ambrumenil, and B. Muzykantskii. *Optimal electron entangler and single-electron source at low temperatures*. Phys. Rev. B 80, 041313(R) [2009].
- H.-S. Sim and E. V. Sukhorukov. *Multiparticle Interference, Greenberger-Horne-Zeilinger Entanglement, and Full Counting Statistics*. Phys. Rev. Lett. 96, 020407 [2006].
- H. Soller and A. Komnik. Charge transfer statistics of transport through Majorana bound states. Physica E 63, 99 [2014].
- H. F. Song, C. Flindt, S. Rachel, I. Klich, and K. Le Hur. Entanglement entropy from charge statistics: Exact relations for noninteracting many-body systems. Phys. Rev. B 83, 161408 [2011].
- H. F. Song, S. Rachel, C. Flindt, I. Klich, N. Laflorencie, and K. Le Hur. *Bipartite fluctuations as a probe of many-body entanglement*. Phys. Rev. B 85, 035409 [2012].
- P. Stegmann, B. Sothmann, A. Hucht, and J. König. Detection of interactions via generalized factorial cumulants in systems in and out of equilibrium. Phys. Rev. B 92, 155413 [2015].
- G. Strübi, W. Belzig, T. L. Schmidt, and C. Bruder. Full counting statistics of Majorana interferometers. Physica E 74, 489 [2015].
- E. V. Sukhorukov and V. V. Cheianov. Resonant Dephasing in the Electronic Mach-Zehnder Interferometer. Phys. Rev. Lett. 99, 156801 [2007].
- S. Takeda, M. Fuwa, P. van Loock, and A. Furusawa. *Entanglement Swapping between Discrete and Continuous Variables*. Phys. Rev. Lett. 114, 100501 [2015].
- S. M. Tan, D. F. Walls, and M. J. Collett. *Nonlocality of a single photon*. Phys. Rev. Lett. 66, 252 [1991].
- Z. B. Tan, D. Cox, T. Nieminen, P. Lähteenmäki, D. Golubev, G. B. Lesovik, and P. J. Hakonen. Cooper Pair Splitting by Means of Graphene Quantum Dots. Phys. Rev. Lett. 114, 096602 [2015].
- G.-M. Tang, F. Xu, and J. Wang. Waiting time distribution of quantum electronic transport in the transient regime. Phys. Rev. B 89, 205310 [2014].

- R. Thalineau, A. D. Wieck, C. Bäuerle, and T. Meunier. *Using a two-electron spin qubit to detect electrons flying above the Fermi sea* [2014]. ArXiv:1403.7770.
- K. H. Thomas and C. Flindt. Electron Waiting Times in Non-Markovian Quantum Transport. Phys. Rev. B 87, 121405(R) [2013].
- K. H. Thomas and C. Flindt. Entanglement entropy in dynamic quantum-coherent conductors. Phys. Rev. B 91, 125406 [2015].
- T. J. Thornton, M. Pepper, H. Ahmed, D. Andrews, and G. J. Davies. One-Dimensional Conduction in the 2D Electron Gas of a GaAs-AlGaAs Heterojunction. Phys. Rev. Lett. 56, 1198 [1986].
- D. J. Thouless, M. Kohmoto, M. P. Nightingale, and M. den Nijs. *Quantized Hall Conductance in a Two-Dimensional Periodic Potential*. Phys. Rev. Lett. 49, 405 [1982].
- A. V. Timofeev, M. Meschke, J. T. Peltonen, T. T. Heikkila, and J. P. Pekola. Wideband Detection of the Third Moment of Shot Noise by a Hysteretic Josephson Junction. Phys. Rev. Lett. 98, 207001 [2007].
- J. Tobiska and Y. V. Nazarov. Inelastic interaction corrections and universal relations for full counting statistics in a quantum contact. Phys. Rev. B 72, 235328 [2005].
- N. Ubbelohde, C. Fricke, C. Flindt, F. Hohls, and R. J. Haug. Measurement of finite-frequency current statistics in a single-electron transistor. Nat. Commun. 3, 612 [2012].
- Y. Utsumi, D. S. Golubev, M. Marthaler, K. Saito, T. Fujisawa, and G. Schön. Bidirectional single-electron counting and the fluctuation theorem. Phys. Rev. B 81, 125331 [2010].
- Y. Utsumi and K. Saito. Fluctuation theorem in a quantum-dot Aharonov-Bohm interferometer. Phys. Rev. B 79, 235311 [2009].
- J. A. Vaccaro, F. Anselmi, and H. M. Wiseman. Entanglement of Identical Particles and Reference Phase Uncertainty. Int. J. Quant. Inf. 1, 427 [2003].
- L. Vaidman. Nonlocality of a Single Photon Revisited Again. Phys. Rev. Lett. 75, 2063 [1995].
- S. J. van Enk. Single-particle entanglement. Phys. Rev. A 72, 064306 [2005].
- B. J. van Wees, H. van Houten, C. W. J. Beenakker, J. G. Williamson, L. P. Kouwenhoven, D. van der Marel, and C. T. Foxon. *Quantized conductance of point contacts in a two-dimensional electron gas.* Phys. Rev. Lett. 60, 848 [1988].
- M. Vanević, Y. V. Nazarov, and W. Belzig. Elementary Events of Electron Transfer in a Voltage-Driven Quantum Point Contact. Phys. Rev. Lett. 99, 076601 [2007].
- M. Vanević, Y. V. Nazarov, and W. Belzig. Elementary charge-transfer processes in mesoscopic conductors. Phys. Rev. B 78, 245308 [2008].

- K. von Klitzing, G. Dorda, and M. Pepper. New Method for High-Accuracy Determination of the Fine-Structure Constant Based on Quantized Hall Resistance. Phys. Rev. Lett. 45, 494 [1980].
- R. Vyas and S. Singh. Waiting time distributions in the photodetection of squeezed light. Phys. Rev. A 38, 2423 [1988].
- A. A. Vyshnevyy, A. V. Lebedev, G. B. Lesovik, and G. Blatter. Two-particle entanglement in capacitively coupled Mach-Zehnder interferometers. Phys. Rev. B 87, 165302 [2013].
- R. A. Webb, S. Washburn, C. P. Umbach, and R. B. Laibowitz. Observation of $\frac{h}{e}$ Aharonov-Bohm Oscillations in Normal-Metal Rings. Phys. Rev. Lett. 54, 2696 [1985].
- E. Weisz, H. K. Choi, I. Sivan, M. Heiblum, Y. Gefen, D. Mahalu, and V. Umansky. *An electronic quantum eraser*. Science 344, 1363 [2014].
- H. M. Wiseman, S. D. Bartlett, and J. A. Vaccaro. Ferreting Out the Fluffy Bunnies: Entanglement Constrained by Generalized Superselection Rules. In Laser Spectroscopy, volume 1, p. 307 (World Scientific, 2004).
- H. M. Wiseman and J. A. Vaccaro. Entanglement of Indistinguishable Particles Shared between Two Parties. Phys. Rev. Lett. 91, 097902 [2003].
- J. Zhang, Y. Sherkunov, N. d'Ambrumenil, and B. Muzykantskii. Full counting statistics of quantum point contacts with time-dependent transparency. Phys. Rev. B 80, 245308 [2009].
- P. Zoller, M. Marte, and D. F. Walls. *Quantum jumps in atomic systems*. Phys. Rev. A 35, 198 [1987].
- W. H. Zurek. Cosmological experiments in condensed matter systems. Phys. Rep. 276, 177 [1996].

Acknowledgments

It would not have been possible to complete the work presented in this thesis on my own, so I would like to thank several important people who have been very helpful in its creation.

First of all, I would like to thank Christian Flindt, whose incredible support and trust in me has brought out the best in this work. He agreed to take over the supervision of my PhD during the difficult time when my original advisor, Markus Büttiker, had passed away. From the beginning, he continuously encouraged me to be creative and work on my own ideas, and has enthusiastically supported even the crazier ones among them. He invited me to work in his newly created group in Helsinki whenever I wanted to go. He has been an extraordinary and competent advisor and friend.

I would like to thank Markus Büttiker, my original supervisor who hired me to work in his group in Geneva and who taught me a lot of things during the one year I had the privilege of working with him, before he sadly passed away.

Then, I would like to thank Eugene Sukhorukov, who took over my formal supervision in Geneva after Markus passed away, for insightful scientific discussions and for ensuring I could continue to work on my thesis in Geneva.

Many thanks to Gianni Blatter and Christian Glattli for agreeing to be part of my thesis committee. During my scientific work, I have immensely benefitted from discussions with people in the electronic transport community, notably Mathias Albert, Géraldine Haack, Préden Roulleau, Michael Moskalets, Peter Samuelsson, Gwendal Fève, Rafael Sanchez, Gordey Lesovik, and many others.

I have been very fortunate to have had some amazing colleagues during my time as a PhD student, both in Geneva and in Helsinki, many of whom have become good friends. From Geneva, I would like to thank Dania Kambly, Pierre Delplace, Jian Li, Johan Ott, Björn Sothmann and Christoph Schenke. I would like to mention in particular Patrick Hofer, who started his PhD just shortly after myself and with whom I thus shared many experiences. We have spent many hours discussing science on the blackboard and have become productive scientific collaborators, but also good friends and band mates.

Then, I would like to thank the members of the quantum information theory group in Geneva, especially Nicolas Brunner, Joseph Bowles and Jonatan Bohr Brask, for a great collaboration mainly on the entanglement aspects of my work and many exciting discussions, and Flavien Hirsch for proofreading the French part of this thesis.

In Helsinki, I have met many interesting and extraordinary people, but I would like to specifically mention Christian's group members, Shuo Mi, Ciprian Padurariu, Kay Brandner and Elina Potanina, for welcoming me into the group and making each day at the office fun, and my other colleagues and friends at Aalto University, especially Anne-Maria Visuri, Joel Röntynen, and Arya Dhar, for welcoming me into their circle

Acknowledgments

of friends and being great companions. They really made a difference, and I am very grateful for the wonderful times I had in Finland.

I would also like to thank Francine Gennai-Nicole and Cécile Jaggi, secretaries of the Department of Theoretical Physics in Geneva, and Nathalie Chaduiron from the physics section, for taking care of all administrative matters. Thanks to Andreas Malaspinas as well, for IT support and help in setting up the group website.

I would like to thank my band members from *Le Fuzzball*, Irwin, Margot, Mona, Andrew, Joe, Amiyna, and Patrick, and my flatmates, Marco, Andrea, Flavien, Nadia, and Joe, for being such a wonderful part of my life here in Geneva.

Last but not least, I would like to thank my parents, Astrid and Dietrich, and my brother, Niklas, for always being there and supportive of everything I do. Thank you.